Lappeenranta University of Technology
School of Engineering Science
LUT Chemistry/ Laboratory of Process Engineering
BJ02A0020 Master's Thesis

Rasmus Peltola

DROPLET COALESCENCE AND BREAKAGE IN REACTIVE LIQUID-LIQUID EXTRACTION

Examiners:	Professor Tuomas Koiranen M. Sc. Jussi Tamminen
Supervisors:	M. Sc. Jussi Tamminen Lic. Tech. Esko Lahdenperä
Lappeenranta	15.05.2017

CONTENTS

1. Introduction 1
2. Liquid-Liquid Extraction 2
3. Droplet Coalescence 3
3.1 Mechanism of Droplet Coalescence 3
3.2 Influencing Parameters 6
3.2.1 Droplet Size 7
3.2.2 Addition of Surfactant and Salt 11
3.2.3 Droplet Interface Mobility 13
3.2.4 Mass Transfer 14
3.2.5 Collision Frequency Parameters 18
3.2.6 Electrochemical Effects 19
3.3 Experimental Setups 21
4. Droplet Breakage 25
4.1 Mechanism of Droplet Breakage 25
4.1.1 Binary Breakup 26
4.1.2 Capillary Breakup 27
4.1.3 Tip Streaming 28
4.2 Influencing Parameters 29
4.2.1 Droplet Size 29
4.2.2 Addition of Surfactant 30
4.2.3 Dilational Elasticity 31
4.2.5 Breakup Frequency Parameters 32
4.2.5 Mass Transfer 34
4.2.6 Flow History and Apparatus Geometry 35
4.3 Experimental Setups 36
5. Mass Transfer of Copper in Reactive Liquid-Liquid Extraction 39
5.1 Introduction to Reactive Mass Transfer 39
5.2 Mechanism of Copper Complex Formation 40
6. Computational Fluid Dynamics and Interfacial Tracking Methods 41
6.1 Computational Fluid Dynamics 42
6.2 Level-Set Method for a Single Droplet 43
6.3 Volume of Fluids 43
7. Image and Video Analysis 45
7.1 Principles of Image and Video Analysis 45
7.2 Concentration Calibration 47

7.3 Data Processing 50
8. Experiments 51
8.1 Experimental Setup 52
8.2 Preparation of Feed Solutions and Calibration Standards 54
8.2.1 Preparation of $CuSO_4$ and $(NH_4)_2SO_4$ solutions 54
8.2.2 Preparation of Acorga M5640 in Exxsol D80 solutions 55
8.2.3 Preparation of Calibration Standards 55
8.2 Binary Droplet Coalescence Procedure 56
8.2 Single Droplet Kinetic Extraction Procedure 57
9. Results and Discussion 58
9.1 Droplet Formation Times 58
9.2 Droplet Volumes 60
9.3 Droplet Rest Times 63
9.4 Droplet Concentration Analysis Results 65
9.5 Droplet Concentration Difference Analysis Results 69
9.6 Single Droplet Kinetic Extraction 70
9.7 Binary Droplet Coalescence: Modelling and Experimental 74
10. Conclusions 75
References

ALKUSANAT

Diplomityö on tehty Lappeenrannan teknillisessä yliopistossa kemiantekniikan osaston prosessitekniikan laboratoriossa. Työn ohjaajina toimivat projektitutkijat Jussi Tamminen ja Esko Lahdenperä sekä tarkastajana professori Tuomas Koiranen. Heitä kiitän suuresti arvokkaasta tuesta kaikissa diplomityön eri vaiheissa. Erityisesti Jussia haluan kiittää erinomaisesta ja kärsivällisestä ohjauksesta sekä aina saatavilla olevista vinkeistä ja neuvoista, joita ilman työ olisi tuskin koskaan valmistunut. Lisäksi kiitokset Eskolle työhön sisältyvän mallinnuksen tekemisestä ja mallinnukseen liittyvistä neuvoista. Lopuksi esitän vielä kiitokseni tuesta ja kannustuksesta perheelleni Raijalle, Timolle, Marukselle ja Jarnolle, sekä opiskelutovereilleni Mikko Brotellille, Antti Paarviolle, Isto Sipilälle ja Veli-Ensio Heiniluodolle.

ABSTRACT

Lappeenranta University of Technology
School of Engineering Science
LUT Chemistry / Laboratory of Process Engineering

Rasmus Peltola

Droplet Coalescence and Breakage in Reactive Liquid-Liquid Extraction

85 pages, 39 figures, 6 tables, 0 appendix

Examiners: Professor Tuomas Koiranen
M. Sc. Jussi Tamminen

Keywords: coalescence, breakage, reactive extraction, liquid-liquid system, mass transfer, kinetic extraction, binary droplet system

Literature survey on droplet coalescence and droplet breakage is presented in this study. Coalescence experiments were performed in a binary droplet system, in addition to single droplet kinetic extraction experiments. Droplet coalescence was simulated with COMSOL Multiphysics modelling software using the level-set method, and comparison of modelling and experimental results was performed. Image and video analysis program developed in MATLAB 2016a was used to analyse the obtained results. The program measures and calculates various droplet parameters such as droplet volumes, droplet concentrations and surface areas, among others. Droplet coalescence times, rest times, and formation times were measured manually from the recorded videos. Droplet rest times were compared for two different binary droplet systems: 20 volume percent Acorga M5640 in Exxsol D80 dispersed in 0.16 M $(NH_4)_2SO_4$ and in 0.16 M $CuSO_4$, respectively. Former droplet rest time distribution was normally distributed, while the latter was normally distributed only when droplet rest times above 0.3 seconds were excluded from the results. The droplet rest time was reduced significantly when copper complex formation was taking place in the system: from average of 9.41 seconds with the continuous phase of 0.16 M $(NH_4)_2SO_4$ to only 0.11 seconds with the 0.16 M $CuSO_4$. This was attributed to the formation of surface tension gradients caused by Marangoni effects. Droplet concentration analysis revealed both the sessile and pendant droplet concentrations just before the coalescence, and the concentrations of combined droplets after the coalescence. Concentrations of sessile and pendant droplets corresponded reasonably well with all phase combinations, while concentrations of combined droplets were lower than expected when compared to sessile and pendant droplet concentrations. Concentration difference analysis did not reveal enhanced mass transfer during a coalescence event within the detection limits of the used image analysis method. Single droplet kinetic extraction experiments were performed in order to determine the mass transfer rate of copper complex from the continuous phase into the dispersed phase as a function of time and to get a point of reference to the mass transfer rate in the coalescence experiments.

TIIVISTELMÄ

Lappeenranta University of Technology
Teknillinen tiedekunta
LUT Kemiantekniikka / Prosessitekniikan laboratorio

Rasmus Peltola

Pisaran yhtyminen ja hajoaminen reaktiivisessa uutossa

85 sivua, 39 kuvaa, 5 taulukkoa, 0 liitettä

Tarkastajat: Professori Tuomas Koiranen
DI Jussi Tamminen

Hakusanat: yhtyminen, hajoaminen, reaktiivinen uutto, neste-neste uutto, aineensiirto, kinetiikka, kahden pisaran systeemi

Tässä työssä esitetään kirjallisuuskatsaus pisaran yhtymiseen ja hajoamiseen liittyen. Kokeelliseen osioon sisältyy kahden pisaran yhtymiskokeet sekä yhdellä pisaralla suoritetut kinetiikkakokeet. Pisaran yhtyminen simuloitiin COMSOL-ohjelmalla käyttäen Level-Set-menetelmää, ja saatuja tuloksia vertailtiin kokeellisiin tuloksiin. MATLAB-ohjelmalla kehitettyä kuva- ja videoanalyysimenetelmää sovellettiin saatujen kokeellisten tulosten analysoimiseen. Analyysiohjelma mittaa ja laskee lukuisia pisaraparametreja, kuten pisaratilavuuksia, pisarakonsentraatioita ja pinta-aloja. Pisaran yhtymisajat, lepoajat ja muodostumisajat määritettiin suoraan videoista. Pisaran lepoaikoja vertailtiin käyttäen kahta erilaista kemiallista systeemiä. Molemmissa oli dispergoituneena faasina 20 tilavuusprosenttinen Acorga M5640 liuos Exxsol D80 öljyyn laimennettuna, ja jatkuvana vesifaasina oli 0.16 molaarinen ammoniumsulfaatti sekä 0.16 molaarinen kuparisulfaatti. Ammoniumsulfaattia käytettäessä lepoajat olivat normaalijakautuneita, mutta kun vesifaasiksi vaihdettiin kuparisulfaatti, lepoajat noudattivat normaalijakaumaa ainoastaan jos yli 0.3 sekuntia kestävät lepoajat poistettiin tuloksista. Lepoajat lyhenivät huomattavasti kun systeemissä muodostui kuparikompleksia: keskimääräinen 9.41 sekunnin lepoaika ammoniumsulfaattia käytettäessä lyheni vain 0.11 sekunnin keskimääräiseen lepoaikaan kun jatkuvaksi faasiksi vaihdettiin kuparisulfaatti. Tämän oletettiin johtuvan pisaroihin muodostuvista pintajännitysgradienteista, jotka aiheutuvat niin sanotusta Marangoni-ilmiöstä. Pisarakonsentraatioanalyysilla saatiin selvitettyä molempien yhdistyvien pisaroiden konsentraatiot juuri ennen yhtymistä, sekä yhdistyneiden pisaroiden konsentraation juuri yhtymisen jälkeen. Pisarakonsentraatiot ennen yhtymistä olivat lähes saman suuruisia kaikissa koesarjoissa, mutta yhdistyneiden pisaroiden konsentraatiot olivat oletettua pienempiä kun niistä verrattiin konsentraatioihin ennen yhtymistä. Konsentraatioeroanalyysi osoitti, ettei aineensiirto tehostu pisaran yhtymisen aikana käytetyn kuva-analyysiohjelman mittaustarkkuuden puitteissa. Yhden pisaran kinetiikkakokeet suoritettiin, jotta kuparikompleksin aineensiirtoa jatkuvasta vesifaasista dispergoituneeseen orgaaniseen faasiin voitiin tutkia ajan funktiona. Lisäksi saatiin vertailukohta aineensiirtoon yhtymiskokeissa.

LIST OF SYMBOLS AND ABBREVIATIONS

A	Absorbance	AU
c	Concentration of a droplet	$\mathrm{mmol/dm^3}$
Δc	Concentration difference	$\mathrm{mmol/dm^3}$
d	Droplet diameter	cm
G	Shear strain rate	$\mathrm{s^{-1}}$
L	Optical path length	mm
l	Chord length	mm
n	Amount of copper in droplet	mmol
R	Droplet radius	cm
t_c	Required contact time for coalescence to occur	s
t_d	Required time to reach critical film thickness	s
V	Droplet Volume	µL

Dimensionless Numbers

Bo	Bond number, describes relevance of body forces (buoyancy) to interfacial tension forces.
Ca	Capillary number, describes the ratio of viscous stress that deforms the drop, and that of restoring stress induced by interfacial tension of a drop.
N_{coa}	Number of coalescence events, used in calculation of coalescence efficiency.
N_i	Number of droplet interactions, used in calculation of coalescence efficiency.
We	Weber number, describes relation of inertia to surface tension.

Greek Letters

λ	Viscosity ratio (η_d/η_c)	-
γ_{d_1,d_2}	Coalescence efficiency for droplets d_1 and d_2	-
ε	Molar absorptivity	$\frac{\mathrm{L}}{\mathrm{mmol\,mm}}$

φ	Droplet radius ratio	-
σ	Interfacial tension	$\mathrm{N/m}$
η	Viscosity	mPa s

Subscripts

0	Initial
ch	Chord
coa	Coalescence
co	Combined
crit	Critical
d	Droplet
eq	Equivalent
i	Interaction
p	Pendant
pi	Pixel position
s	Sessile

Abbreviations

CFD	Computational Fluid Dynamics
CMC	Critical Micelle Concentration
DSD	Droplet Size Distribution
EFCE	European Federation of Chemical Engineers
LED	Light Emitting Diode
LIX	Liquid Ion Exchanger
OBR	Oscillatory Baffled Reactor
PDDC	Pulsed Disc and Doughnut Column
PLIC	Piecewise Linear Interface Calculation
SLIC	Simple Linear Interface Calculation
VOF	Volume of Fluids

1 INTRODUCTION

In liquid-liquid systems one fluid is immersed in an ambient phase. For example, industrial oil droplets are frequently found in the form of water-oil emulsions and involve both coalescence and breakage of droplets (Ata *et al.*, 2010, Eow and Ghadiri, 2003; Urdahl *et al.*, 2001). In addition to petrochemical manufacture, liquid-liquid systems are found in a broad variety of industrial processes, such as in environmental treatment operations, pharmaceutical industry, wastewater treatment, hydrometallurgy, distillation, nuclear industry, and various other chemical industries (Gebauer *et al.*, 2015; Villwock *et al.*, 2014; Wegener *et al.*, 2013).

Although there has been a significant amount of research on the subject over the years, most results found in literature are dependent on the used reagents and experimental conditions. Subsequently, it has been a difficult task for researchers to create reliable mathematical expressions for droplet coalescence and breakage as the effect of all the influencing variables are not completely understood. Additionally, mass transfer and absorption of surfactants or contaminants may also strongly affect these processes. According to Bothe and Fleckenstein (2013), any detailed mathematical models describing mass transfer are not able to provide exact analytical solutions since the involved flow patterns are highly complex. However, by considering the overall process as an interaction of single droplets, which is the smallest unit of liquid-liquid extraction, the number of influencing factors can be diminished and experimental investigation becomes more straight forward.

Mass transfer coefficients, extraction kinetics and droplet coalescence times, among others, can be determined in binary droplet systems and then applied to liquid-liquid systems of larger scale. In this thesis, single droplet extraction kinetics and binary droplet coalescence are experimentally studied. Literature survey on binary droplet coalescence and droplet breakage is presented, and mass transfer between these two related phenomena is investigated.

2 LIQUID-LIQUID EXTRACTION

Often separation of the phases and extraction of specific transfer components is necessary in order to obtain required level of purification or concentration of a product. According to Bart (2001) liquid-liquid extraction has been utilized on industrial scale since end of 19th century. First patent concerning a liquid-liquid extraction column was published in Germany, and since solvent extraction has been applied e. g. in uranium ore processing during 2nd World War and in hydroxyoxime type extractants used for copper selective extraction in 1960s. The main applications today concern separation and purification processes, enrichment processes and conversion of salts. Separation can be enhanced by dissolving a suitable component within a solvent. Purpose of this is to promote selectivity or separation efficiency, and the term reactive liquid-liquid extraction (or just reactive extraction) is typically used to describe the method. According to Bart (2001), major applications for reactive extraction are related to hydrometallurgy, chemical and biochemical industry, and environmental engineering.

Liquid-liquid systems include coalescence and breakage of droplets, mass transfer of components and adsorption of surfactants or contaminants. Especially the coalescence process has not been completely understood. One should also consider fluid dynamics in design of liquid-liquid systems, and interactions between these different phenomena create additional complexity. In order to tackle this problem, liquid-liquid system can be reduced into a binary droplet system, where only one droplet is moving in an ambient continuous phase. Even for a single droplet system there are usually no models that are based on analytical equations, so computational methods such as CFD has to be applied. In most cases, best results are obtained by careful combination of experimental research, numerical calculations and empirical models according to Wegener *et al.* (2014).

3 DROPLET-DROPLET COALESCENCE

3.1 Mechanism of Droplet Coalescence

Understanding the interaction between two droplets in a liquid-liquid system is of quintessential importance since it is the smallest transfer unit in liquid-liquid extraction operations. The droplet size distribution (DSD) of a system is affected by droplet coalescence together with droplet breakup and mass transfer. It has been demonstrated by numerous researchers that coalescence process occurs when two drops collide with each other and an interfacial film between the drops is formed. The drops are then deformed and the film between interfaces of the two drops takes a lenticular shape. Consequently, a so-called dimple is formed in the center of the continuous phase, while in the periphery the droplet interfaces are closer to each other (Klaseboer *et al*., 2000). Eiswirth (2014) estimated that this outer ring of the dimple accounts only for about maximum of 5 % of the total contact area. In this area the droplet surfaces are close enough to each other so that attractive as well as repulsive forces are able to interact. As the interfacial film drains to a certain thickness called the critical film thickness, it ruptures and coalescence occurs. At the critical film thickness any disturbance or instability will result into the rupture of the film. A liquid bridge is formed between the droplets, creating a new coalesced droplet. This is called the film drainage model. The solved form of the film drainage model for two droplets d_1 and d_2 as formulated by Coulaloglou and Tavlarides (1977) is the following:

$$\gamma_{d_1,d_2} = \exp(-\frac{t_d}{t_c}) \tag{1}$$

where t_c is the contact time required for the coalescence to occur and t_d is the time required to reach the critical film thickness for droplets d_1 and d_2. Coulaloglou and Tavlarides (1977) described coalescence probability based on the equivalent droplet diameter:

$$\gamma = \exp(-c_1 * d_{eq}^4) \tag{2}$$

where c_1 is an adjustable parameter and d_{eq} is the equivalent droplet diameter of droplets d_1 and d_2 ($d_{eq} = 2\frac{d_1 * d_2}{d_1 + d_2}$ where d_1 and d_2 are droplet diameters).

Coalescence efficiency of two colliding droplets at value interval of [0, 1] can be described in the following way:

$$\gamma_{d_1,d_2} = \frac{N_c}{N_i} \tag{3}$$

where N_c is the number of coalescence events and N_i is the number of droplet interactions (i. e. colliding droplet pairs).

The equations mentioned above form the basis for all film drainage models, some of which may be much more elaborated. They are mainly used to describe the propensity of droplets to coalescence in agitated liquid-liquid dispersions involving continuous coalescence and breakage of multiple droplets. The major differences between various models concern usually properties of phase interfaces and affect the computation of film drainage time. The drainage time may increase or decrease depending on the surface properties of droplets (e. g. droplet shape and size, deformability of the surface and characteristics of the interfacial area). According to an estimate made by Eiswirth (2014), a typical interaction time of a binary droplet collision in a standard toluene/acetone/water system recommended by the European Federation of Chemical Engineers (EFCE) lasts roughly 40 ms, and is affected by the system conditions. He noticed that coalescence time is generally about half of the total contact time of the droplets, the coalescence event typically being around 20 ms. In the experimental work of this thesis similar results were obtained: the coalescence time was approximately 23 ms in all of the performed coalescence experiments. However, the film drainage time, i. e. the contact time of the droplets before coalescence occurs, was drastically affected by the phase properties and is discussed in more detail in Section 9.3.

Binary droplet coalescence of two toluene drops in continuous water phase is illustrated in Fig. 1.

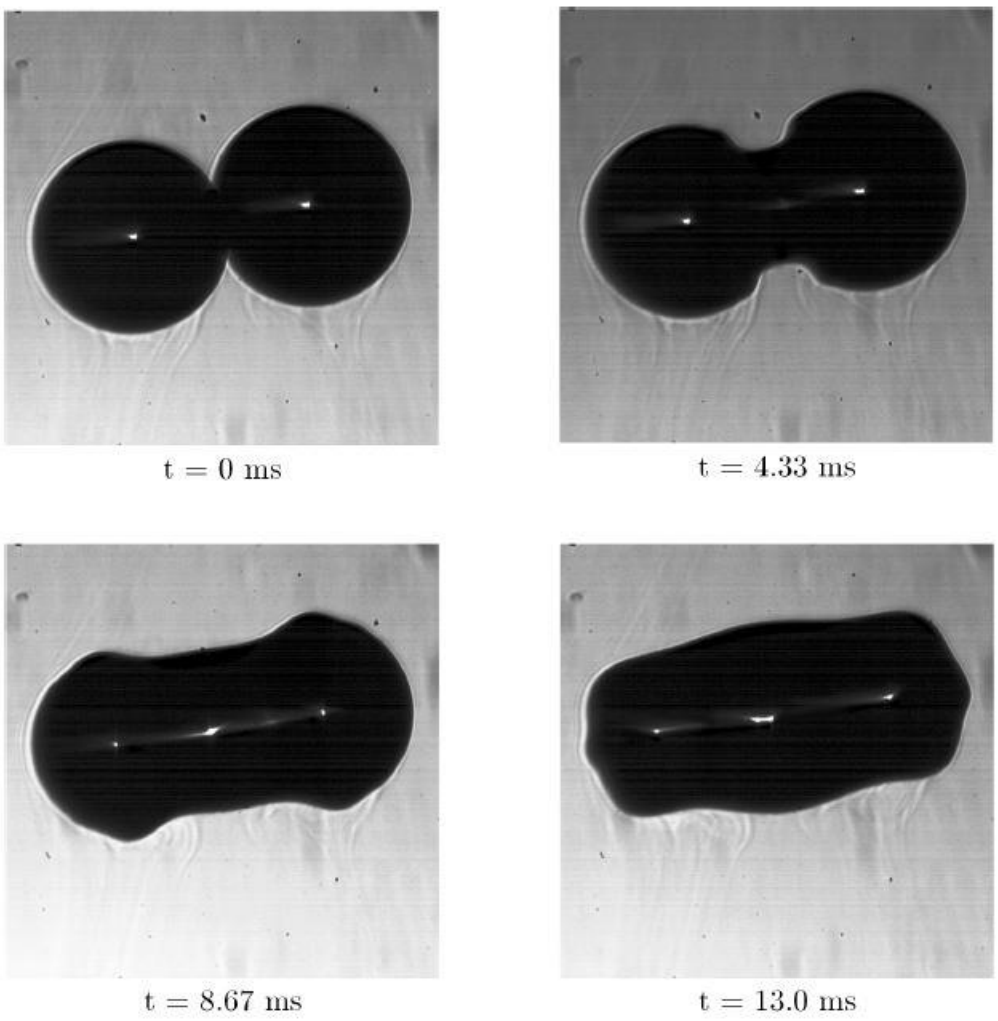

Figure 1. Binary droplet coalescence of two toluene droplets dispersed in continuous water phase captured with a digital camera by Eiswirth (2014).

Eiswirth *et al.* (2012a) observed that when there is a difference in droplet sizes in a binary droplet system, the internal energy of the smaller droplet is higher than that of the larger droplet due to higher internal pressure. When the film ruptures in a coalescence event, the fluid from the smaller droplet migrates to the larger droplet due to pressure gradient between the droplets. They noticed a vortex forming as the fluid was transferring from the smaller droplet.

In addition to the above described film drainage theory, a critical velocity model (Lehr *et al.*, 2002; Lehr and Mewes, 1999) and an energy model (Howarth, 1964; Sovova, 1981) have been developed. The critical velocity model is based on the

empirical assumption that the crucial factor in coalescence efficiency is the approach velocity of drops towards each other. Experimental results suggesting the phenomena were first obtained by Doubliez (1991) and later by Duineveld (1994). On the other hand, the energy model assumes that rather than the relatively weak attraction forces at the droplet interface, the collision impact of droplets determines whether or not coalescence occurs. In this model the energetic collisions between the droplets at certain critical velocities are solely responsible for coalescence event and film thinning is not taken into account. The film drainage model and energy model are considered as physical coalescence models, while the critical velocity model is considered an empirical model.

Different kind of coalescence models are categorized in Fig. 2 as suggested by Liao and Lucas (2010).

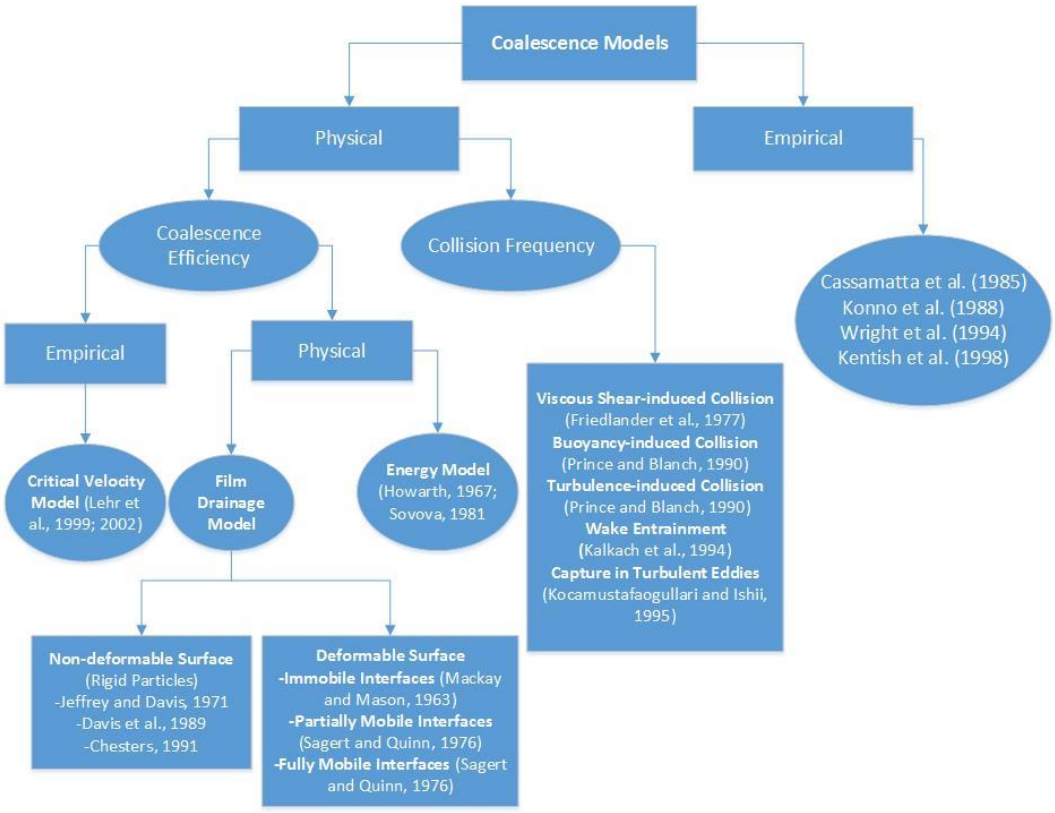

Figure 2. Classification of coalescence models based on the classification presented by Liao and Lucas (2010).

3.2 Influencing Parameters

Coalescence processes may be influenced by several factors. These include the contact time of the drops, the time of film drainage and the critical film thickness. These parameters in turn depend on the properties of the droplets (e. g. DSD), the physical properties of the phases (such as fluid viscosity and density), and other properties of the system. Usually the time of film drainage is controlling factor in coalescence processes. According to Rommel *et al*. (1992), the rate of film thinning is affected by external pressure and may be hindered by Marangoni effects (see Section 3.2.4) when there are surfactants present in the system.

3.2.1 Droplet Size

Eiswirth (2014) studied the effect droplet diameter on terminal velocity of droplets in his dissertation. It was observed that droplets with a diameter up to 2.5 mm maintained their spherical shape, while droplets above the value started to deform gradually into more and more ellipsoidal shape. Eiswirth (2014) demonstrated in his experiments that for small droplets (diameter below 0.2 mm) internal circulation did not affect the terminal velocity remarkably. However, when droplet diameter was increased up to 1.5 mm, the internal circulation assumed a more significant role in incrementing the terminal velocity of droplets. As the droplet shape started to deform to an ellipsoidal one at larger diameters, the terminal velocity began to decrement again due to increased drag coefficient.

In a binary droplet system one should also consider the radius ratio of colliding droplets. According to Eiswirth (2014) droplets do not mix effectively when the radius ratio of the two droplets is close to one. In this case the boundary between the drops remains rather stable due to symmetrical droplet interaction. The deformation of the coalesced droplet is identical on both sides of the drop, leading to forces that tend to counter-balance each other. Consequently, the pressure gradient across the droplet axis is small, resulting also in negligible velocity variations within the drop, meaning that the velocity gradient is very low. On the other hand, when the radius ratio differs clearly from the value of one, a vigorous internal mixing of coalesced droplet can be observed. As the pressure inside the smaller droplet tends to be higher compared to that in a larger droplet, the internal energy in the smaller droplet is also high. Eiswirth (2014) noticed in his coalescence

experiments that the droplet interface transforms asymmetrically when there is a radius difference between the droplets. At around 12 ms after the start of coalescence event the larger droplet minimizes its surface energy by rapidly devouring fluid from the smaller droplet inside. The rapid circulation inside the droplet and following deformation of the interface at approximately 15 ms give rise to an impulse that pushes the remaining fluid from the smaller droplet into the larger droplet. In the experimental work performed in this thesis the radius ratio of colliding droplets was approximately one in all coalescence experiments, and no significant differences in the internal circulation of the droplets could be observed during a coalescence event.

A coalescence event with droplet radius ratio of $\varphi = 0.98$ is illustrated in Fig. 3.

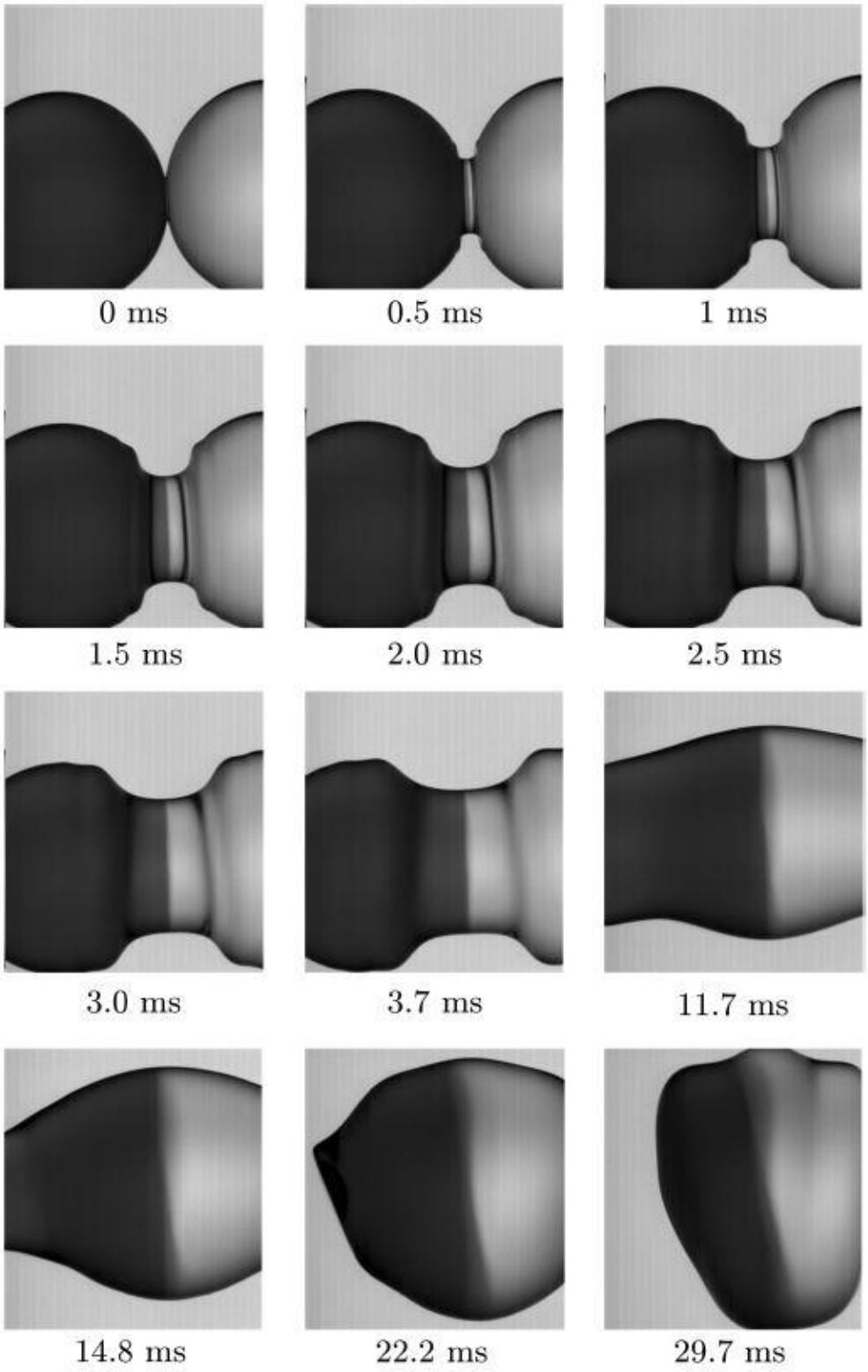

Figure 3. Binary droplet coalescence event with droplet radius ratio of φ = 0.98 as experimentally demonstrated by Eiswirth (2014). Toluene droplets were dispersed in continuous water phase, and Disperse Blue

14 C. I. 61500 dye, which is only soluble in the organic phase, was used to colorize the toluene of the other droplet.

A coalescence event with droplet radius ratio of $\varphi = 0.69$ is illustrated in Fig. 4.

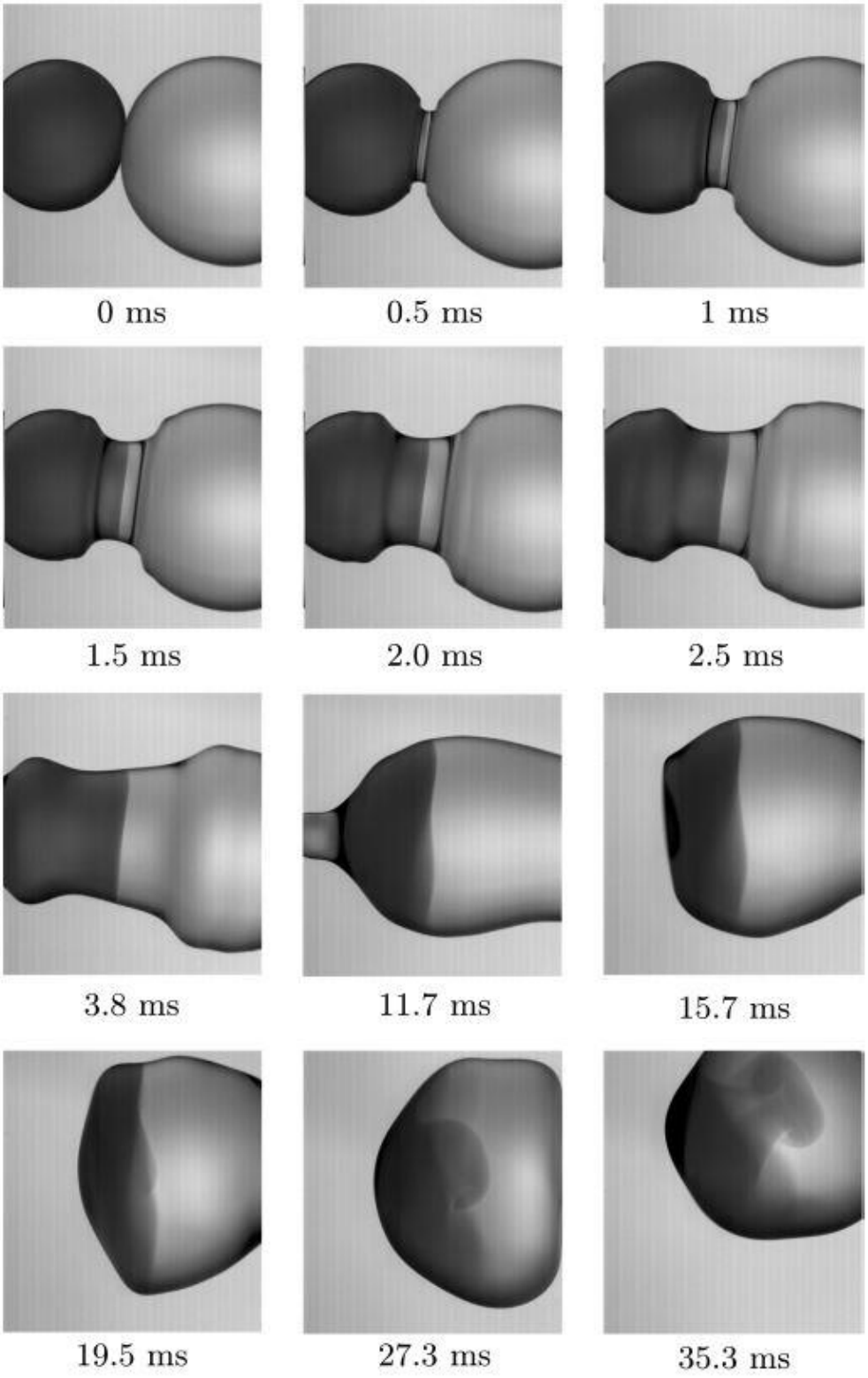

Figure 4. Binary droplet coalescence event with droplet radius ratio of φ = 0.69 as experimentally demonstrated by Eiswirth (2014). Toluene droplets were dispersed in continuous water phase, and Disperse Blue 14 C. I. 61500 dye, which is only soluble in the organic phase, was used to colorize the toluene of the other droplet.

3.2.2 Addition of Surfactant and Salt

Adsorption of surfactants may have multitude of substantial effects on liquid-liquid systems including alternation of physicochemical attributes, blocking of droplet's interface and inhibiting the interface movement during droplet formation, reduction of droplet's internal circulation, and reduction of interfacial tension. Wegener and Paschedag (2011) found out that when using Triton-X 100 as surfactant, even minimal surfactant concentration may result in considerable decrease in droplet rise velocity. They also observed that the smaller the droplet surface is, the faster its surface is occupied by the surfactant. Surfactants also dampen velocity variations of droplets and as the surfactant concentration is increased, the maximum velocity of droplets occurs at higher droplet sizes. Mitra and Ghosh used both anionic surfactant (sodium dodecyl benzene sulfonate, SDBS) and cationic surfactant (cetyl trimethyl ammonium bromide, CTAB) in their binary droplet coalescence experiments. It was observed that the total interaction time of droplets was increased from 0.8 seconds with the lowest surfactant concentrations (0.001 mM) up to 25 seconds with highest surfactant concentrations (0.14 mM). In the experimental work of this thesis similar result was obtained in a binary droplet system when salt concentration of 0.16 M $(NH_4)_2SO_4$ was used in the continuous phase. The highest interaction time was around 26 seconds, while the average value was about 9.4 seconds. The effect of coalescence on the surfactant distribution on the droplet surface is illustrated in Fig. 5.

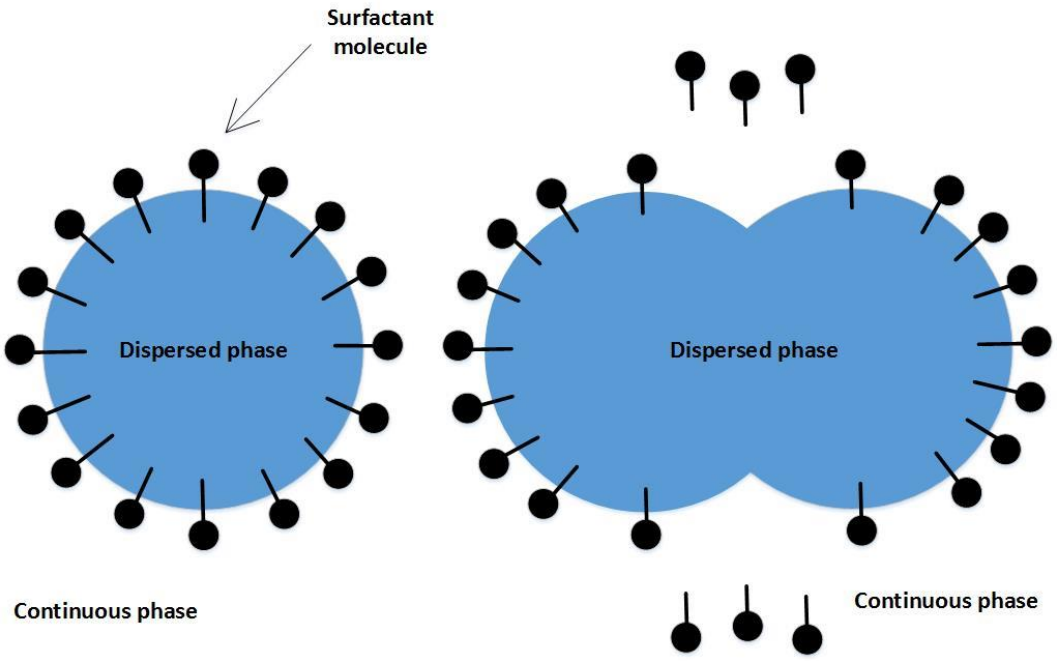

Figure 5. Illustration of surfactant molecule absorption and rearrangement of the molecules during droplet coalescence based on the schematic diagram of Wang *et al.* (2014). Surfactant is absorbed homogeneously from the continuous water phase onto the surface of oil droplet at low concentrations (left side picture). As the surface is elongated and the saturated adsorption is reached, the excess molecules in the bulk diffuse to the depleted region (right side picture), weakening the Marangoni effect (i. e. interfacial tension gradients).

Mitra and Ghosh (2007) among others have studied the effect of salt addition on the coalescence process. Results indicated that with small concentrations of salt (e. g. 0.1 M of NaCl), there was an increment in coalescence time. As the concentration of NaCl was gradually increased, the coalescence time started to decrease until it was lower than in the absence of the salt at 1 M of NaCl. It was observed that salt addition reduced interfacial tension of the droplets, meanwhile the surface excess (concentration of the salt at the droplet interface) was increased. It was assumed that the salt addition diminished repulsive forces at droplet interface, gradually enhancing droplet coalescence. Stevens *et al.* (1990) investigated the effect of adding ionizing salt in the continuous phase. They found out that the salt increased coalescence time when dispersed phase consisted of polar organic liquids, e. g.

butyl acetate. In contrast, when dispersed phase consisted of nonpolar droplets, e. g. heptane, the coalescence time remained unchanged. Stevens *et al.* (1990) came into the conclusion that increased viscosity of the interfaces could be the main reason behind this phenomenon. Eiswirth (2014) observed in his experiments that when adding 1 $mmol/dm^3$ of sodium sulfate to aqueous phase saturated with toluene, the coalescence probability was higher than in the absence of the salt. Also, the coalescence probability was decreasing as the pH of the continuous phase was increased. Maximum coalescence probability of 63 % was obtained at a pH of 5. In general, highest coalescence probability for all systems in his experiments (with or without salt addition) was obtained between the pH values of 4.5 – 5.5.

3.2.3 Droplet Interface Mobility

Many researchers emphasize the importance of system purity in coalescence processes. It has been demonstrated that even negligible concentrations of impurities may alter the coalescence behavior significantly (Wegener *et al*., 2009). This can be observed by the mobility of droplet interface. Entirely mobile interface indicates that the system is completely impurity free, and has no molecules that are active at the interface (such as surfactants). In this case the droplet has full internal circulation and can obtain the maximum terminal velocity in a specific system. For a slightly contaminated system (for example in the case of salt or surfactant addition), the interface is only partly mobile. This leads to a decrease in internal circulation and in reduction of the terminal velocity. In a strongly contaminated systems the interface is fully immobilized. For example, a high concentration of surfactants that entirely saturate the droplet interface may completely immobilize the droplet surface. In this case the surface can be considered as rigid, implying that the maximum terminal velocity that can be reached is similar to that of a rigid sphere. According to Wegener *et al.* (2013), the terminal velocity is also affected by the shape of droplet interface. They discussed the following three categories: 1) in spherical regime the terminal velocity increases with incremented drop diameter; 2) in transition regime deformation takes place and droplets assume an increasingly oblate shape, while the terminal velocity reaches a maximum at certain point after which it starts to decrease as the droplet diameter is increased; 3) in oscillatory regime the terminal velocity decreases to a certain extent as the drop diameter is

increased, and the droplets may oscillate as the shape assumes more and more irregular form. The effect of droplet interface mobility on droplet velocity profile is illustrated in Fig. 6 as presented by Wegener *et al.,* (2013).

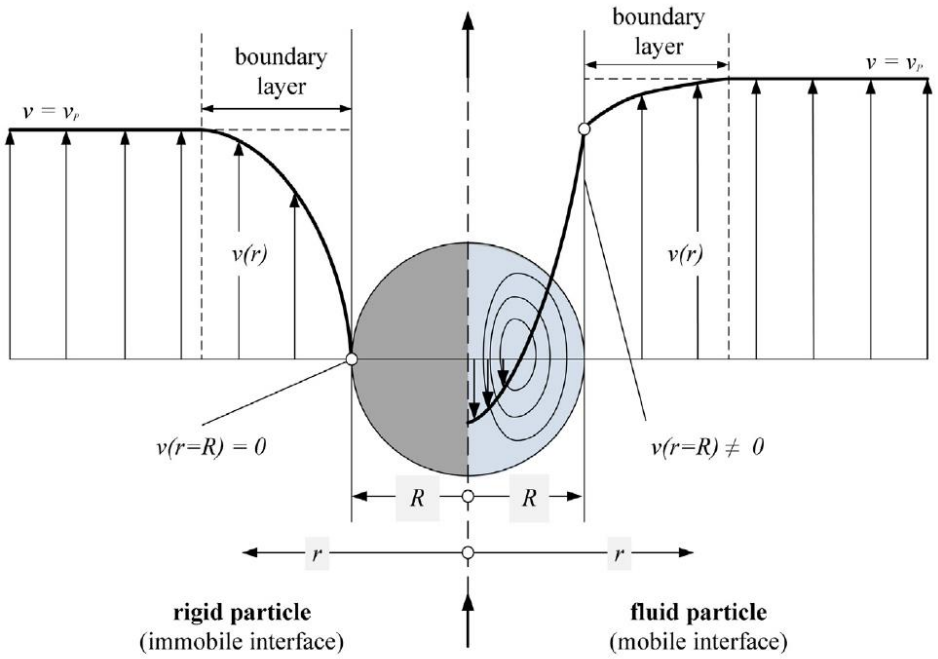

Figure 6. Velocity profile inside and at proximity of a spherical rigid droplet (left side) and spherical droplet with fully mobile interface (right side) as illustrated by Wegener *et al.* (2014). R is droplet radius and v_P is velocity of droplet.

3.2.4 Mass Transfer

Ban *et al.* (2000) and Chevaillier *et al.* (2006) among others have investigated the effect of mass transfer in a binary droplet system. In a standard toluene/acetone/water system it has been observed that with mass transfer direction from continuous phase to dispersed phase the film drainage time is increased and coalescence is hindered, while with inverted mass transfer direction from dispersed to continuous phase the drainage time is reduced and coalescence is accelerated (Ban *et al.*, 2000). Similar observations have been made also on systems with different mass transfer components. Kopriwa *et al.* (2012) contributed this phenomenon to changes in film drainage due to surface tension gradients and

miscibility variations of phases caused by the presence of a solute. Experimental studies by Kamp and Kraume (2014) suggests that mass transfer of dispersed acetone droplets to continuous water phase results in coalescence at practically 100 % probability, while with inverted mass transfer direction the coalescence probability is reduced to practically 0 %. This is contributed to the increase in film drainage time, which becomes higher than the total contact time of drops in the case of mass transfer from continuous to dispersed phase. The results also suggest that this phenomenon is not dependent on the droplet sizes or the relative velocities of the droplets. The effect of mass transfer direction is illustrated in Fig. 7.

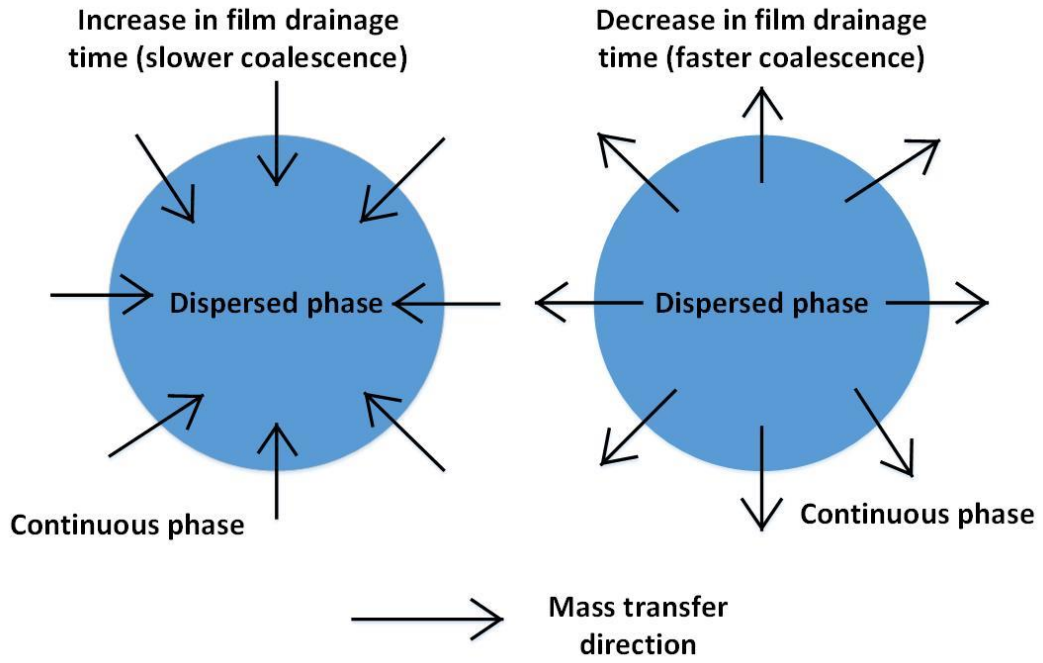

Figure 7. The effect of mass transfer direction on film drainage time and speed of coalescence based on the work of Ban *et al.* (2000), Chevaillier *et al.* (2006) and Kamp and Kraume (2014).

Eiswirth (2014) discovered a formation of micro-droplets consisting of continuous phase in a case with mass transfer from disperse to continuous phase. The continuous phase becomes entrapped between the droplet interfaces and thus will not migrate from the droplets instantly. He speculated that this phenomenon might affect real-life liquid-liquid extraction processes because part of the continuous phase is abducted into the dispersed phase. Eiswirth (2014) noted that when adding even small amounts of acetone in the dispersed phase, the coalescence probability

becomes higher compared to a system without a transfer component. He observed that the probability of coalescence event is 100 % for all acetone concentrations with the pH of 3, and even at pH of 11 and acetone concentration of 1 wt % the coalescence probability was still 90 %. When pH was adjusted to 6, the same acetone concentration was sufficient to raise the coalescence probability back to 100 %. At the same conditions but without a mass transfer component, the probability was reduced to 48 %. Contrary results were obtained when mass transfer direction was reversed from continuous to dispersed phase. Coalescence probability was reduced only to 10 % with acetone concentration of 0.05 wt %, suggesting that even negligible concentrations of mass transfer components are able to strongly hinder the coalescence process in this mass transfer direction.

The representation of mass transfer on two horizontally arranged droplets during coalescence event as suggested by Ban *et al.* (2000) is presented in Fig. 8.

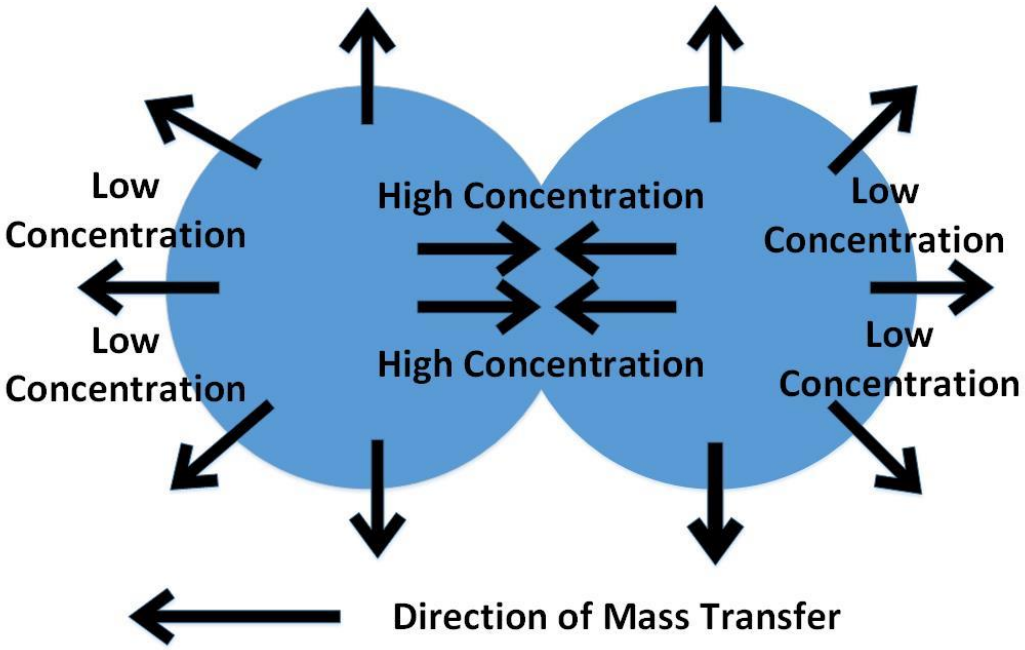

Figure 8. The effect of mass transfer during binary droplet coalescence based on the illustration by Ban *et al.* (2000).

As the concentration of the solute is increased in the droplet, the interfacial tension of the droplet is decreased. The differences in concentration leads to differences in

interfacial tension, which in turn results in promoted droplet coalescence. The interfacial tension gradients caused by the mass transfer as suggested by Ban *et al.* (2000) are presented in Fig. 9.

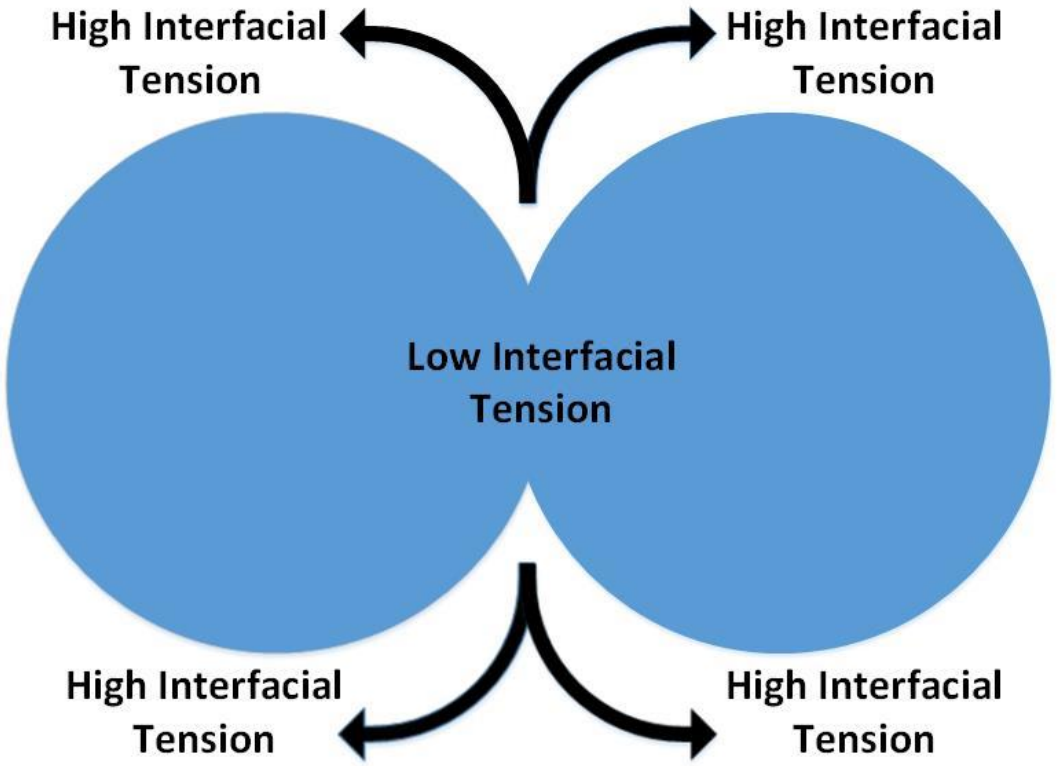

Figure 9. The effect of mass transfer on interfacial tension of the droplets based on the illustration by Ban *et al.* (2000).

In literature, these effects are referred to usually as Marangoni effects. According to COMSOL encyclopedia, the Marangoni effects can be divided in the two separate cases depending on the driving force: in solutocapillary effect the surface tension gradient is driven by the changes in concentration, and in thermocapillary effect the surface tension gradient is dependent on the temperature. Both of these effects can take place simultaneously.

Single droplet coalescence process with and without mass transfer is illustrated in Fig. 10 as suggested by Wegener *et al.* (2014).

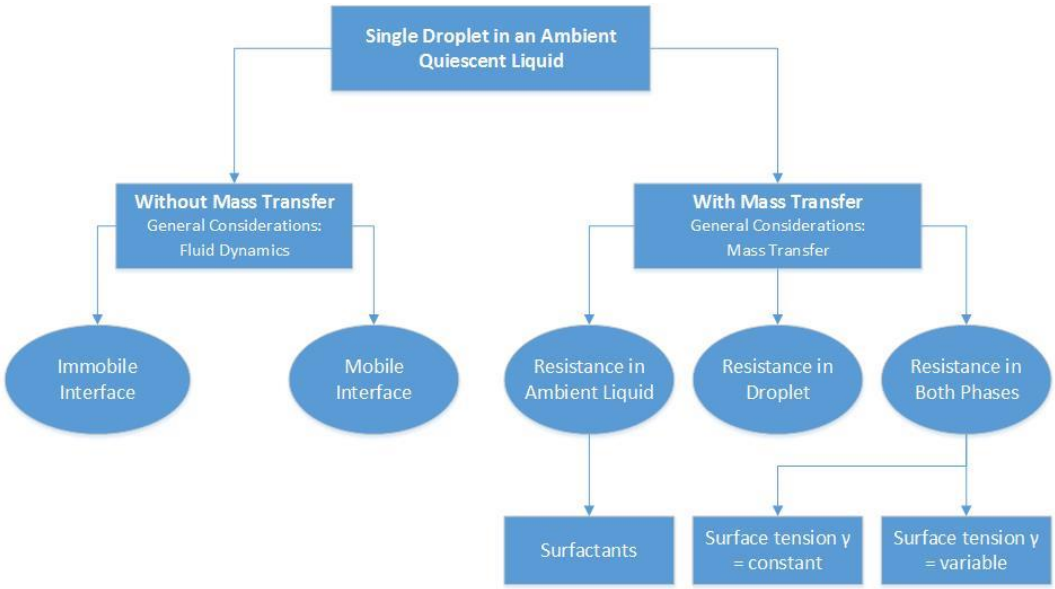

Figure 10. Single droplet coalescence with and without mass transfer in an ambient quiescent liquid with the general considerations to be taken into account. Figure is based on classification by Wegener *et al.* (2014).

3.2.5 Collision Frequency Parameters

The effect of collision frequency on droplet coalescence has been extensively researched over the years (Colella *et al.*, 1999; Chesters, 1991; Hikibi *et al.*, 2001; Kalkach *et al.*, 1994; Kocamustafaogullari and Ishii, 1990; Lehr *et al.*, 2002; Prince and Blanch, 1990; Wang *et al.*, 2005; Wu *et al.* 1998). According to Liao and Lucas (2010) usually five parameters have been assumed to induce collisions between droplets in agitated liquid-liquid dispersions: 1) turbulence; 2) buoyancy; 3) viscous shear; 4) wake-entrainment and 5) capture in turbulent eddies.

From these parameters turbulence is considered to have the most significant impact on droplet collision frequency, while the other parameters are typically given little consideration or neglected. Turbulent movement of surrounding fluid induces droplet collisions, and according to Liao and Lucas (2010), the fluid particle behavior is usually assumed to be similar to the movement of gas molecules in classical kinetic gas theory. However, this assumption is not completely accurate since fluid particles differ in various aspects from gas particles (e. g. surface properties, collision elasticity). The theory assumes that the effective volume swept

by randomly floating particles per unit time can be used to predict the collision frequency of droplets. In this model the relative velocity of two colliding droplets is a crucial parameter since it is included in all equations. According to Coulaloglou and Tavlarides (1977), the colliding droplets have velocity similar to an equally sized eddy.

The buoyancy induced collisions differ from the turbulent collisions in the aspect that relative velocities are calculated based on the rise velocities, which are in turn caused by the buoyant forces of fluid particles according to Prince and Blanch (1990).

The viscous shear induced collisions are caused by linearly moving particle flow (Friedlander, 1977). In other words, the fluid movement is assumed to be laminar and the particles in the uniform flow collide because of velocity gradients.

Wake-entrainment refers to a phenomenon where amount of liquid is accelerated in so-called wake region behind a freely rising bubble. It has been noted by various researchers that these wakes play an important role especially in bubble interaction (Komosawa *et al.,* 1980; Bilicki and Kestin, 1987; Stewart, 1995). The collisions caused by the wakes may result in coalescence if the surrounding fluid has suitable physical properties.

Finally, the capture in turbulent eddies refers to a mechanism where collision frequency is solely determined by local shear in turbulent eddies. This model assumes that DSD is significantly smaller that the size of eddies in the turbulent flow, suggesting that the velocities of droplets will be very close to that of continuous phase flows (Chesters, 1991). So far, it has been a difficult task for researchers to determine the cumulative effect of all the parameters described above. This usually results in various simplifications and assumptions that may or may not affect the reliability of coalescence models.

3.2.6 Electrochemical Effects

According to Mousavichoubeh *et al.* (2010), applying an electrical field to a coalescence process has significant impact on film thinning process, and may results in substantial shortening of the required coalescence time. The major drawback of electro-coalescence processes is the break-up and formation of fine sized secondary drops as a consequence of too strong electric field or the generation of too large drops (Aryafar and Kavehpour, 2009; Eow *et al.,* 2002; Eow and Ghadiri, 2003; Tsouris *et al.,* 1998). By using surfactants, the interfacial tension is reduced and the effect of electrical forces are intensified.

Zhang *et al.* (2012) observed that as the surfactant concentration is increased, droplets will be aligned in the maximum direction of the electric field and coalescence occurs at adjoining drops. This results in a chain-like structure that bridges the electrodes and leads to a significant increase in conductivity of fluid. As DSD increases, this configuration will be dismantled due to gravitational forces, resulting in decremented conductivity.

In general, droplet charges and ionic strengths can be described by DLVO-theory (named after its developers Deryaguin, Landau, Verwey and Overbeek). The theory describes electrostatic repulsion and van der Waals attraction forces of charged colloidal particles dispersed in a fluid phase. Tobin and Ramkrishna (1992) suggested that droplet charges are both pervasive and intrinsic in many aqueous mixtures, and consequently can affect coalescence processes. There have been numerous zeta potential measurements of organic droplets in a water phase, and the results suggest that droplets may carry significant negative charges. This is attributed usually to an increased adsorption of hydroxide ions onto droplet surface when the concentration of hydroxides is increased in continuous phase. This leads to an incremented surface potential of the droplets, stabilizing the system and preventing coalescence. It was also observed that charges vary with the pH of the water phase, and according to Reddy and Fogler (1980) the stability of an organic-in-water dispersion can be significantly increased by applying higher pH values.

Tobin and Ramkrishna (1992) demonstrated in their experiments that increased pH narrows the DSD, resulting in smaller drops. On the other hand, they noticed that higher ionic strength leads to an enhanced coalescence rate, especially for larger

droplets. This can be noticed from substantially spread DSD at high ionic strengths, suggesting that small drops are mostly left unaffected while larger drops continue to enlarge due to coalescence. The decremented repulsion between particles at the higher ionic strengths is attributed to the decrease of electrical double layer that surrounds every charged particle. Tobin and Ramkrishna (1992) concluded that as small drops remain relatively unaffected to electrostatic forces, there is some critical droplet size after which coalescence takes place unhindered. They also emphasized the importance of droplet size, as the larger droplets continue to coalescence more easily when the electrostatic forces are diminishing, while smaller droplets remain unchanged.

3.3 Experimental Setups

Based on the literature, experimental setups used for binary droplet coalescence can be divided into two categories: a static setup where two stagnant droplets are fixed on needles either horizontally or vertically, or a dynamic setup where at least one drop is freely moving relative to the other drop. A static setup is more commonly utilized in coalescence studies since experiments can be more easily implemented compared to dynamic setups, and it also offers better observability and droplets can be more easily adjusted. On the other hand, dynamic setups represent real-life dynamics more accurately, but they offer inferior observability and are more complex in design. As the different steps of coalescence process occur in a relatively short period of time (from milliseconds to seconds), high speed imaging is required in order to inspect coalescence phenomena. However, a high reproducibility of collisions between the droplets, in addition to moderately high repetition rate, is required in order to establish a data base that is statistically plausible. An experimental setup used by Eiswirth (2014) in his coalescence experiments with free rising droplets is illustrated in Fig. 11.

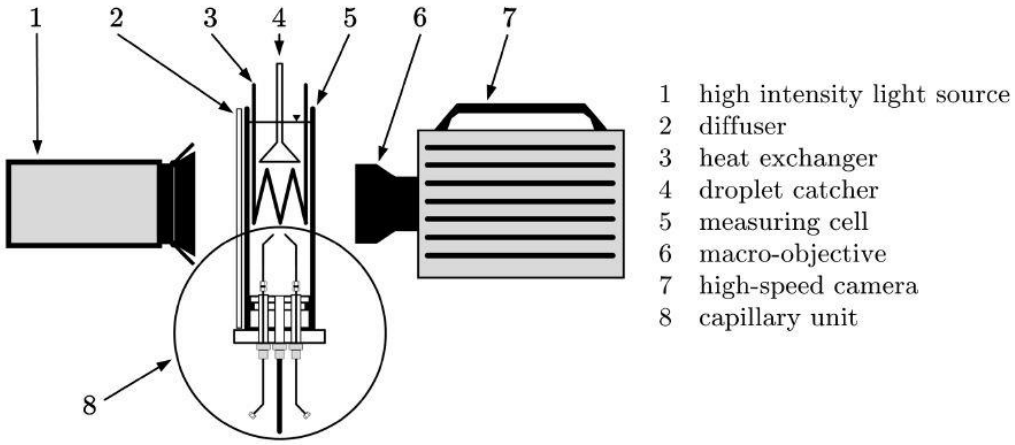

Figure 11. Small scale experimental setup for high speed investigations of rising droplets. Droplet shape, velocity and coalescence were measured with the setup (Eiswirth 2014).

An experimental setup first developed and described by Kamp and Kraume (2014) and later improved by Gebauer *et al.* (2016) is illustrated in Fig. 12.

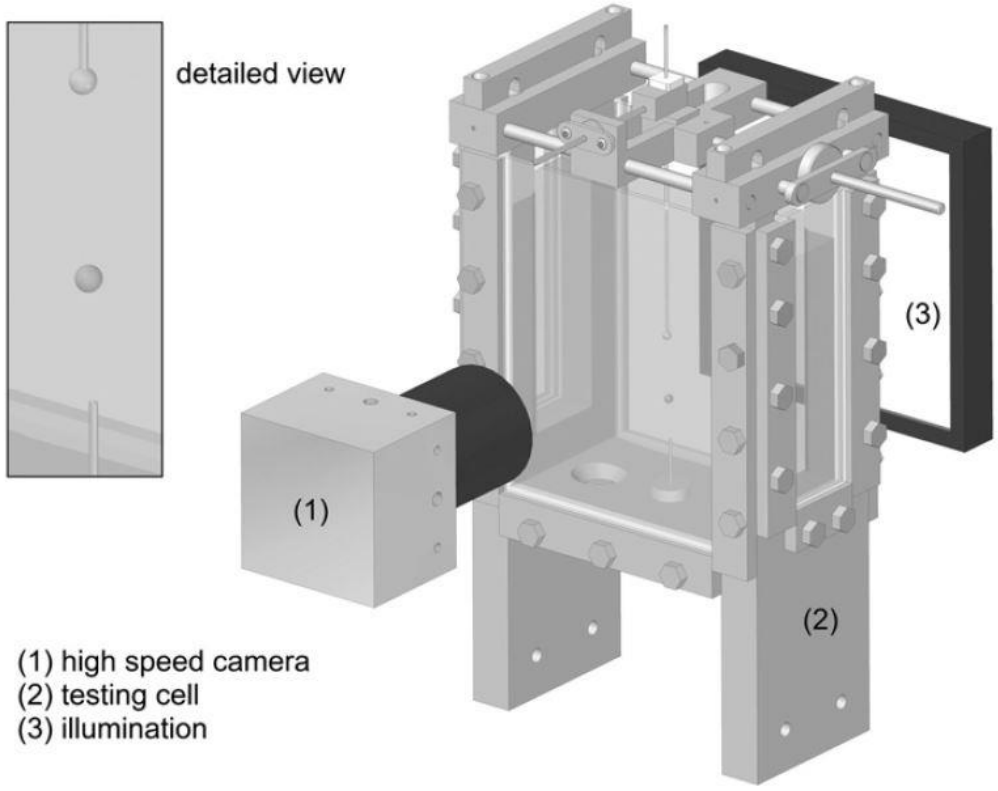

Figure 12. Experimental setup used in the investigation of free rising droplet and fixed pendant droplet dispersed in continuous water phase (Gebauer *et al.* (2016).

In Fig. 13 the setup used by Ata *et al.*, (2011) is presented.

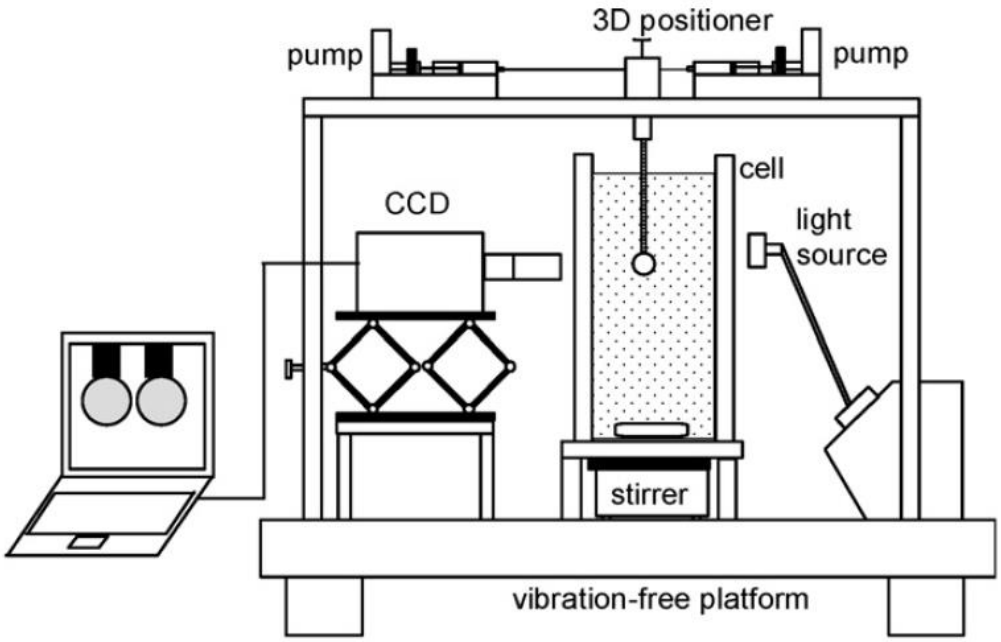

Figure 13. Experimental setup used by Ata *et al.* (2011) for the investigation of binary droplet coalescence of kerosene droplets dispersed in continuous water phase. Two programmable syringe pumps were used to pump the oil droplets and high speed video camera was used for image acquisition.

A method in which droplet coalescence is implemented by placing a droplet on a fluid interface and allowing it to coalesce with the bulk phase is called a droplet rest process. According to Mitra and Ghosh (2007) this setup has been applied in majority of experimental coalescence investigations. Gaitzsch *et al*. (2011) among others have utilized counter-flow cell in their coalescence experiments, offering realistic dynamic collisions of drops, but having the drawbacks of optical distortion and poor lateral motion of drops. In addition to the typical rising and pendant droplet collisions, also horizontally colliding drops have been investigated (Scheele and Leng, 1971). This setup requires either small density differences between continuous and dispersed phase or a high droplet velocity in order to avoid vertical drifting of droplets due to buoyancy. Thoroddsen *et al.* (2005b) noted that coalescence with at least one fixed droplet evolves slower compared to coalescence with freely moving drops. When a droplet is fixed on capillary, movability of its boundary becomes hindered and less surface energy is available to be released at coalescence event. If the setup allows for freely moving droplets, fluid from the

droplet transfers quickly from the bulk of droplet into the "neck region", i. e. to the region joining the two droplets together. The unhindered coalescence is accompanied by vigorous deformation of droplet surface. Kamp and Kraume (2014) designed a new test cell combining the benefits from various setups including dynamic droplet collisions with good observability, exact generation and variability of droplet sizes without changes in the setup, and variability of relative droplet velocities and continuous phase properties.

4 DROPLET BREAKAGE

4.1 The Mechanism of Droplet Breakage

The breakage of fluid droplets in immiscible continuous phase is of great importance for performance of numerous industrial devices and reactors that are based on efficient contact between the two liquid phases. According to Mignard *et al*. (2004), droplet breakage determines essential process parameters such as droplet size distributions, volume fractions and interfacial areas of dispersed phase. Consequently, it has a significant role in process design and optimization of numerous industrial processes including chemical reactions, liquid-liquid extraction, blending of polymers, emulsification and adsorption (Han *et al*., 2014).

According to Briscoe *et al*. (1999), an important parameter describing the breakup probability of a droplet is the Capillary number. It may be considered as the ratio of viscous stress that deforms the drop, and that of restoring stress induced by interfacial tension of a drop. When the viscous stress becomes higher than the restoring effect of droplets surface tension, the droplet will rupture. In a system with laminar flow conditions, the capillary number can be defined as follows:

$$\mathrm{Ca} = \frac{\eta_c G R}{\sigma} \tag{4}$$

where G is the shear strain rate, R is the initial droplet radius, σ is the interfacial tension, and η_c is the viscosity of continuous phase.

Thus, the critical capillary number in which a droplet breakup takes places is dependent on the viscosity ratio ($\lambda = \eta_d/\eta_c$), η_d is the viscosity of dispersed phase. A droplet breaks into two smaller daughter droplets just above the critical capillary number of the mother droplet. In addition, a few tiny satellite droplets are generated according to Briscoe *et al*. (1999). Other commonly used breakup parameters include the Weber number (*We*) and the Bond number (*Bo*). These parameters, however, are considered to have smaller impact on droplet breakup compared to the Capillary number according to Lan *et al.* (2017). Droplet breakup using different Capillary numbers and viscosity ratios is illustrated in Fig. 14.

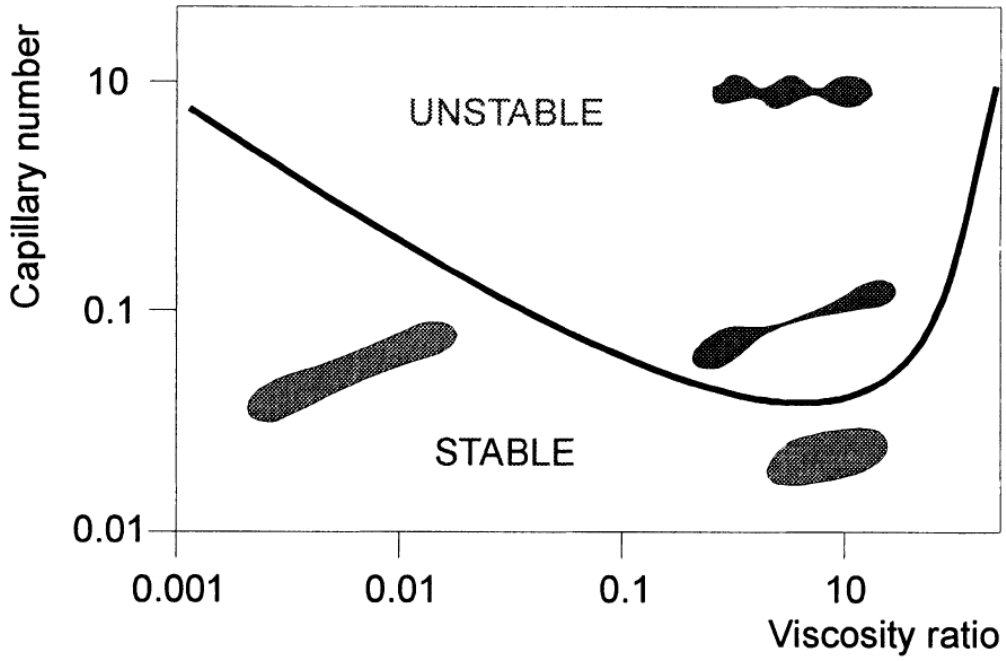

Figure 14. Droplet breakage under simple shear flow as illustrated by Briscoe *et al.* (1999).

The mechanism of droplet breakage has been immensely researched for decades, starting from the work of Taylor in 1930s. According to Jansen et al. (2000) droplet breakup can be divided into the following three categories: 1) binary breakup; 2) capillary breakup and 3) tip streaming. These mechanisms are discussed in the following paragraphs.

4.1.1 Binary Breakup

The first mechanism is called binary breakup, in which a droplet will split into two daughter droplets. This will continue until such droplet size is obtained that the droplet can survive the prevailing hydrodynamic conditions of the system. For a single droplet, the binary breakup is controlled by interaction between viscous forces and Laplace pressure (defined as σ/R). As described above, breakup depends on the Capillary number, above which breakage occurs. When viscosity ratio is close to one, Ca_{crit} is of order unity, and as viscosity η decreases in a system, Ca_{crit} increases steadily. According to Jansen *et al.* (2000), Ca_{crit} reaches an asymptote at viscosity ratio of $\lambda = 3.8$, meaning that in a binary breakup mechanism droplets cannot be fragmented in shear flows at viscosity ratios above 3.8. The curve describing a single droplet breakup is called the Grace curve (first introduced by Grace in 1982), and is formulated as follows:

$$Ca_{crit} = f_{grace}(\lambda) \tag{5}$$

When concentration of a system is increased, the relation of Eq. (5) does not apply without modification. This is caused by the more frequent interactions between droplets, causing destabilization and resulting in smaller Capillary numbers. This shifts the critical breakup curve to a certain extent, depending on the system properties.

4.1.2 Capillary Breakup

The second mechanism is called capillary breakup, in which flow field is varying to such extent that drops have no time to adapt their shape. Eventually droplets stretch into highly elongated shape that will be fragmented during a single breakup event due to capillary waves. Compared to binary breakup, in which one mother droplet is continuously broken into two daughter droplets, the capillary breakup produces a relatively large number of fragmented droplets in a single event. In capillary breakup the Capillary number of the system is typically increased to values highly above the critical value, resulting in exceedingly unstable droplet shapes that break up as a consequence of capillary waves.

4.1.3 Tip Streaming

The third mechanism is called tip streaming. In this breakup mechanism small droplets are detached at pointed ends of a larger mother droplet. This is a consequence of varying surfactant distribution on the droplet interface, causing low interfacial tension at the extremities of the droplet and high tension elsewhere on the droplet. According to de Bruijn (1989), tip streaming cannot take place when surfactant concentration is extremely low and there isn't local variation of interfacial tension. It neither can occur when surfactant concentration is so high that the surfactant covers droplet interface completely and the interfacial tension will be low all over the droplet. He speculates that tip streaming might have great significance for example in separation processes. Tip streaming requires much smaller shear rates than the other two methods of breakup, and the resulting daughter droplets are typically much smaller in size. De Bruijn (1989) demonstrated in his experiments that the viscosity ratio is not crucial parameter for tip streaming to occur, but the type of fluids applied in the system have a great importance. He observed that even low concentration components in a fluid can prevent tip streaming from taking place. Tip streaming and binary breakup mechanism are compared in Fig. 15.

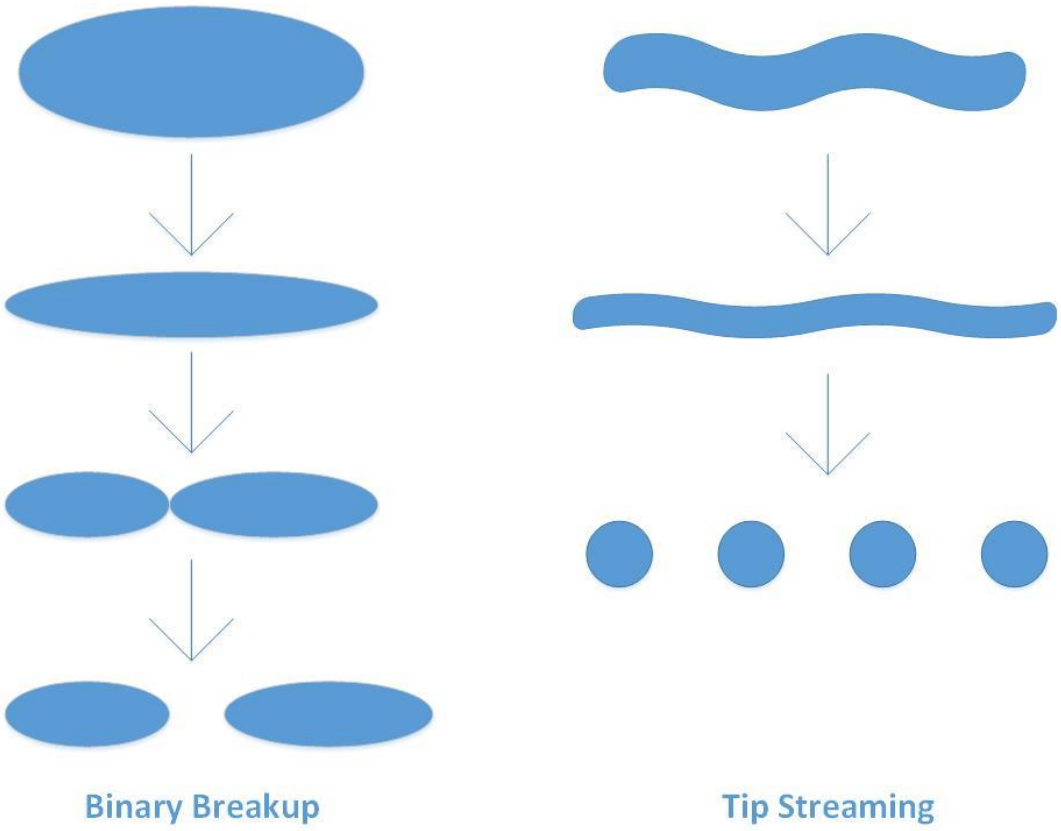

Figure 15. Comparison of binary and tip streaming breakup mechanisms based on the illustration by Briscoe *et al.* (1999).

4.2 Influencing Parameters

Usually the following five parameters has been considered to affect droplet behavior and breakup according to Briscoe *et al*., (1999): 1) the droplet size; 2) the extend and type of the strain field that is applied; 3) the flow history of droplets; 4) the viscosities of dispersed phase and continuous phase; and 5) the interfacial tension between fluids. However, more effort has been put recently into research of additional parameters such as in the effect of experimental apparatus geometry and on the influence of a third component (e. g. surfactant). Additionally, Liao and Lucas (2009) proposed the following four breakup frequency parameters: turbulent fluctuation, viscous shear forces, shearing-off process and interfacial instability.

4.2.1 Droplet Size

Depending on literature source, there seems to be two distinct viewpoints on how increasing a radius of mother droplet affects breakup process. Some studies indicate that increasing the droplet diameter linearly increases breakup frequency of droplets (Han *et al.*, 2011a; Wang *et al.*, 2003; Luo and Svendsen, 1996). On the other hand, some researchers have made the conclusion that breakup frequency reaches maximum at a certain point, after which increasing the droplet diameter results in decreased breakup frequency (Anderson and Anderson, 2006b; Coulaloglou and Taylarides, 1977). Han *et al.* (2014) observed that increased mother droplet size was corresponding to a widening daughter droplet size distribution after the breakup. As the turbulent dissipation rate was increased, the breakup frequency was also increased and simultaneously the critical breakup diameter was decreasing. Bak and Podgorska (2013) discovered that decreasing mother droplet size retards the breakage rate because of smaller differences between disruptive and stabilizing forces, which are inversely proportional to the droplet diameter.

4.2.2 Addition of Surfactant

The influence of surfactant addition on breakup process has been widely studied over the years (Bak and Podgorska, 2012; Briscoe *et al.*, 1999; Stone and Leal, 1990; Wang *et al.*, 2013, among others). Wang *et al.* (2013) used oil soluble sorbitan monooleate (Span 80) as surfactant in their experiments. They speculated that at low surfactant concentrations molecular rearrangement dominates the interfacial phenomena. This results in increased dilational elasticity, establishing stronger resistance to droplet deformation and thus preventing breakage of droplets. They suggested that the DSD increases to a certain point as concentration of surfactant is increased, despite weakened interfacial tensions on the droplets. As the surfactant concentration exceeds a critical value, molecular diffusion from the continuous phase begins to gradually govern the system, leading to a reduced breakage resistance. Wang *et al.* (2013) also noted that when surfactant concentration exceeds critical micelle concentration (CMC), droplets are more easily fragmented into smaller droplets as a consequence of decreased interfacial tension and elastic modulus.

Bak and Podgorska (2012) used polyoxyethylene sorbitan monolaurate (Tween 20) and polyoxyethylene sorbitan monooleate (Tween 80) as surfactants in their experiments. By increasing Tween 20 concentration from 0.0012 mM to 0.0060 mM, the droplet size distribution was reduced by almost twofold. Simultaneously, film drainage was hindered and droplet coalescence slowed down. By using Tween 80, however, droplet coalescence was faster.

Briscoe *et al.* (1999) emphasize that interfacial properties of droplets are affected dynamically by surfactants. In many cases, diffusion of surfactant causes changes in the surfactant concentration within a system. They observed that if surfactant concentration is low enough, there may not be enough surfactant molecules to cover the interface of a quickly expanding droplet. Additionally, if the surfactant molecules are relatively large, they might not be able to cover the expansive droplet surface in time. Each of these factors have effect on variation of surfactant concentration, and consequently, in increasing the variation of surface tension on a droplet.

4.2.3 Dilational Elasticity

Wang *et al.* (2013) observed that as elasticity of a droplet interface is increased, dispersed droplets become more stable and are more able to resist deformation. On the other hand, as the dilational elasticity of an interface is decreased, drops are broken much more easily. When small concentration of surfactant is added into the system, unsaturated molecule adsorption at the interface is increased. Further increase in the concentration promotes molecular rearrangement, leading to an incremented Gibbs elasticity of the surface and strengthened Marangoni convection. At the same time molecules transfer more efficiently between the surface layer of the dispersed phase and bulk of the continuous phase, balancing interfacial tension gradients and invoking deformation of droplet surface. Consequently, the elastic modulus is initially increased at low surfactant concentrations, and then gradually begins to decrease as the concentration of surfactant is increased. This shows that the interfacial dilational properties (especially dilation elasticity) may have a major effect on droplet breakup.

4.2.4 Breakup Frequency Parameters

Models for the breakup frequency of droplets are divided into four mechanisms as suggested by Liao and Lucas (2009): turbulent fluctuation, viscous shear forces, shearing-off process and interfacial instability. These mechanisms are illustrated in Fig. 16.

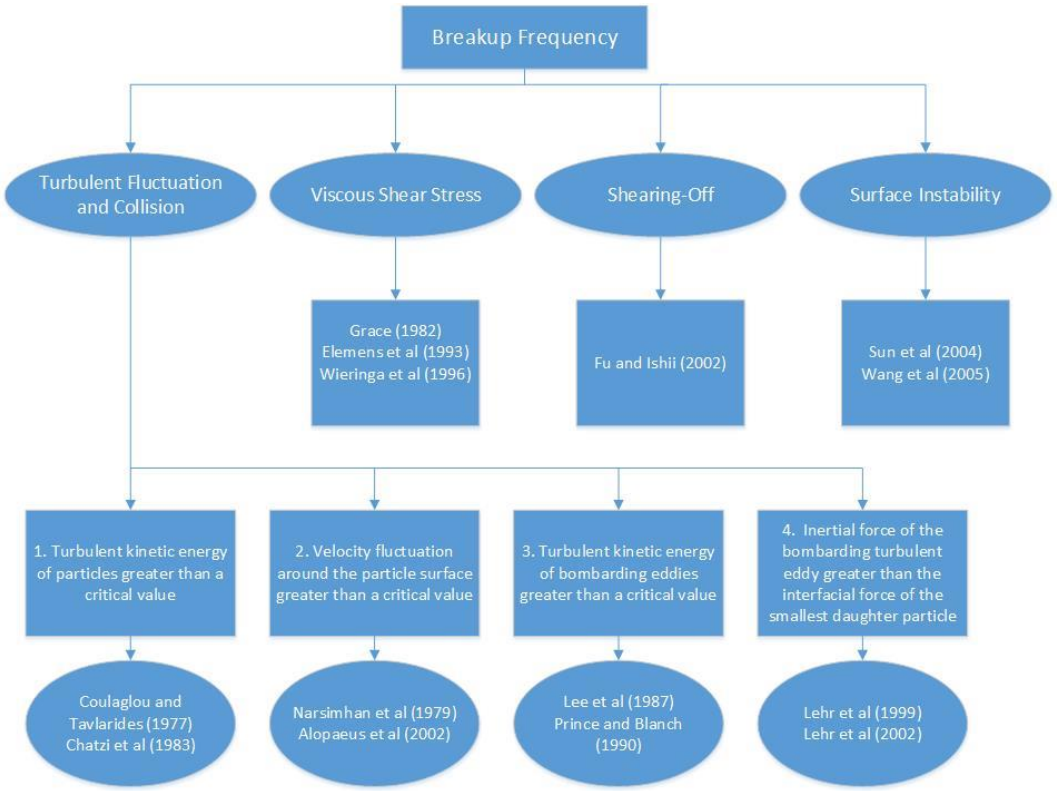

Figure 16. Breakup frequency parameters based on the classification by Liao and Lucas (2009).

Some studies have investigated a breakup process based on eddy-drop collision models (Han *et al.*, 2011a; Luo and Svendsen, 1996; Wang *et al.*, 2003). According to Wang *et al.* (2003) increasing a droplet diameter results in increased number of eddies with equal or smaller sizes than that of the droplet. This results in turn to increased eddy-drop collision frequency, thus promoting the breakup of droplets. Additionally, as energy dissipation rate is increased, both the drop-eddy collision rate and kinetic energy of an eddy is increased, thus resulting in enhanced breakup. Coulaloglou and Tavlarides (1977) formulated the breakage rate of droplet as the

product of inverse breakage time and the fraction of overall number of breaking droplets. They suggested that the kinetic energy of turbulent eddies will break up a droplet if the distributed energy is higher than the surface energy of a mother droplet. Additionally, Prince and Blanch (1990) suggested that the breakup frequency can be expressed as the product of breakup efficiency and collision rate between droplets and eddies of suitable sizes. In their model the breakup efficiency is the fraction of eddies that possess enough energy to promote breakup.

Effect of various strain fields on a breakup process have been also investigated. According to Ni *et al.,* (2001), the breakup frequency is increased when either oscillation frequency or oscillation amplitude of continuous phase is increased in continuous Oscillated Baffled Reactor (OBR). When the oscillation amplitude was increased from 10 mm to 12 mm, the droplets with diameters between 750 – 1000 µm were most clearly influenced. Further increment in the amplitude to 15 mm affected mostly smaller droplets with diameters between 200 – 600 µm. When the oscillation frequency was incremented from 1 to 2 Hz, the coalescence rate constant was decreased by tenfold, indicating that more breakage was taking place. Further increase in the amplitude, however, did not promote substantial increase in the droplet breakage. They deducted that the frequency has greater impact on a breakup process than the amplitude. This was indicated by narrowed DSD of particles at increased fluid oscillation rate. Increasing either oscillation amplitude or oscillation frequency invokes enhanced mixing in a reactor or a column, which in turn leads either to increased collision and drainage rates of droplets, or to reduced contact time between droplets, inhibiting the coalescence and promoting the breakage. Typical droplet image taken in the OBR by Ni *et al.,* (2001) is presented in Fig. 17.

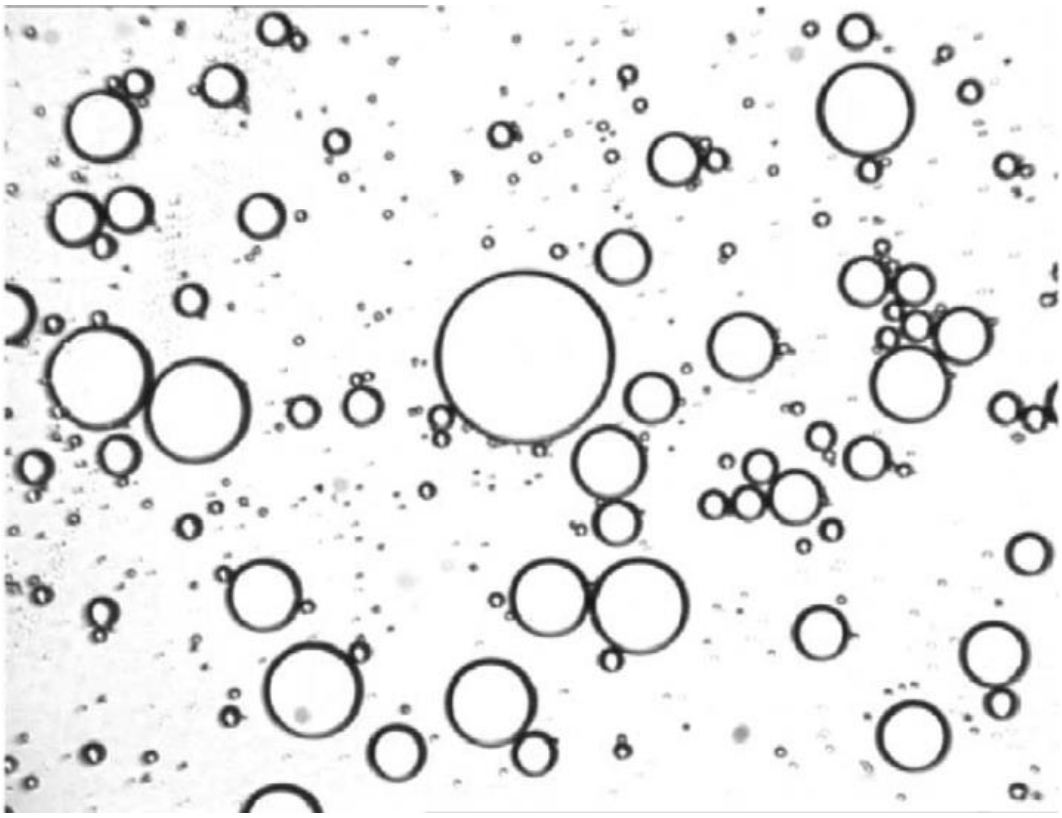

Figure 17. Typical image of silicone oil droplets dispersed in continuous water phase in OBR (Ni *et al.*, 2001).

4.2.5 Mass Transfer

Most studies found in the literature have only investigated mass transfer during a free rising of droplets in a column or a vessel, thus making the assumption of instantaneous droplet breakage and therefore neglecting the mass transfer during the breakage event. However, according to a study by Bozorgzadeh (1980) the mass transfer coefficient during the droplet breakup was found out to be enhanced compared to predictions made for oscillating droplets. Bozorgzadeh (1980) concluded that the increased surface area of the droplets led to the improved mass transfer rate. Skelland and Kanel (1992) studied mass transfer in a batch agitated liquid-liquid dispersion. Their simulations suggested that the mass transfer during the breakage of droplets contributed from two to seven percent of the total mass transfer when the continuous phase consisted of water. However, when the phases were reversed (i. e. water was dispersed) the mass transfer during the breakage was almost negligible (from 0.13 % to 0.65 %). In their study this was accounted for by the destruction of concentration gradients during the violent breakage process of

droplets, resulting to enhanced extraction rate. The mass transfer is controlled by the dispersed phase when continuous phase consists of water, but as the phases are reversed, the continuous phase begins to dominate the mass transfer. Skelland and Kanel (1992) argued that the internal mixing of droplet caused by the breakage is not as significant when the mass transfer resistance is governed by the continuous phase. They also observed that the percentage of solute transferred due to droplet breakup and the resulting oscillations seemed to be independent of mass transfer direction.

4.2.6 Flow History and Apparatus Geometry

The flow history of droplets refers to the fact that swift changes in systems flow conditions can agitate droplet breakup even at values below critical strain rates. According to Rallison (1984), this has also effect on the number of droplets that are generated after the breakup and on the amount of shear stress that is needed to initiate the breakup. This demonstrates that breakup process is closely related to the flow history and its type. The effect of apparatus geometry is not usually taken into account when considering droplet breakup, and flow fields of a system are assumed to be practically infinite. However, Pozrikidis (1990) demonstrated that when a droplet is near a neighboring wall, it may have an effect in the droplet deformation process. In his experiments a droplet moving away from a plane wall adopts a progressively elongated shape at low surface tension values, and ultimately a tail is formed behind the droplet. As the surface tension is increased the formation of the tail is prevented, and the droplet can thus maintain its initial spherical shape. On the other hand, when a droplet moves towards a wall, its shape becomes more and more oblate. If the surface tension is sufficiently low, the droplet becomes a thinning layer of fluid that spreads radially. Again, as the surface tension is increased, the spreading can be constrained and the droplet maintains a more stable form. According to Podzrikidis (1990) the mechanism of droplet deformation induced by a neighboring wall does not depend substantially on either the viscosity ratio or the initial configuration of the droplet. His experiments were in agreement with the film drainage theory when the surface tension was relatively high and the viscosity of the continuous phase was of the same or higher magnitude as the viscosity of dispersed phase.

4.3 Experimental Setups

Droplet breakup has been studied in various experimental settings such as in turbulent pipe flow (Rozentsvaig and Strashinskii, 2016), in shear flow (Lan *et al.*, 2017, Xu *et al.,* 2006) and in pulsation (Liu *et al.,* 2016). Lan *et al.* (2017) researched droplet breakage in a co-flowing microfluidic device illustrated in Fig. 18. The researchers noted that in this kind of microfluidic devices the droplet breakup can be divided into two discrete regimes: dripping in vicinity of capillary tip where the droplets pinch off, and jetting in an extended thread further from the capillary tip. In the dripping region the droplet breakup is governed by shear-driven breakup mechanism.

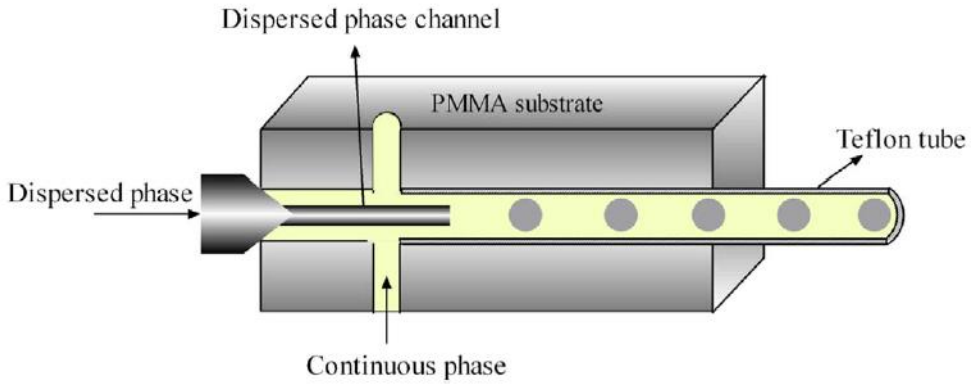

Figure 18. Co-flowing microfluidic device used by Lan *et al.* (2017) in their droplet breakup experiments.

Mignard *et al.* (2004) conducted their droplet breakage experiments by utilizing a continuous Oscillatory Baffled Reactor (OBR). In this device the more typical impeller is replaced by a pulsed flow and stationary baffles. Mignard *et al.* (2014) speculated that this kind of experimental setup provide the formation of suitable sized eddies and fractionation of the dispersed phase, creating more homogenous conditions in the reactor compared to stirring tanks. The OBR is illustrated in Fig. 19.

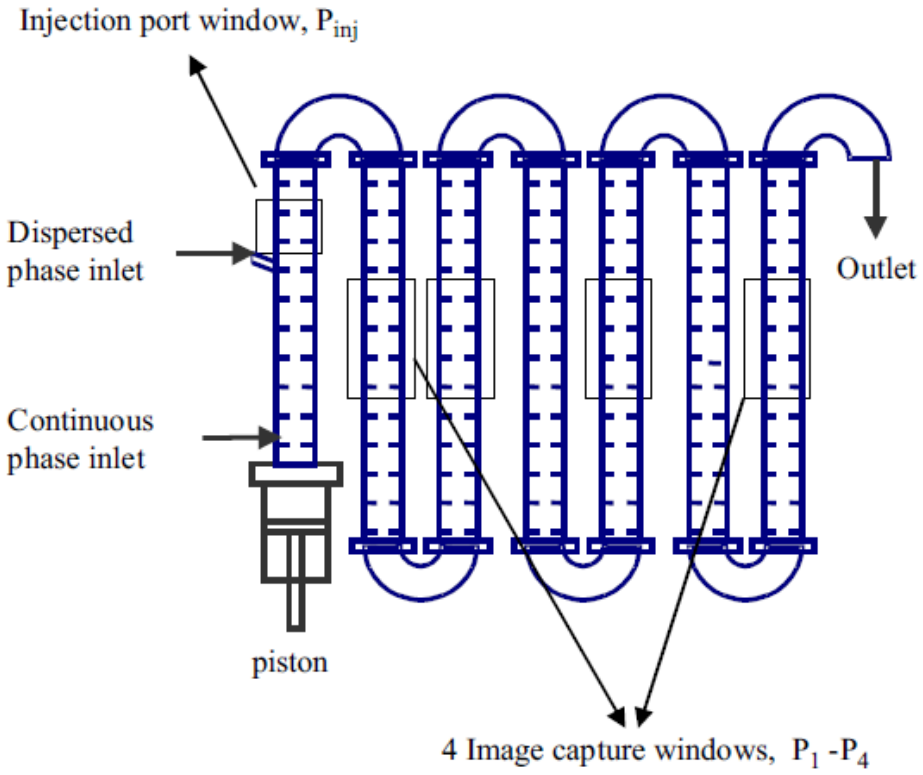

Figure 19. Top view diagram of Oscillated Baffled Reactor used by Mignard *et al.* (2014). Similar setup was also used by Ni *et al.* (2001).

Pulsed disc and doughnut column (PDDC) was used by Liu *et al.* (2016). This relatively recently developed extraction column enhances droplet breakage by pulsation and has numerous advantages compared to traditional columns according to Liu *et al.* (2016). These advantages include weaker channeling effect and stronger unloading capacity, but Liu *et al.* (2016) admit that the prediction of droplet size distribution, which is crucial in designing and scaling up the PDDC, is still a problematic task. The PDDC setup applied by Liu *et al.* (2016) is illustrated in Fig 20.

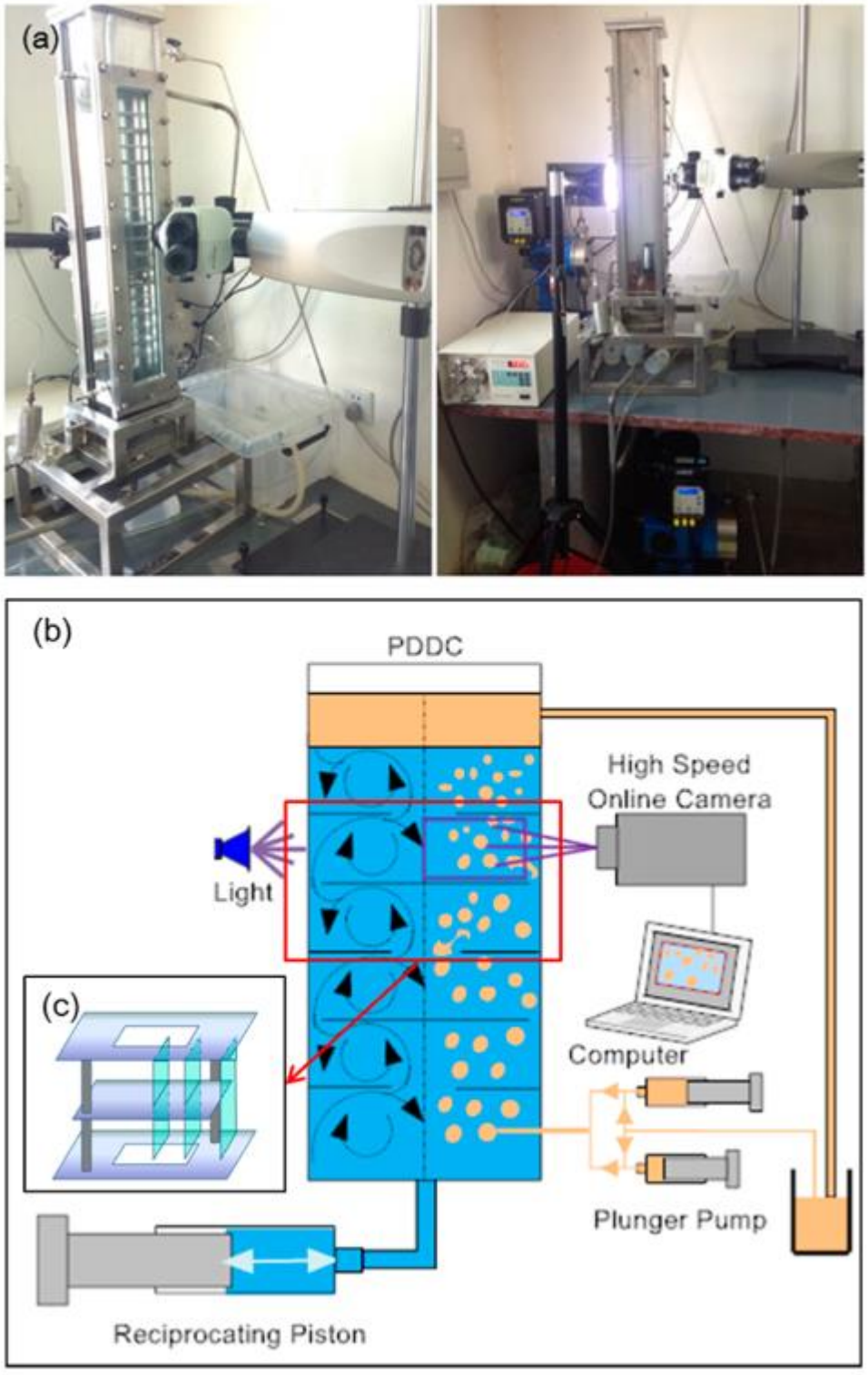

Figure 20. The pulsed disc and doughnut column used by Liu *et al.* (2016) as photographed (a), and illustrated by a schematic diagram from the outside (b) and inside (c).

5 MASS TRANSFER OF COPPER IN REACTIVE LIQUID-LIQUID EXTRACTION

5.1 Introduction to Reactive Mass Transfer

Mass transfer in systems with liquid-ion exchangers may be divided into the following regimes: chemical reaction regime, diffusional controlled regime, or combination of these regimes including both the diffusional and kinetic resistances. According to Bart (2001) the mass transfer with reactive extraction is fundamentally achieved by the numerous chemical reactions occurring in a liquid-ion exchanger and solute system. Industrial liquid-ion exchangers are designed to preferably dissolve in the organic solvent phase in order to prevent losses, and the reaction site is therefore the interface between organic and aqueous phases.

According to Bart (2001) the overall equilibrium reaction of a certain stoichiometry can be divided into the various elementary steps, which may be either instantaneous or rate determining and may include the following: 1) the solute-ion exchanger complexation, 2) the interfacial adsorption or desorption reaction, 3) the aggregation or dissociation of the organic ion exchanger, 4) the complexation reaction with chelating agents, 5) the removal of solvating water molecules by an organic compound, 6) the additional solvation of the solute-ion exchanger complex stoichiometry to form higher complexes, and 7) the competitive reaction of another solute, among others.

Bart (2001) notes that the typically higher organic phase viscosity and the higher molecular weights of the generated organic complexes may result in dominating diffusional resistances in the organic phase. Furthermore, this is enhanced by presence of surfactants. In industry, the enrichment of surfactants at the interface of liquids is very common. This results in more rigid interface that is arduous for the solute to penetrate. Consequently, the diffusional mass transfer is restricted if these adsorption layers aren’t handled accordingly. On the other hand, if the mass transfer is restricted by an interfacial reaction, the transport of reactants or products from the interface becomes irrelevant. Induced charge at the interface has an effect on interfacial kinetics of ionic solutes. The electrostatic interactions affecting solute

concentrations at the interface leads to either in enhanced or reduced chemical rate of reaction. At high aqueous salt concentrations the effect is diminished as a consequence of dampened polarization effects. If high surfactant concentrations at the interface are present, however, an interfacial blockage may cause significant reduction of mass transfer rate according to Bart (2001).

5.2 Reaction Mechanism of Copper Complexation

The complexation of copper in a binary droplet system was included in the experimental work of this thesis, and the complexation mechanism is presented in the following chapter.

Reactive extraction of copper and the involved complexation mechanism has been widely studied over the years. The complexation mechanism begins with the interfacial adsorption of the extractant as introduced by Tamminen *et al.* (2013):

$$\mathrm{HA_{Org}} \rightleftarrows \mathrm{HA} \tag{6}$$

Reaction between the copper cation and hydroxyoxime (HA) yields labile intermediate complex CuA^+ as follows:

$$\mathrm{Cu^{2+} + HA \rightleftarrows CuA^+ + H^+} \tag{7}$$

Reaction of the intermediate complex and another hydroxyoxime molecule yields complex (CuA_2) as described in Eq. (8):

$$\mathrm{CuA^+ + HA \rightleftarrows CuA_2 + H^+} \tag{8}$$

Because the overall charge of complex is neutral, the diffusion of the complex from interface into organic bulk phase is occurring:

$$\mathrm{CuA_2 \rightleftarrows CuA_{2,org}} \tag{9}$$

Taking the equations described above into account, the overall reaction of copper complex formation in organic phase can be given in the following way:

$$Cu^{2+} + 2\,HA_{org} \rightleftarrows CuA_{2,org} + 2H^{+} \quad (10)$$

When reaction in Eq. (8) is rate determining, the reaction rate of copper extraction can be calculated as follows:

$$r = k\frac{[Cu^{2+}][HA]_{org}{}^{2}}{[H]^{+}} - \frac{k}{k_E}[CuA_2]_{org}[H^{+}] \quad (11)$$

where k is kinetic constant and K_E is equilibrium constant. The equilibrium constant of copper extraction can be calculated by the following equation:

$$k_E = \frac{[CuA_2]_{org}[H^{+}]^2}{[Cu^{2+}][HA]_{org}{}^{2}} \quad (12)$$

6 COMPUTATIONAL FLUID DYNAMICS AND INTERFACIAL TRACKING METHODS

Modelling of binary droplet coalescence and breakage has been extensively studied by numerous researchers (Ata *et al.*, 2010; Eiswirth, 2014; Gebauer *et al.*, 2015; Kamp and Kraume, 2014; Mitra and Ghosh, 2007; Reichert and Walker, 2015; Villwock *et al.*, 2014; Wegener and Paschedag, 2011; Zhang *et al.*, 2012, among others). Results from these studies usually depend strongly on the used phase properties and experimental data. There is a broad range of models and correlations available in literature, but as the interface phenomena of single droplets can be highly complex, the selection of most suitable method may be difficult and time consuming. Analytical equations are available for a few simplified cases, but most studies include a combination of experimental, empirical and numerical methods. While empirical methods may give satisfactory results effortlessly, the acceptability of the applied equations has to be checked thoroughly.

Most frequently used computational methods described in literature include the level-set method (Deshpande and Zimmerman, 2006), the diffuse interface method (Verschueren *et al.*, 2001), the volume of fluid method (Rider and Kothe, 1998), the front tracking method (Unverdi and Tryggvason, 1992) and the Lattice-Boltzman method (Takada *et al.*, 2000). According to Deshpande and Zimmerman (2006) each of these methods have their own advantages and disadvantages, and the selection of the most suitable method should be made carefully.

In the following chapters computational fluid dynamics method is discussed and the level-set method and the volume of fluids method are presented in more detail.

6.1 Computational Fluid Dynamics

Numerical methods such as Computational Fluid Dynamics (CFD) present increasingly accurate results, but the results from these simulations should be always confirmed against experimental measurements. According to Laakkonen *et al.* (2006) rigorous CFD demands immense computational resources and thus is currently too heavy for the optimization of various mathematical parameters. However, a multi-block model with certain simplifications considering local DSDs and mass transfer is more applicable for most purposes. According to Alopaeus *et al.* (2014) one of the most typical simplifications concerns the flow patterns. Real-life reactors contain typically intensive multiphase fluid flows, and some parts of the flow are of high turbulent intensity, while other regions are more quiescent. However, in most computational fluid dynamic models the local variations of flow conditions are neglected in order to lessen the computational burden, and the flow region is considered as ideally mixed everywhere in the reactor or the column. These variations, however, can affect the dynamics of a droplet population and thus the operation of vessels. The simplifications can be accounted for by simultaneous modelling of fluid flow, multiphase behavior and chemical reactions in a rather straightforward but computationally heavy manner.

The flow of a polydisperse multiphase flow have been simulated e. g. by Ramkrishna (2000) by coupling the population balance equation with the CFD model. This method was also utilized by Marchisio *et al.* (2003), Marchisio and

Fox (2005); Silva *et al.* (2008), and Silva and Lage (2011). However, the researchers noted that the selection of most suitable coalescence and breakage models strongly affect the accuracy of the obtained simulation results as the parameters need to be adjusted according to the properties of the system (Liao and Lucas, 2009).

6.2 Level-Set Method for a Single Droplet

Level-set method is one of the numerous computational methods used in the simulation of multi-phase flows. It was first introduced by Osher and Sethian (1988) and has been since applied in various fields. The method is known for easy and accurate capture of interfaces according to Wang *et al.* (2006). The level-set method is especially useful in its distinct representation of dispersed and continuous phases. More specifically, the method describes the interface topology and its changes entirely by the zero set of the level-set function. According to Wang *et al.* (2006), the method is both stable and easy to code, while the computation of geometric parameters and three-dimensional problems can be effortlessly implemented. However, Wang *et al.* (2006) admit that the level-set method treats the interface less accurately compared to boundary-fitted coordinates method. Yang and Mao (2005) calculated the mass transfer in single dispersed drops with resistances in both continuous and dispersed phase. While the results predicted by the method were in excellent agreement with the experimental studies, Wang *et al.* (2006) noted that the mass transfer during the acceleration step of falling and rising droplets were not taken into account. According to Annaland (2006), in the situations where the droplet interface is drastically deformed, the level-set methods may suffer from mass or volume loss and therefore accuracy of the method is reduced.

6.3 Volume of Fluids

Volume of fluid (VOF) method was first introduced by Hirt and Nichols (1981). This numerical method is used to solve the Navier-Stokes equations for incompressible transient two-phase flows. The fundamental idea of the method is to use so-called phase indicator function to implicitly capture the position of an interface according to Bothe and Fleckenstein (2013). Additionally, orientation of

the interface needs to be defined, which is derived from the gradient of the phase indicator function. According to Annaland *et al.* (2005), the VOF methods can be roughly divided into the following two categories depending on the representation of the interface: simple line interface calculation (SLIC) and piecewise linear interface calculation (PLIC). Traditionally VOF methods have been characterized by the SLIC-algorithm (Hirt and Nichols, 1981), but more recent VOF methods include the PLIC-algorithm which has significantly improved accuracy and capability compared to the older VOF-algorithms according to Annaland *et al.* (2005). Major drawback of VOF-algorithm concerns the so-called artificial coalescence of interfaces, which occurs when the mutual distance of the interfaces becomes smaller than the size of a computational cell. However, in systems where coalescence prevails, this method does not require particular algorithms for the merging or breaking of interfaces.

Different modelling methods are compared in Table I as presented by Annaland *et al.* (2005).

Table I. Comparison of the methods used for modelling of multiple flows with sharp interfaces based on the work of Annaland *et al.* (2005).

Method	**Advantages**	**Disadvantages**
Level-Set	Conceptually simple and easy to implement	Limited accuracy and loss of mass (volume)
SLIC VOF	Conceptually simple and straight forward extension to 3D	Numerical diffusion, limited accuracy and automatic merging and breaking of interfaces
PLIC VOF	Relatively simple and accurate, accounts for significant topology changes in interface	Difficult to implement in 3D and automatic merging and breaking of interfaces
Lattice-Boltzmann	Accurate and accounts for significant topology changes in interface	Difficult to implement and automatic merging and breaking of interfaces
Front-Tracking	Extremely accurate and robust, accounts for significant topology changes in interface	Mapping of interface mesh onto Eulerian mesh requires dynamic remeshing, merging and breaking of interfaces requires sub-grid model

7 IMAGE AND VIDEO ANALYSIS

7.1 Principles of the Image and Video Analysis

The obtained experimental results were analyzed using the image and video analysis program developed in MATLAB (2016a). The program uses concentration analysis method presented by Tamminen *et al.* (2017). The recorded still images and video frames were imported into the program, and droplet volumes, droplet concentrations, surface areas among others were automatically measured and

calculated. To obtain full shape of the droplets, an ellipse fitting to the image data was used, assuming that the shape of the droplets is oblate spheroid. The droplet formation times, rest times and coalescence times were measured manually from the videos by going through the frames one by one.

The droplet concentration analysis is based on the observation of changing intensity inside the droplet image. As copper forms complex with hydroxyoxime (see Eq. (10)), the color change can be clearly observed inside the droplet and recorded by a digital camera. The concentration analysis with the camera is based on the Lambert-Beer equation:

$$A = \varepsilon L c \tag{13}$$

where A is absorbance, c is concentration, L is optical path length and ε is molar absorptivity.

The concentration of droplets can be calculated using the absorbances from the green channel of the camera when the droplet geometry is taken into consideration. The optical path length describing the distance which light moves through a droplet affects the absorbance as follows from Eq. (13), and by assuming that a droplet is oblate spheroid this can be accounted for by calculating the chord lengths (analogous to the optical path length) of the droplet at each pixel position. The effect of light scattering can be taken into consideration by computing the molar absorptivity at each pixel position of a droplet image as a function of the chord length. The apparent absorptivity increases at shorter chord lengths due to refraction and scattering of light, and this can be observed as a dark edge of the droplet. By inserting the calculated chord lengths and absorptivities into the Lambert-Beer equation, the concentrations at each pixel of the droplet image can be calculated in the following way:

$$c_p = \frac{A}{\varepsilon l_{ch}} \tag{14}$$

where c_p is the concentration at the position of the pixel and l_{ch} is the chord length at the position of the pixel. The volume of each pixel can be taken into account by using the image scale, i. e. the distance per pixel (l_p), together with the calculated chord lengths (l_{ch}) as follows:

$$V_p = l_p^2 l_{ch} \tag{15}$$

where V_p is the volume of the pixel. When the pixel volume and measured pixel concentration are known, the amount of copper at the position of each pixel can be computed by the following equation:

$$n_p = c_p V_p \tag{16}$$

By summing all of the copper amounts together, the overall copper concentration of a droplet can be calculated as follows:

$$c = n/V_d \tag{17}$$

where *n* is the sum of copper transferred to the droplet and V_d is the volume of droplet.

Full description of the image analysis method is presented in the article by Tamminen *et al.* (2017).

7.2 Concentration Calibration

The calibration lines used in the image analysis program are presented in Fig. 21. The calibration standards of known concentrations were imaged as droplet in the coalescence cell. The calibration was made separately for both 10 and 20 volume percent Acorga M5640 in Exxsol D80.

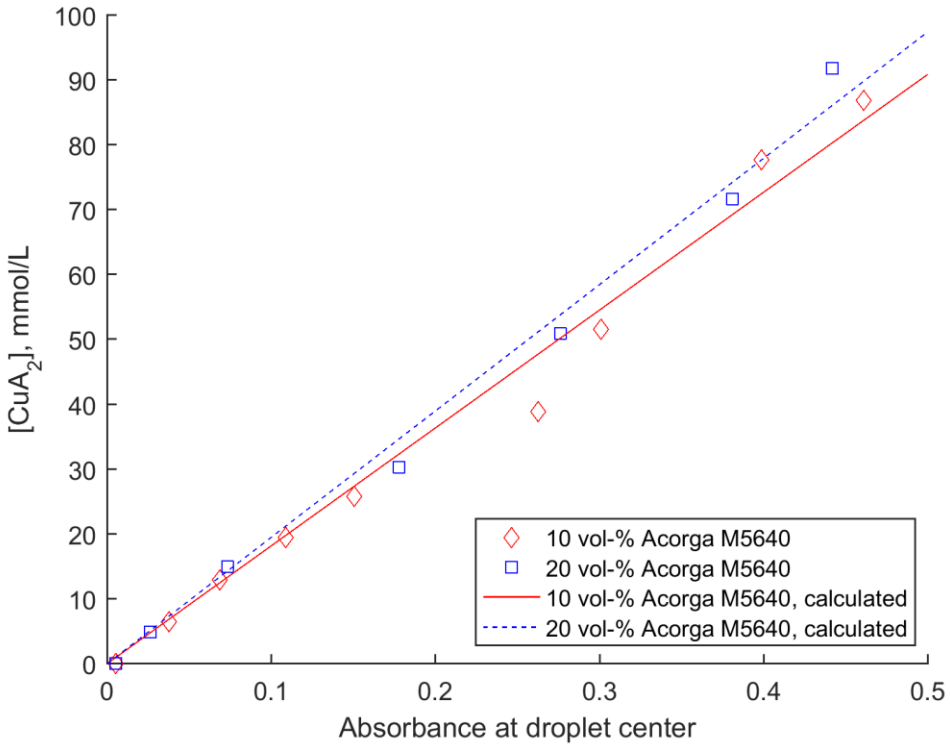

Figure 21. The concentration of copper complex in the calibration standards at droplet center using the green channel of the camera. Calibration line equation for 10 vol-% Acorga M5640: $[CuA_2] = 181.8 \cdot$ absorbance, and for 20 vol-% Acorga M5640: $[CuA_2] = 194.8 \cdot$ absorbance. Analysis was made from extracted video frames.

In kinetic extraction experiment analysis was made from still images instead, which slightly affected the calibration line equations: for 10 vol-% Acorga M5640 $[CuA_2] = 167.6 \cdot$ absorbance, and for 20 vol-% Acorga M5640: $[CuA_2] = 184.1 \cdot$ absorbance.

The interpolation functions that were used to calculate the molar absorptivities at each pixel position are presented in Fig. 22 and in Fig. 23 for 10 vol-% Acorga M5640 and 20 vol-% Acorga M5640, respectively. The interpolation function that was applied in the calculation of apparent absorptivity is the following:

$$\varepsilon = a/\ln(l_{ch} + 1) + b \tag{18}$$

The function parameters were fitted to the droplet data in order to compute concentration profiles and average concentrations of droplets.

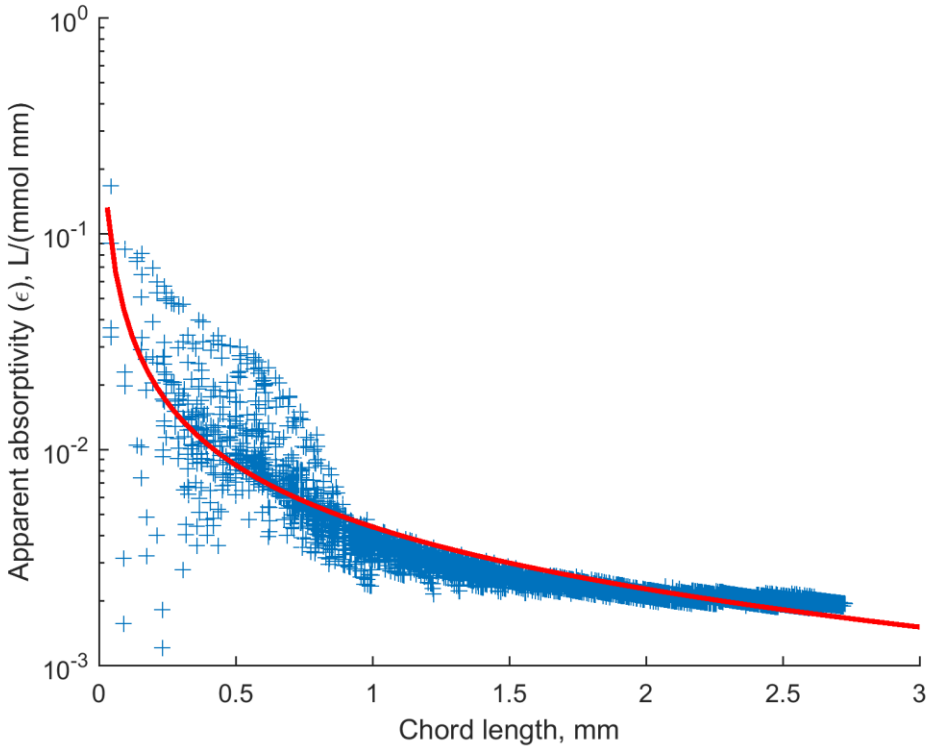

Figure 22. Apparent absorptivity for 10 vol-% Acorga M5640 standard solution sample using the green channel of the camera. The 13 mM standard solution was imaged as a droplet in the coalescence cell. Parameters used in Eq. (18): a = 0.004013 and b = -0.001381.

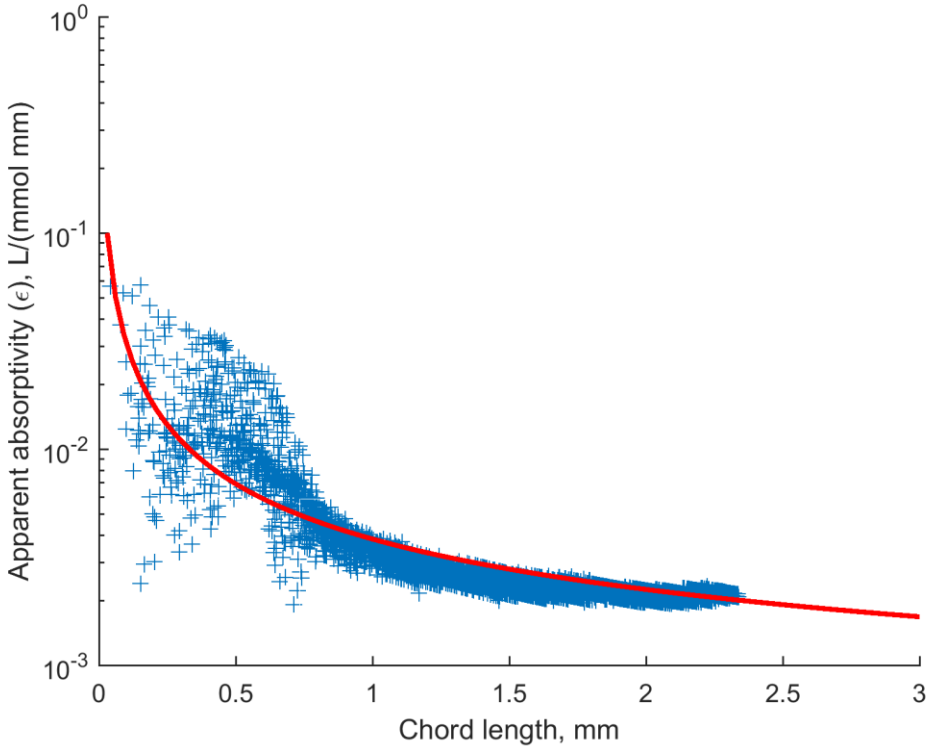

Figure 23. Apparent absorptivity for 20 vol-% Acorga M5640 standard solution sample using the green channel of the camera. The 15 mM standard solution was imaged as a droplet in the coalescence cell. Parameters used in Eq. (18): a = 0.003012 and b = -0.0004867.

7.3 Data Processing

The results obtained from the image and video analysis programs were rounded up to three decimals. Mode of distribution describes the most frequently appearing values of a data set, and it was selected to represent the results in this thesis. Concentration difference was calculated based on the measured droplet volumes and concentrations as follows:

$$\Delta c = \frac{n_c}{V_c} - \frac{n_s + n_p}{V_s + V_p} \tag{19}$$

where n_c is the amount of copper in combined droplet, n_s is the amount of copper in sessile droplet, n_p is amount of copper in pendant droplet, V_c is the volume of combined droplet, V_s is the volume of sessile droplet and V_p is the volume of pendant

droplet. Flow chart of the overall image analysis and data processing method is presented in Fig. 24.

Figure 24. Different steps of data processing used in the image and video analysis method.

8 EXPERIMENTS

Experiments conducted in this thesis consisted of binary droplet coalescence experiments, in addition to single droplet kinetic extraction experiments. The experiments mentioned above are discussed in more detail in the following chapters.

8.1 Experimental Setup

All experiments were performed in a coalescence cell illustrated in Fig. 25. Two needles could be freely adjusted vertically in order to obtain the required distance between the needle tips in the cell. In order to produce droplets of desired volumes, two syringe pumps (World Precision Instruments model no. AL-1000) were used. In both the coalescence and kinetic experiments the pumps were programmed to yield droplets with volume of 8 µL with the pump rate setting of 400 µL/min. 10 mL syringes with the diameter of 15.5 mm were used in both pumps in all performed experiments, and these syringes were connected to the upper and lower needles with tubes. Pumps were started manually and sessile and pendant droplets were formed at the tips of the 0.91 mm needles at approximately the same time. The distance between the needle tips was 5 mm ± 0.5 mm. Casio EX-F1 digital camera was used for the video recording of the coalescence experiments at 300 frames per second and for the capture of still images in the kinetic extraction experiments. The camera was calibrated with the settings of ISO 100 (describing the sensor's sensitivity to light), aperture value of F 4.6 and shutter speed of 1/320 s, which were kept constant in all experiments in order to ensure the comparability and reproducibility of the obtained results. LED-panel (by Epistar, color 3000 K, power 36 W, size 300 mm · 300 mm) was used as a background light.

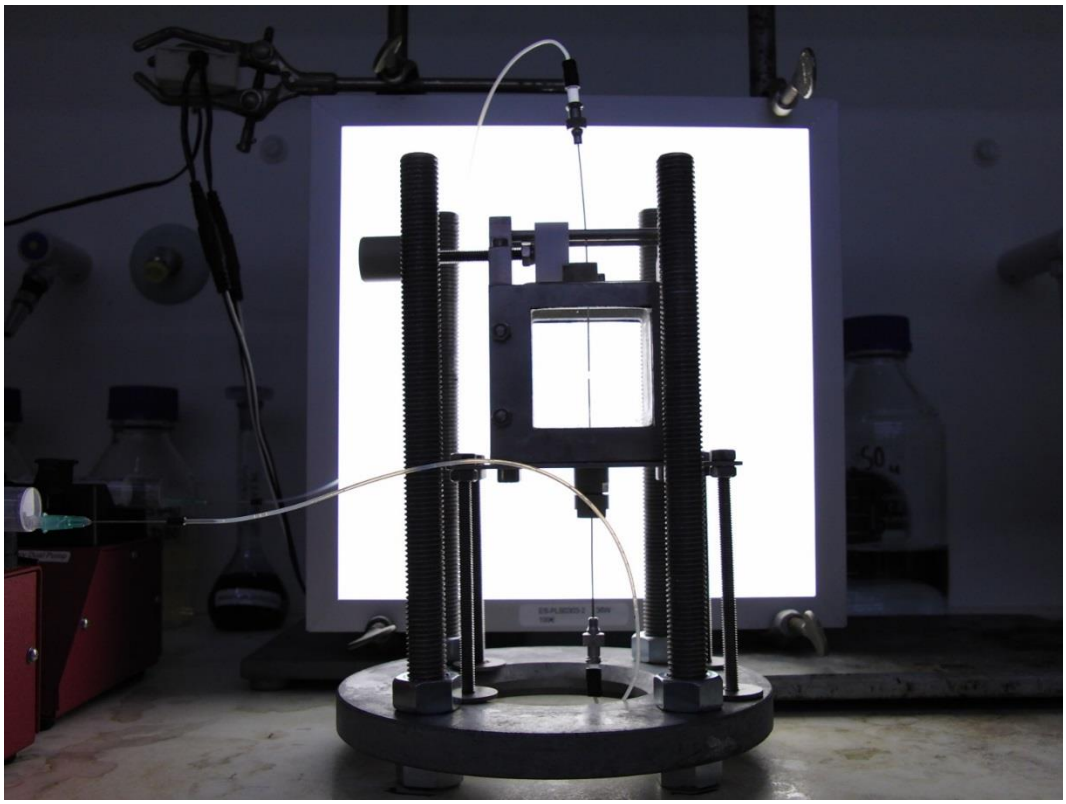

Figure 25. The coalescence cell used in the experiments with two syringe pumps connected to upper and lower needles with tubes and illuminated by LED-panel.

A schematic diagram of the setup for binary droplet coalescence experiments is given in Fig. 26.

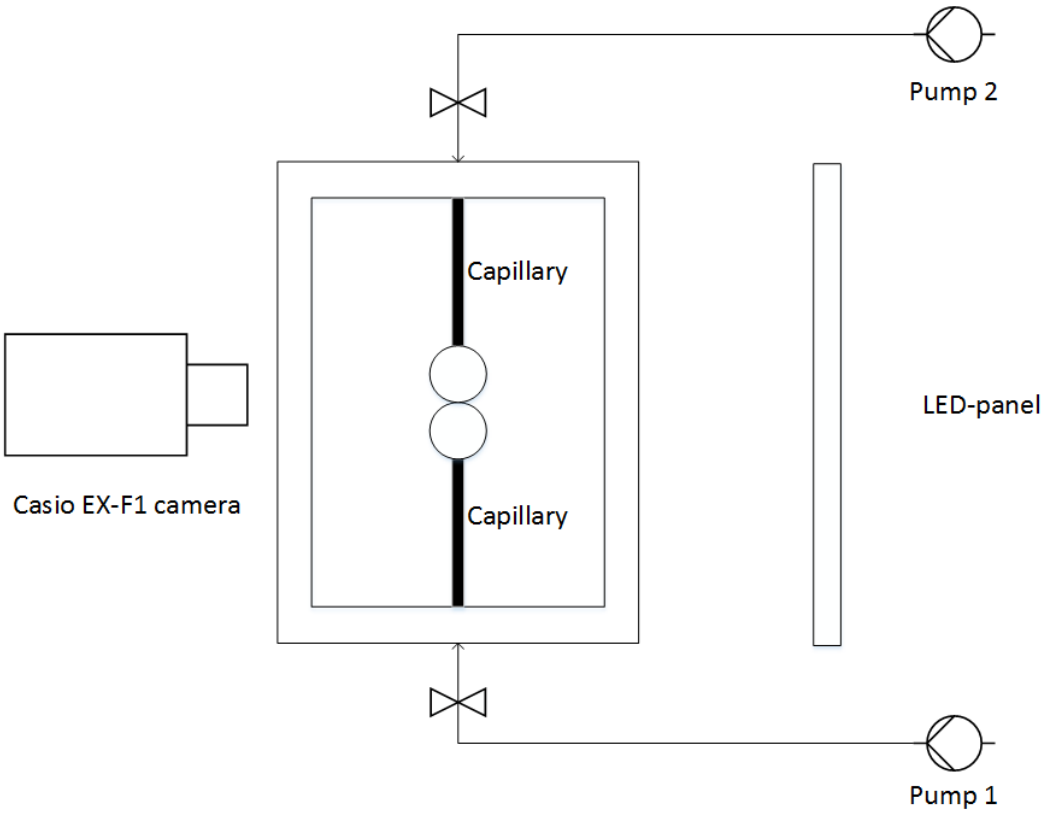

Figure 26. Casio EX-F1 camera was positioned in front of the coalescence cell at the distance of 112 mm to the front glass panel of the cell. The LED-panel was behind the coalescence cell at the distance of 262 mm to the camera lens. The width of the coalescence cell was 40 mm and height was 60 mm.

In the single droplet kinetic experiments the setup was similar to that used in the binary droplet coalescence experiments expect for the removal of the upper needle and second syringe pump.

8.2 Preparation of Feed Solutions and Calibration Standards

Preparation of $CuSO_4$ and $(NH_4)_2SO_4$ solutions, dilution of Acorga M5640 solutions, and preparation of standard solutions used in concentration calibration are presented in the following chapters.

8.2.1 Preparation of $CuSO_4$ and $(NH_4)_2SO_4$ solutions

The continuous phase concentrations applied both in the binary droplet coalescence experiments and in single droplet kinetic extraction experiments are tabulated in Table II. The required amounts of copper (II) sulfate pentahydrate and deionized water were weighted with an analytical scale. The salt and the water were mixed in 1000 mL Erlenmeyer flask using a magnetic stirrer to ensure that all of the salt was dissolved. pH of the solution was then measured with Consort multiphase analyzer C3010 and adjusted to 3.1 for all solutions by adding required amounts of 3.0 M HNO_3. The preparation procedure of ammonium sulfate solutions was similar to that described above.

8.2.2 Preparation of Acorga M5640 in Exxsol D80 solutions

Acorga M5640 solvent extraction reagent (by Cytec Solvay Group) was diluted in Exxsol D80 (by Exxon) in order to yield 10 volume percent and 20 volume percent solutions. The 10 vol-% Acorga M5640 solution had density of 0.8183 g/µL and viscosity of 2.30 mPas, while the 20 vol-% Acorga solution had density of 0.8335 g/µL and viscosity of 2.99 mPas. Required amounts of Acorga and Exxsol were weighted with an analytical scale and poured into a 500 mL flasks. A centrifuge was used in order to clarify the Acorga solutions, and the clarified solutions were then transferred into new flasks by using a pipette and a pump.

8.2.3 Preparation of Calibration Standards

Two methods were used to prepare the calibration standards. In the first method equilibrated copper complex solutions were prepared by adding required amounts of the prepared copper sulfate solutions of known concentrations and Acorga M5640 in Exxsol D80 solutions into a separation funnel. Volumes of the aqueous phase and the organic phase were kept equal. The dispersion was mixed for 30 minutes to ensure that the equilibrium was reached and then left to settle overnight. Finally, the aqueous phase was removed from the organic phase by using the separation funnel. To determine the copper contents of the aqueous phases, Agilent 8543 UV/VIS-spectrophotometer was used to perform analysis. Organic copper concentrations were then computed based on mass balances.

In the second method the calibration standards were diluted from the equilibrated copper complex solutions. By using a micropipette, required amounts of the equilibrated organic phase and pure Acorga solution were measured to yield calibration standards of known concentrations.

8.3 Binary Droplet Coalescence Experiment Procedure

First part of the binary droplet coalescence experiments consisted of total 150 experiments with the continuous phase of 0.16 M $CuSO_4$ and the dispersed phase of 20 volume percent Acorga M5640 in Exxsol D80. The experiments were made in series of 10 droplet pairs after which the cell was emptied and carefully rinsed with water and ethanol to prevent impurities. By using copper sulfate solutions as the continuous phase the formation of copper complex occurred, and the effect of mass transfer could be investigated during the coalescence experiments. Since mass transfer between the phases begins immediately, an extra care was paid to the minimization of residual droplets volume and the residual droplet copper complex concentration. Needle distance was adjusted to around 5 mm so that the coalescence of 8 µL droplets will occur. Videos of each coalescence process were recorded with Casio EX-F1 digital camera at 300 frames per second. The videos were then manually analyzed in order to determine droplet formation times, droplet rest times and droplet coalescence times. Additionally, droplet volumes, concentrations, needle distances and relative positions of the droplets were measured as described in section 7.1. Droplet rest time distribution was constructed based on the results.

The second part of binary droplet coalescence experiments consisted of experiments with varied dispersed and continuous phase properties (tabulated in Table II). The impacts of continuous phase concentration and extraction reagent volume fraction on the coalescence event and on the mass transfer of copper complex were investigated. Experimental procedure was identical to that described above, with each of the phase combinations including 10 consecutive coalescence experiments.

The final part of the binary droplet coalescence experiments consisted of total 150 experiments with the continuous phase of 0.16 M $(NH_4)_2SO_4$ and the dispersed

phase of 20 volume percent Acorga M5640 in Exxsol D80. Since no reaction occurred in the system, the binary droplet coalescence could be investigated without the effect of mass transfer between the phases. Again, the experiments were made in series of 10 droplet pairs and droplet rest time distribution was constructed. Comparison of droplet rest time histograms with and without mass transfer was performed (see section 9.4).

Table II. The combination of dispersed and continuous phases used in the performed binary droplet coalescence experiments and single droplet kinetic extraction experiments.

Organic phase (Acorga M5640 in Exxsol D80)	Continuous phase	Number of experiments
10 vol-% Acorga	0.16 M $CuSO_4$	10
10 vol-% Acorga	0.24 M $CuSO_4$	10
10 vol-% Acorga	0.32 M $CuSO_4$	10
10 vol-% Acorga	0.40 M $CuSO_4$	10
10 vol-% Acorga	0.50 M $CuSO_4$	10
10 vol-% Acorga	0.85 M $CuSO_4$	10
20 vol-% Acorga	0.16 M $CuSO_4$	150
20 vol-% Acorga	0.24 M $CuSO_4$	10
20 vol-% Acorga	0.32 M $CuSO_4$	10
20 vol-% Acorga	0.40 M $CuSO_4$	10
20 vol-% Acorga	0.50 M $CuSO_4$	10
20 vol-% Acorga	0.85 M $CuSO_4$	10
20 vol-% Acorga	0.16 M $(NH_4)_2SO_4$	150

8.4 Single Droplet Kinetic Extraction Experiment Procedure

Single droplet kinetic extraction experiments were performed in the coalescence cell using the phase combinations tabulated in Table II (excluding experiments with 0.16 M $(NH_4)_2SO_4$ since no reaction occurs). Single sessile droplet with volume of about 8 µL was formed at the tip of 0.91 mm needle at the beginning of each experiment. The pump was started simultaneously with a stop watch and pictures were taken in predetermined time intervals so that the concentration change could

be observed as a function of time from the image series. During the first 60 seconds images were taken as fast as possible with the camera, and as experiment continued on the time interval was gradually decreased as tabulated in Table III.

Table III. Time intervals between the taken pictures in the experiment.

Total experiment time	Time Interval (s)
0 – 60 seconds	6 (approximate)
1 – 2 minutes	10
2 – 4 minutes	20
4 – 8 minutes	30
8 – 16 minutes	60
16 – 20 minutes	120

9 RESULTS AND DISCUSSION

The results from binary droplet coalescence experiments and from single droplet kinetic extraction experiments are presented in the following chapters. Additionally, simulation result of coalescence event with COMSOL Multiphysics software using the level-set method is presented (performed by Esko Lahdenperä) and compared to the experimental results.

9.1 Droplet Formation Times

Droplet formation time describes the required time for a droplet to reach its final volume, i. e. the time interval between starting of the syringe pump and the first contact between the droplets. The droplet formation times are presented in Fig. 27.

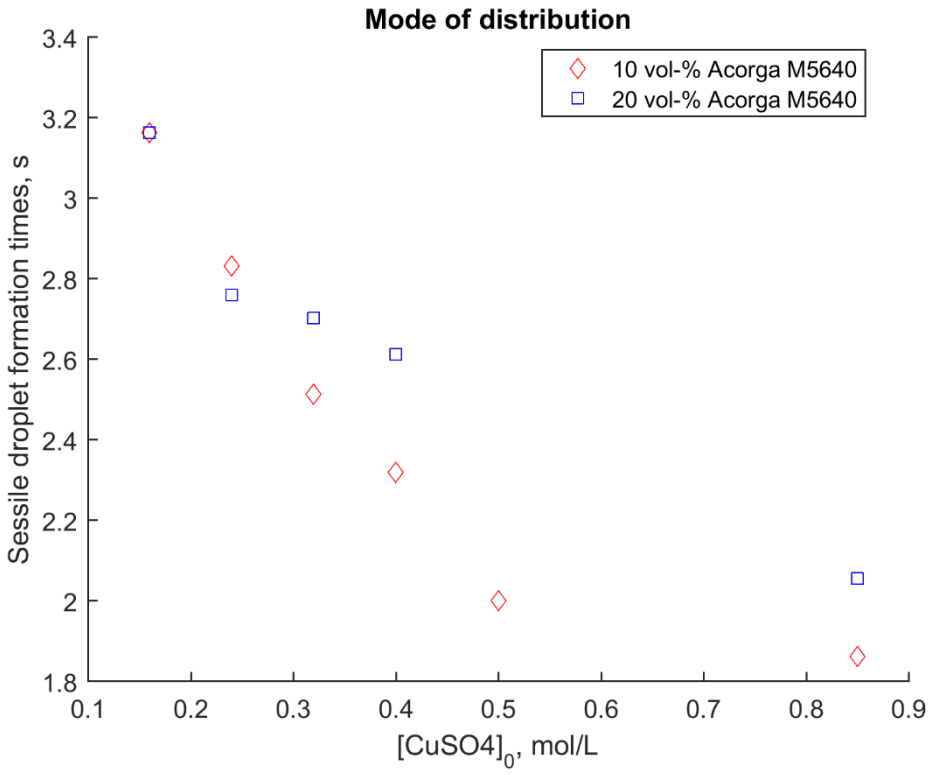

Figure 27. Sessile droplet formation times as a function of continuous phase concentration.

From Fig. 27 it can be clearly seen that droplet formation times were decreasing as the concentration of continuous phase was increased. Also, the formation times for 10 volume percent Acorga M5640 were generally lower compared to those for 20 volume percent Acorga solutions. Formation of the pendant droplets occurred generally about 0.3 seconds later than the formation of sessile droplets due to manual starting of the pumps. The increasing density difference between the phases at higher continuous phase concentrations was considered affect the droplet formation times. Simultaneously, the buoyancy of the system was increasing, which has an impact on the geometry of the droplets. The sessile droplet became more and more oblong as the buoyancy in the system was increased, while the pendant droplet tended to move upwards more readily and became more oblate. These changes in droplet geometry may contribute to the decreasing droplet formation times. Formation times for both pendant and sessile droplet are presented in Table IV.

Table IV. Pendant droplet and sessile droplet formation times in all performed binary droplet coalescence experiments including copper complexation. Times are presented as modes of distribution.

Continuous phase *c* ($CuSO_4$)	Dispersed phase (Acorga M5640)	Sessile droplet formation time (s)	Pendant droplet formation time (s)
0.16 M	10 vol-%	3.163	2.553
0.24 M	10 vol-%	2.833	2.690
0.32 M	10 vol-%	2.513	6.469
0.40 M	10 vol-%	2.320	2.073
0.50 M	10 vol-%	2.000	1.543
0.85 M	10 vol-%	1.863	2.92
0.16 M	20 vol-%	3.163	4.233
0.24 M	20 vol-%	2.760	3.013
0.32 M	20 vol-%	2.703	2.486
0.40 M	20 vol-%	2.613	2.296
0.50 M	20 vol-%	3.686	3.340
0.85 M	20 vol-%	2.056	1.67

9.2 Droplet Volumes

Droplet volumes were measured separately for both sessile and pendant droplets just before the coalescence event, i. e. at the time when both droplets have reached their final volumes. The volume of combined droplet just after the coalescence was also measured at approximately 0.1 seconds after the rupture of the interfacial film. The combined volumes of sessile and pendant droplets before the coalescence event and the volume of combined droplet after the coalescence event for 10 volume percent Acorga solutions are presented in Fig. 28.

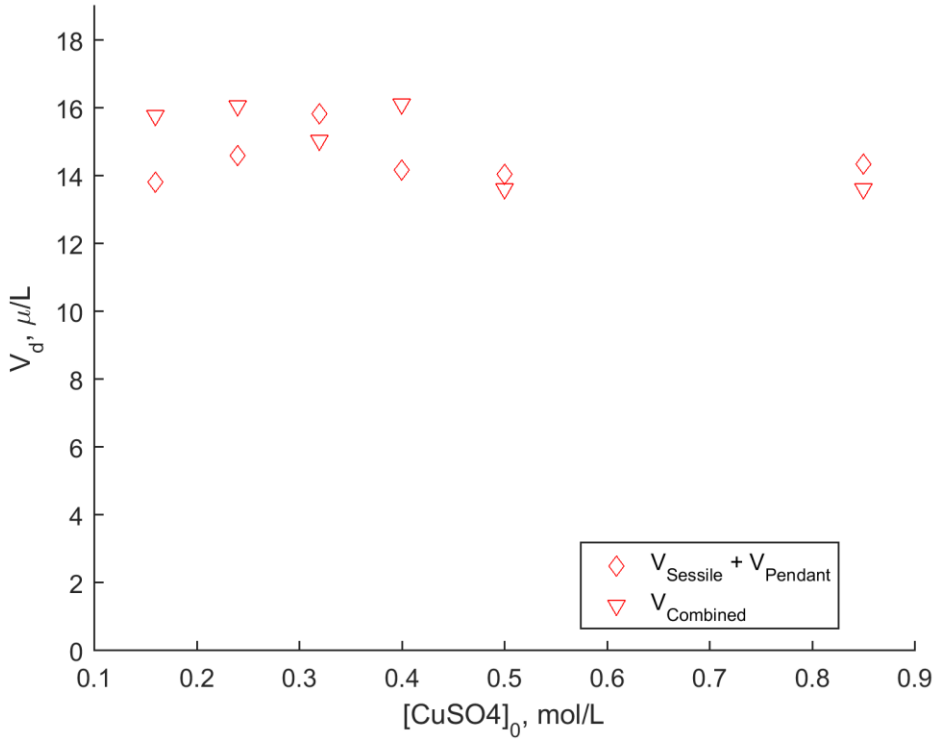

Figure 28. Droplet volumes with 10 vol-% Acorga M5640 as a function of continuous phase concentration. $V_{Sessile} + V_{Pendant}$ describe the combined volumes of the droplet just before the coalescence event, while $V_{Combined}$ describes the volume of the combined droplet just after the coalescence.

Similarly, the droplet volumes for 20 volume percent Acorga solutions are presented in Fig 29.

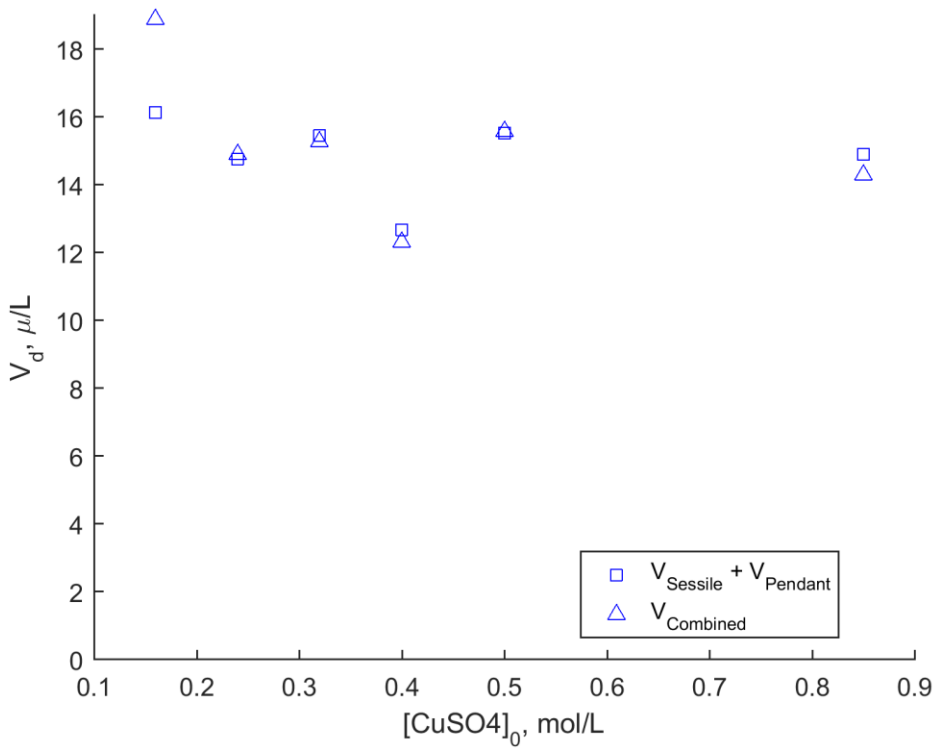

Figure 29. Droplet volumes with 20 vol-% Acorga M5640 as a function of continuous phase concentration. $V_{Sessile} + V_{Pendant}$ describe the combined volumes of the droplet just before the coalescence event, while $V_{Combined}$ describes the volume of the combined droplet just after the coalescence.

From the Fig. 28 and Fig. 29 it can be seen the combined pendant droplet and sessile droplet volumes before the coalescence corresponded fairly well with the volumes of the combined droplets after the coalescence. Differences in the droplet volumes between different data series are mainly due to the accuracies of the syringe pumps. It was also observed that with longer formation times the droplets volumes were generally slightly higher. This was caused by the slow increase in the droplet volumes after the pump was paused, originating from the pumping mechanism. Differences in the volumes before and after the coalescence are related to the accuracy of the analysis method and to the formation of additional daughter droplet. In most of the coalescence experiments small daughter droplet was formed and could be barely observed from the recorded videos. The daughter droplet reduces the volume of the combined droplet by detaching from it during the coalescence event, but due to their extremely small sizes the daughter droplets could not be

analyzed. Consequently, the accuracy of ellipse fitting in the analysis step was considered to have the major impact on the volume differences.

9.3 Droplet Rest Times

Droplet rest time describes the time required for the coalescence to occur after the initial contact between the droplets. In the film drainage model this is described as the drainage time of the interfacial film. As the film begins to thin it eventually reaches the critical film thickness and ruptures, leading to coalescence. In order to investigate the effect of copper complex formation on the droplet rest time, 150 experiments were performed with both 0.16 M $(NH_4)_2SO_4$ (no reaction) and with 0.16 M $CuSO_4$ (reaction). Droplet rest times are presented based on the experimental results. In Fig. 30 droplet rest time distributions using different salts are compared.

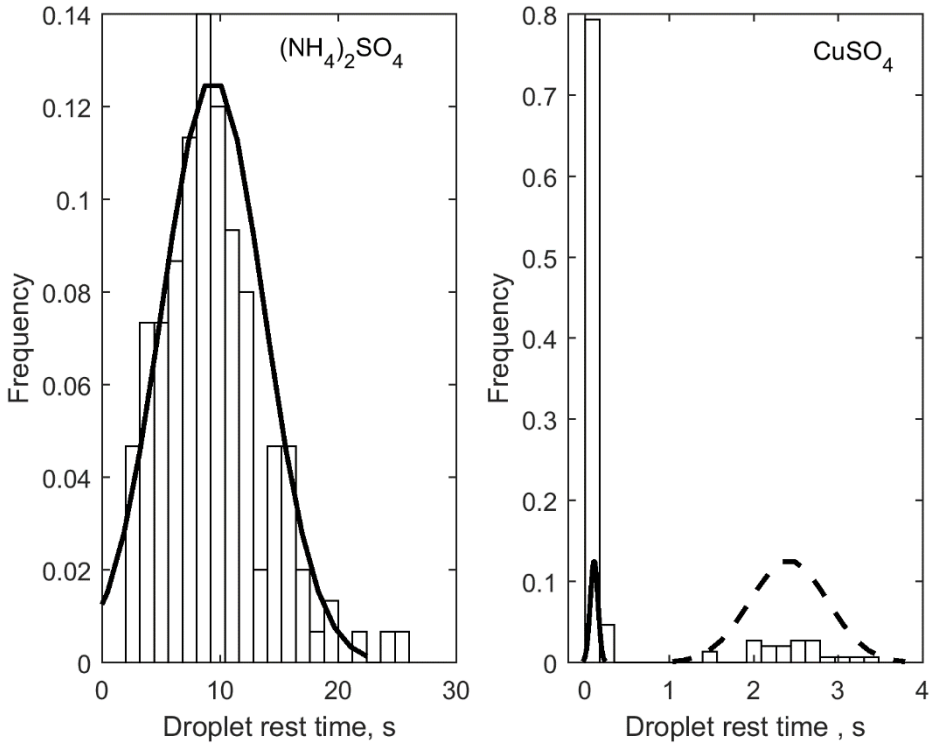

Figure 30. 20 vol-% Acorga M5640 was dispersed in 0.16 M $CuSO_4$ and 0.16 M $(NH_4)_2SO_4$. Both data sets contain 150 experiments.

As seen in Fig. 30 the droplet rest times for the ammonium sulfate system are normally distributed, while in the system with copper sulfate pentahydrate the results follow the normal distribution only when they are separated into two different data sets. Droplet rest times below 0.4 seconds form the first distribution with total of 127 data points included, having the average rest time of about 0.11 seconds. The second distribution contains 23 data points with the average droplet rest time of about 2.42 seconds. In Fig. 31 the droplet rest times above 0.3 seconds are excluded from the system with 0.16 M $CuSO_4$ in order to have more detailed view on the distribution.

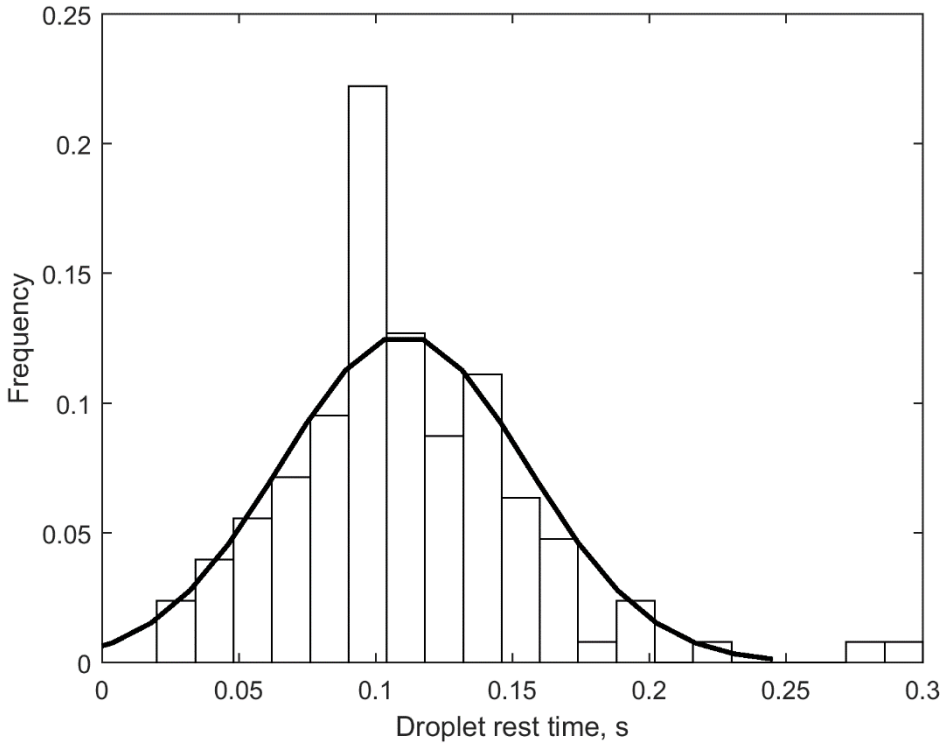

Figure 31. Droplet rest time histogram including 127 experiments with 0.16 M $CuSO_4$ and 20 vol-% Acorga M5640. Droplet rest times above 0.3 seconds are excluded from the distribution.

From Fig. 32 it can be clearly seen that the droplet rest times were drastically reduced in the system including the formation of copper complex. The average droplet rest time with the continuous phase of 0.16 M $(NH_4)_2SO_4$ was about 9.41 seconds, while the average rest time was reduced to only about 0.11 seconds with the use of continuous phase of 0.16 M $CuSO_4$. The effect of mass transfer between the phases in different chemical systems has been observed to strongly affect the

coalescence based on the studies found in literature (Ban *et al.*, 2000; Kamp and Kraume, 2014; Kopriwa *et al.*, 2012). This phenomenon is typically contributed to changes in film drainage induced by the mass transfer. Kopriwa *et al.* (2012) speculated that surface tension gradients caused by the Marangoni effects are responsible for the instability of the droplet, in addition to miscibility variations of dispersed and continuous phases caused by the solute (see Section 3.2.4.). It is assumed to be the main reason for the reduced droplet rest times also in the experimental studies performed in this thesis. The second distribution in right side of Fig. 30 could be explained by the hindered Marangoni convection during the film drainage phase of droplets at these particular experiments. In the experiments with longer droplet rest times it was assumed that the surface tension gradients caused by the Marangoni effects were weaker compared to the rest of the experiments. This could be explained by differences in mass transfer rate and internal circulation of the droplets leading to a more stabilized coalescence event and thus longer droplet rest times.

9.4 Droplet Concentration Analysis Results

Droplet concentrations were determined for both the sessile and pendant droplets just before the coalescence event and for the combined droplet just after the coalescence event. In Fig. 32 sessile droplet concentrations are presented, and in Fig. 33 pendant droplet concentrations are given.

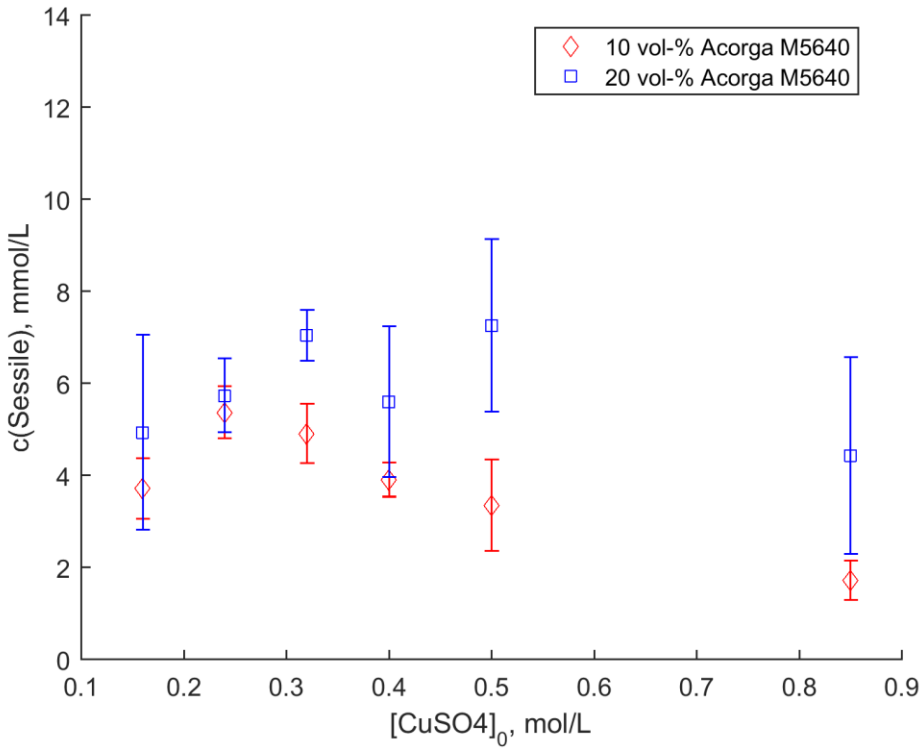

Figure 32. Mode of distribution for sessile droplet concentrations measured just before the coalescence event. The error bars describe the standard deviations of each data set.

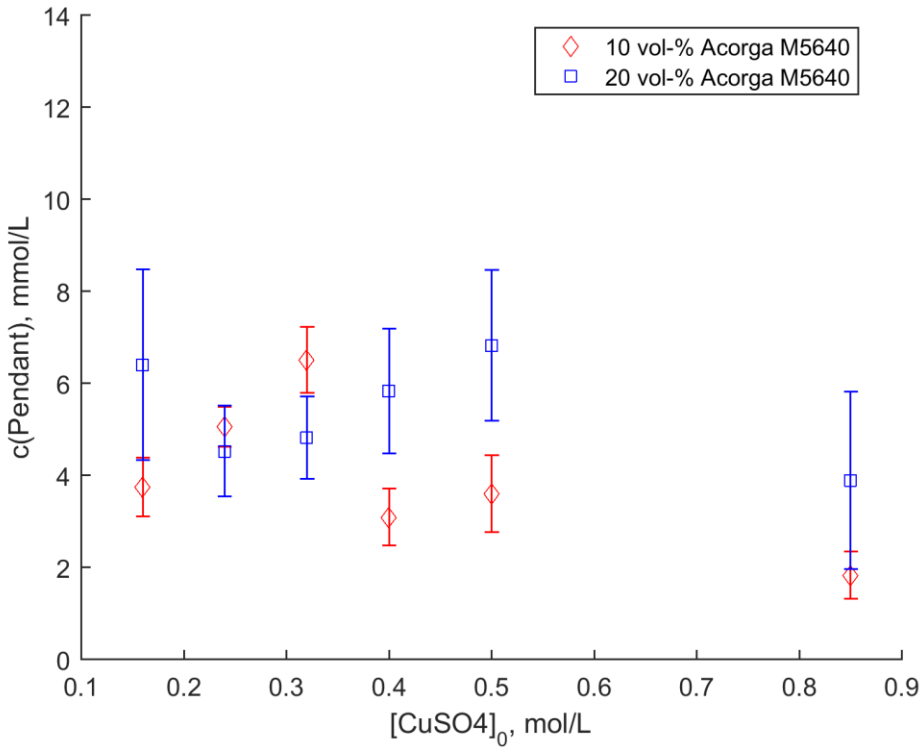

Figure 33. Mode of distribution for pendant droplet concentrations measured just before the coalescence event. The error bars describe the standard deviations of each data set.

In Fig. 34 the combined droplet concentrations just after the coalescence event are presented.

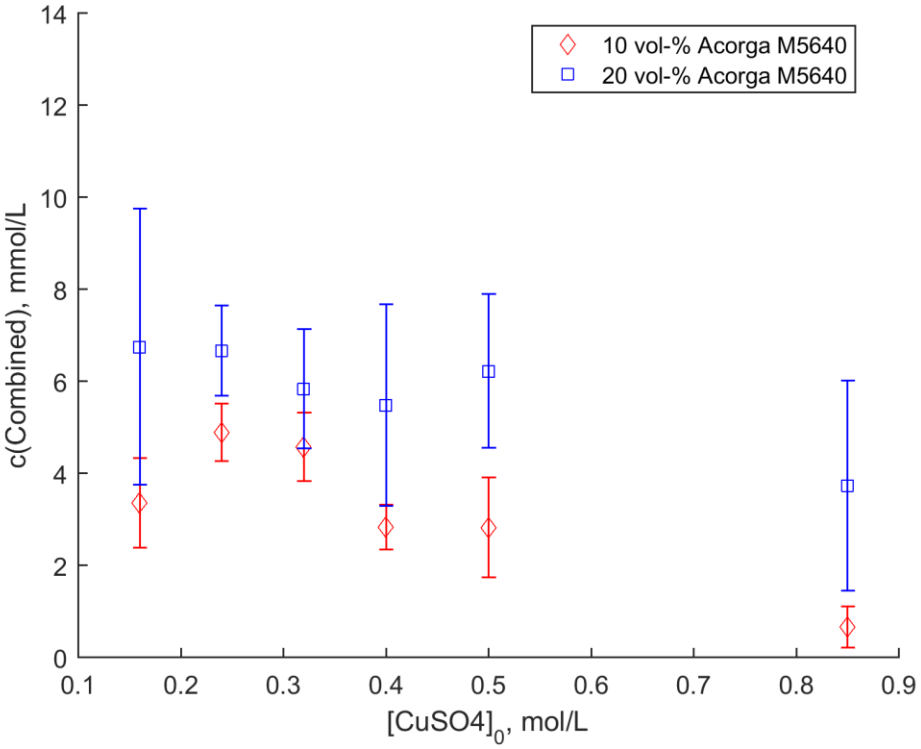

Figure 35. Mode of distribution for combined droplet concentrations just after the coalescence event. The error bars describe the standard deviations of each data set.

From the Figs. 33 – 35 it can be observed that the droplet concentrations stayed generally unaffected as the concentration of the continuous phase was increased. However, the droplet concentrations using the 10 volume percent Acorga M5640 solutions were generally lower compared to the concentrations using the 20 volume percent Acorga M5640 solutions. This was to be expected, when the reagent capacities are taken into account. Concentrations of pendant and sessile droplet corresponded reasonably well with each other, with no significant concentration differences between the droplets. The concentrations were similar because there were no significant differences in either formation times of the sessile and pendant droplets (see Section 9.1) or in the droplet volumes (see Section 9.2). Because the formation times of droplets were similar, it also meant that the time available for the mass transfer of copper complex was approximately equal in both droplets. Similarly, because there were no major differences in the droplet volumes, the mass transfer areas of both droplets were also close to equal.

The concentrations of combined droplets were generally smaller than what was expected when compared to sessile and pendant droplet concentrations just before the coalescence. This may be due to measurement errors in the analysis step, or errors conducting the experimental part. Experimental errors concerning the droplet concentration analysis may originate from minimization efficiency of the residual droplet concentration at the beginning of each experiment, and from the defective focusing of the digital camera used for the imaging of droplets.

9.5 Droplet Concentration Difference Analysis Results

Droplet concentration differences were calculated based on the measured droplet volumes and concentrations as described in Eq. (9). In Fig. 35 the droplet concentration differences for all phase combinations are given.

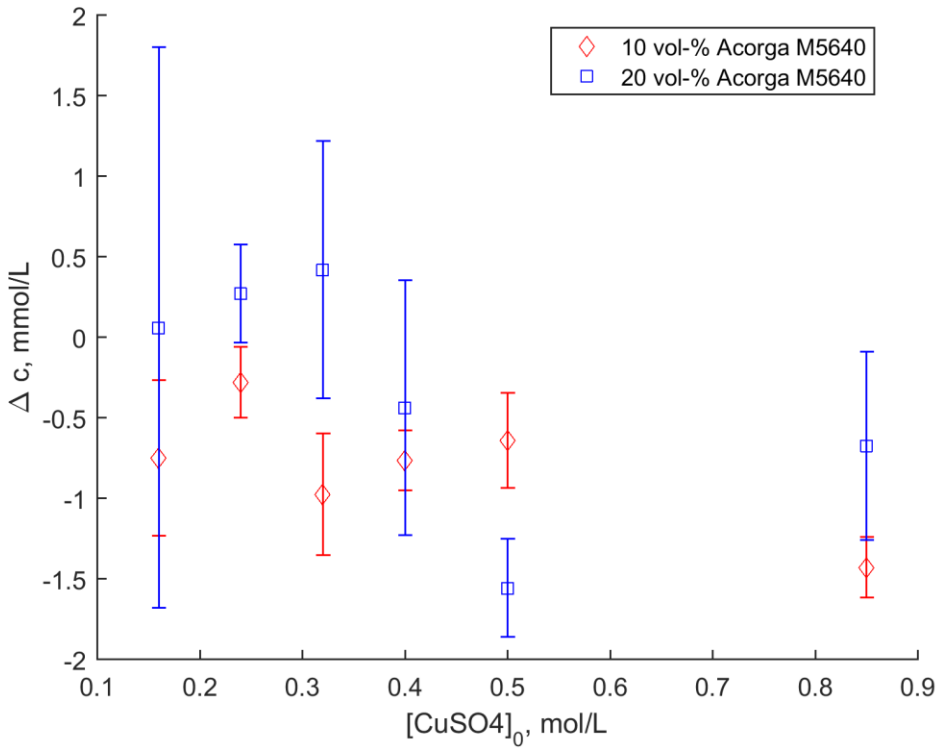

Figure 35. Mode of distribution for droplet concentration differences calculated by Eq. (16). The error margins describe the standard deviations of each data set.

In Fig. 36 the droplet concentration difference distributions for each phase combination is given.

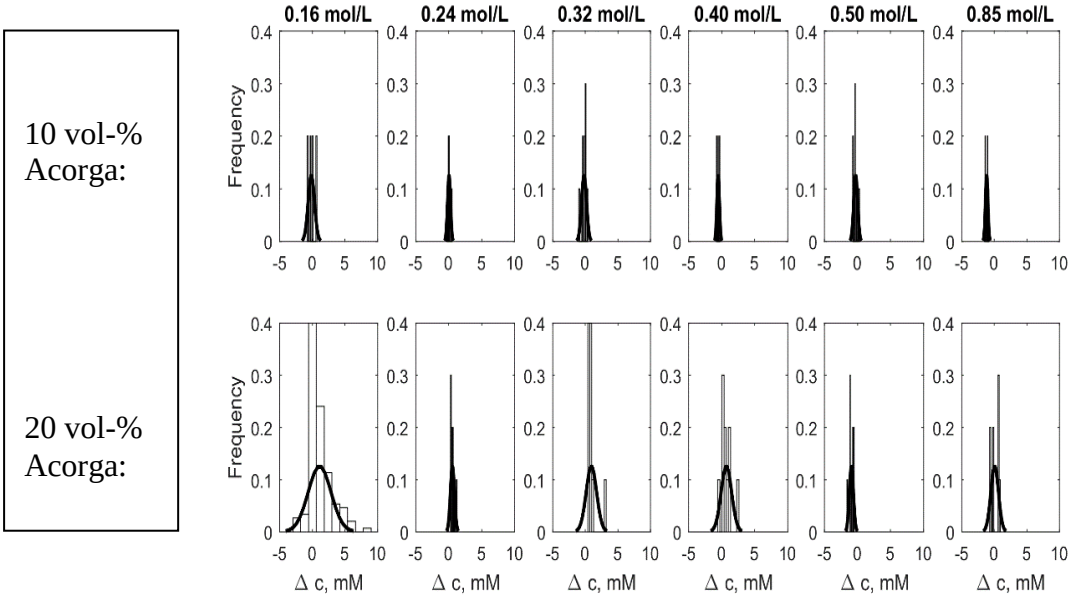

Figure 36. Droplet concentration difference distributions for all phase combinations that include copper complexation.

As can be seen from Fig. 35 and Fig. 36, the droplet concentration differences in all data sets are close to zero or negative. The loss of mass during the coalescence event is physically ineligible, so the measurement error originates from the repeatability of the experiments and from the limit of quantification. It is assumed that the largest data set including 150 experiments with 20 vol-% Acorga M5640 dispersed in 0.16 M $CuSO_4$ provides to most accountable value (Δc = 0.059) for the concentration change. Other data sets including only 10 experiments each do not seem to provide enough statistically plausible data to measure the extremely small concentration change reliably, resulting in most likely false negative values. This can be also seen from the relatively high values of standard deviations of each data set in contrast to the very small concentration change values. Reliability of the obtained concentration change results could be enhanced by increasing the number of experiments for each of the data sets. However, in the scope of this study it was not feasible to increase the number of performed experiments to such extent. Additionally, the accuracy of the concentration analysis method was slightly reduced at higher continuous phase concentrations. This was a consequence of more

unstable binary droplet system as the density difference between the phases was increasing at higher copper sulfate concentrations. The increased density difference led to higher buoyancy within the system, and the resulting instability reduced the quality of the usable analysis frames. Based on the obtained results, it was assumed that the mass transfer during coalescence event was not clearly enhanced within the detection limits of the used image analysis method.

In Table V both the sessile droplet and pendant droplet concentrations are presented in addition to the results from concentration difference analysis.

Table V. Concentration analysis results. Droplet concentrations and concentration differences are given as modes of distribution.

Continuous phase ($CuSO_4$)	Dispersed phase (Acorga M5640)	Sessile droplet *c* (mmol)	Pendant droplet *c* (mmol)	Concentration difference Δc (mmol)
0.16 M	10 vol-%	3.711	3.747	-0.751
0.24 M	10 vol-%	5.367	5.057	-0.28
0.32 M	10 vol-%	4.907	6.509	-0.976
0.40 M	10 vol-%	3.900	3.092	-0.765
0.50 M	10 vol-%	3.347	3.605	-0.641
0.85 M	10 vol-%	1.718	1.826	-1.429
0.16 M	20 vol-%	4.934	6.402	0.059
0.24 M	20 vol-%	5.735	4.526	0.271
0.32 M	20 vol-%	7.040	4.817	0.420
0.40 M	20 vol-%	5.595	5.830	-0.438
0.50 M	20 vol-%	7.257	6.818	-1.557
0.85 M	20 vol-%	4.427	3.891	-0.674

9.6 Single Droplet Kinetic Extraction

Kinetic extraction experiments with a single sessile droplet were performed in order to get a point of reference to the mass transfer rate of copper complex without a coalescence event. In the kinetic experiments mass transfer of copper complex was observed as an increase of droplet concentration in the coalescence cell as a function

of time. Kinetic extraction experiments performed with both 10 and 20 volume percent Acorga M5640 in Exxsol D80 in different continuous phase concentrations are given in the Fig. 37 and Fig. 38, respectively.

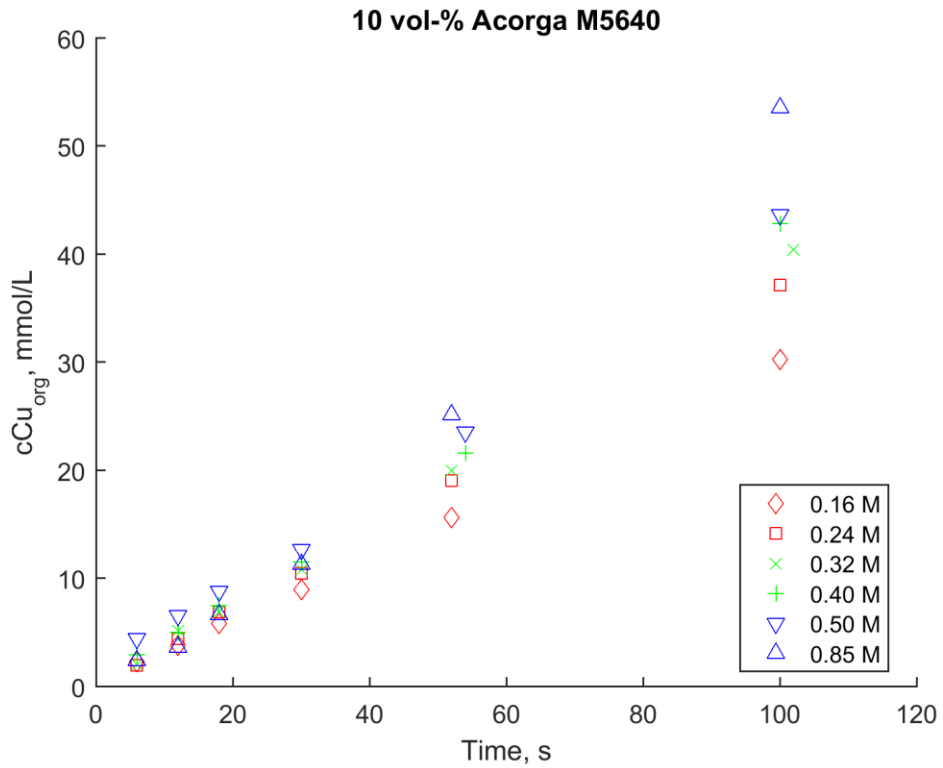

Figure 37. Concentration of copper complex in the droplet as a function of time. Initial aqueous phase concentration was varied between 0.16 – 0.85 M $CuSO_4$.

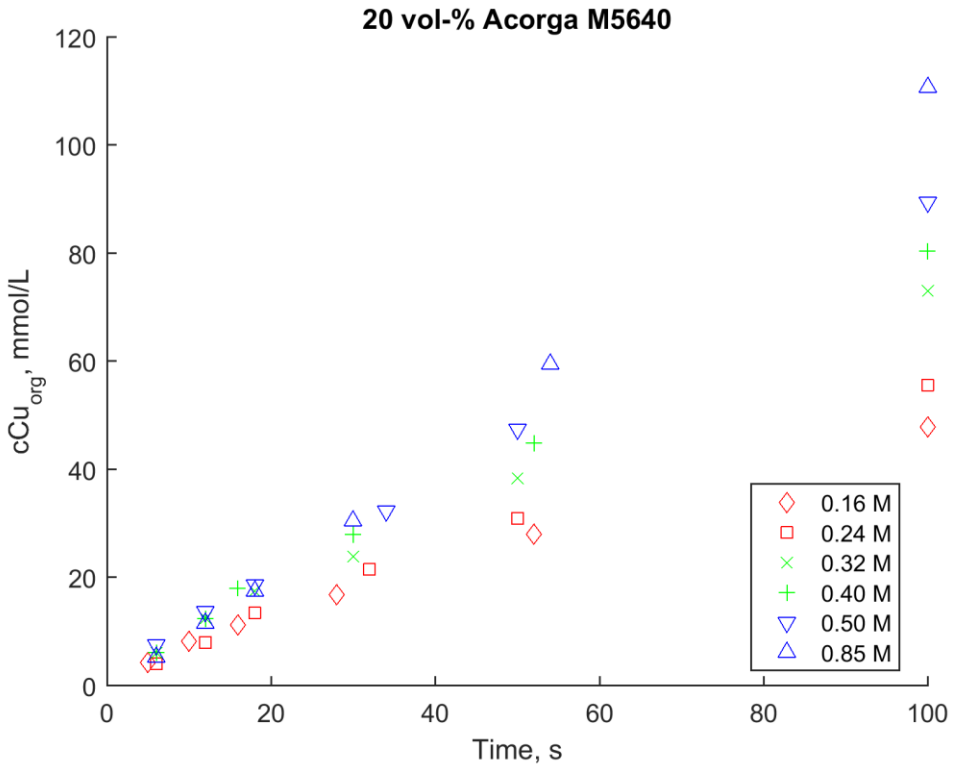

Figure 38. Concentration of copper complex in the droplet as a function of time. Initial aqueous phase concentration was varied between 0.16 – 0.85 M $CuSO_4$.

From Fig. 37 and Fig. 38 it can be seen that the copper complex concentration increased linearly up to around 60 seconds, and then began to gradually slow down. Both in the binary droplet coalescence experiments and in the single droplet kinetic extraction experiments the initial concentration c_0 was considered to be zero at the beginning of each experiment, thus making the assumption of negligible droplet residual concentration. Since a coalescence experiment lasts approximately 10 seconds, taking the droplet formation time into account, it can be said that the concentration increase and thus mass transfer rate of copper complex was linear in all coalescence experiments. As the continuous phase concentration was increased, it was observed that the mass transfer rate of copper complex was also increasing, as expected. However, in the time interval of the coalescence experiments, the differences in the copper complex concentrations between different test runs were not substantial. If mass transfer during the coalescence event is considered, the increase in copper complex concentration during this time interval can be calculated with Eq. (11) by assuming that the increase in concentration during the whole

experiment is linear. However, as the time interval of a coalescence event is very short (about 30 ms), the calculated mass transfer during the coalescence was considered to be close to negligible.

9.7 Binary Droplet Coalescence: Modelling and Experimental

COMSOL Multiphysics software was used to model binary droplet coalescence with the level-set method. The continuous phase and dispersed phase properties used in the simulation were similar to those used in the coalescence experiments with ammonium sulfate and 20 volume percent Acorga M5640 in Exxsol D80 (continuous phase density was 1025 kg/m^3 and was viscosity of 1.1 mPa · s, dispersed phase density was 834 kg/m^3 and viscosity was 3.0 mPa · s). Feed rate was 400 µL/min and needle diameter was 0.91 mm. Comparison of experimental and simulated coalescence is presented in Fig. 39.

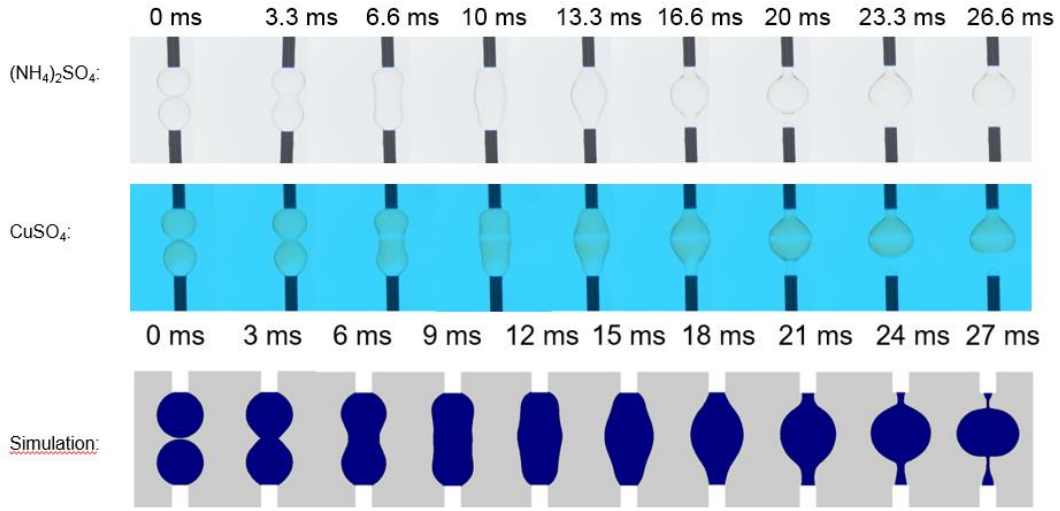

Figure 39. First row: 20 vol-% Acorga dispersed in the continuous phase of 0.16 M $(NH_4)_2SO_4$. Second row: 20 vol-% Acorga dispersed in the continuous phase of 0.16 M $CuSO_4$. Third row: simulation of the coalescence event with COMSOL using the level-set method.

It can be seen from Fig. 39 that the coalescence event was virtually unaffected by the change of salt in the continuous phase. While the inclusion of mass transfer drastically affected the droplet rest time distributions (see Section 9.3), the coalescence event itself seemed to remain rather unaffected by mass transfer. It was

assumed that the coalescence event was affected mainly by physical properties of the system such as density differences and viscosities, while the droplet rest times were more inclined to be affected by interfacial phenomena such as mass transfer and surface tension gradients. No significant differences could be observed between the simulated and experimental results. The slightly longer coalescence time obtained in the modelling could be a result of small differences concerning droplet shapes and phase properties. While in the simulation the droplets were considered to be identical in shape and volume, in the experiments there was always some small variation both in the relative droplet volumes and droplet shapes (see Sections 9.1 and 9.2), and this could lead to small differences also in the coalescence times.

10 CONCLUSIONS

Coalescence experiments were performed in binary droplet system, in addition to single droplet kinetic extraction experiments. By analysing the videos manually, droplet formation times, rest times and coalescence times were obtained. Additionally, droplet volumes, concentrations and surface areas, among others, were obtained by using image and video analysis program. Droplet formation times decreased as the concentration of continuous phase was increased due to increasing density differences between the phases, while droplet coalescence times were constant in all experiments. Droplet rest times were compared for two different binary droplet systems: 20 volume percent Acorga M5640 in Exxsol D80 dispersed in 0.16 M $(NH_4)_2SO_4$ and in 0.16 M $CuSO_4$, respectively. Former droplet rest times were normally distributed, while the latter were normally distributed only when droplet rest times above 0.4 seconds were excluded from the results. The droplet rest times were significantly reduced when copper complex formation was taking place in the system: from average of 9.41 seconds with the continuous phase of 0.16 M $(NH_4)_2SO_4$ to only 0.11 seconds with the continuous phase of 0.16 M $CuSO_4$. This was due to Marangoni effect causing surface tension gradients in the droplet interfaces and reducing the stability of the binary droplet system. Droplet concentration analysis revealed both the sessile and pendant droplet concentrations just before the coalescence, and the concentrations of combined droplets just after the coalescence. Sessile and pendant droplet concentrations corresponded reasonably well with each other in all used phase combinations, but the combined

droplet concentrations were lower than expected when compared to the sessile and pendant droplet concentrations just before the coalescence event. These values could be affected by measurement errors in the analysis step or errors conducting the experimental part. It was assumed that mass transfer during a coalescence event was not enhanced within the detection limits of the used image analysis method. The calculated values from single droplet kinetic extraction experiments confirmed that mass transfer during the whole coalescence experiment was linear and gradually increased as the continuous phase concentration was increased. However, the mass transfer during coalescence event itself was close negligible, mostly due to short coalescence time of about 30 ms. Experimental results were in good agreement with the modelling of coalescence event when using the level-set method, and no significant differences in the coalescence time was observed.

REFERENCES

Alopaeus, V., 2014, Analysis of Concentration Polydispersity in Mixed Liquid-Liquid Systems, Chem. Eng. Research and Design Vol. 92, pp. 612 - 618.

Anderson, R. and Anderson, B., 2006b, Modelling the Breakup of Fluid Particles in Turbulent Flows, Fluid Mech. and Transport Phenomena Vol. 52, pages 2020 - 2030.

Annaland, M. S., Deen, N. G. and Kuipers, J. A. M., 2005, Numerical Simulation of Gas Bubbles Behaviour using a Three-Dimensional Volume of Fluid Method, Chem. Eng. Science Vol. 60, pp. 2999 – 3011.

Aryafar, H., Kavehpour, H.P., 2009, Electrocoalescence: Effects of DC Electric Fields on Coalescence of Drops at Planar Interfaces, Langmuir Vol. 25, pp. 12460 – 12465.

Ata, S., Pugh, R. J. and Jameson, G. J., 2010, The Influence of Interfacial Ageing and Temperature on the Coalescence of Oil Droplets in Water, Colloids and Surfaces A: Physicochem. Eng. Aspects Vol. 374, pp. 96 - 101.

Bak, A. and Podgorska, W., 2012, Investigation of Drop Breakage and Coalescence in the Liquid-liquid System with Non-ionic Surfactants Tween 20 and Tween 80, Chem. Eng. Science Vol. 74, pp. 181 - 191.

Bak, A. and Padgorsta, W., 2013, Drop Breakage and Coalescence in the Toluene/Water Dispersions with Dissolved Surface Active Polymers PVA 88% and 98%, Chem. Eng. Research and Design Vol. 91, pp. 2142 - 2155.

Ban, T., Kawaizumi, F., Nii, S., Takahashi, K., 2000, Study of Drop Coalescence Behavior for Liquid-Liquid Extraction Operation, Chem. Eng. Science Vol. 55, pp. 5385 – 5391.

Bart, H. J., 2001, *Reactive Extraction,* Springer, Berlin, Germany.

Bilicki, Z. and Kestin, J., 1987, Transition Criteria for Two-phase Flow Patterns in Vertical Upward Flow, Int. Journal of Multiphase Flow Vol. 13, pp. 283 - 294.

Bothe, D. and Fleckenstein, S., 2013, A Volume of Fluid based method for mass transfer processes at fluid particles, Chem. Eng. Science Vol. 101, pp. 283 – 302.

Bozorgzadeh, F., 1980, Study of Mass Transfer during Droplet Splitting Using a New Optical Technique, Ph.D. Dissertation, University of Newcastle upon Tyne.

Briscoe, B. J., Lawrence, C. J. and Mietus, W. G. P., 1999, A Review of Immiscible Fluid Mixing, Advances in Colloidal and Interface Science Vol. 81, pp. 1 - 17.

Casamatta, G. and Vogelpohl, A., 1985, Modeling of Fluid Dynamics and Mass Transfer in Extraction Columns, German Chem.Eng. Vol. 8, pp. 96 – 103.

Chatzi, E., 1983, Analysis of Interactions in Fluid-Fluid Dispersion Systems in Agitated Vessels, Cleveland State University Press, Cleveland, OH.

Chesters, A. K., 1991, The Modelling of Coalescence Processes in Fluid-liquid Dispersions: A review of Current Understanding, Chen. Eng. Research and Design Vol. 69, pp. 353 - 361.

Chevaillier, J. P., Klaseboer, E., Masbernat, O. and Gourdon, C., 2006, Effect of Mass Transfer on the Film Drainage Between Colliding Droplets, Journal of Colloid and Interface Science Vol. 299, pp. 472 – 485.

Colella, D., Vinci, D., Bagatin, R., Masi, M. and Bakar, E. A., 1999, A Study on Coalescence and Breakage Mechanisms in Three Different Bubble Columns, Chem. Eng. Science Vol. 54, pp. 4767 - 4777.

Coulaloglou, C. A., Taylarides, L. L., 1977, Description of Interaction Process in Agitated Liquid-liquid Dispersions, Chem. Eng. Science Vol. 32, pp. 1289 - 1297.

De Bruijn, R. A., 1989, Deformation and Breakup of Drops in Simple Shear Flows, Ph.D. Thesis, Eindhoven University.

Deshpande, K. B. and Zimmerman, W. B., 2006, Simulation of Interfacial Mass Transfer by Droplet Dynamics using the Level-Set Method, Chem. Eng. Science Vol. 61, pp. 6486 – 6498.

Duineveld, P. C., 1994, Bouncing and Coalescence of Two Bubbles in Water, Ph. D. Dissertation, University of Twente, Netherlands.

Doubliez, L., 1991, The Drainage and Rupture of a Non-foaming Liquid Film Formed upon Bubble Impact with a Free Surface, Int. Journal of Multiphase Flow Vol. 17, pp. 783 - 803.

Eastwood, C. D., Armi, L. and Lasheras, J. C., 2004, The Breakup of Immiscible Fluids in Turbulent Flows, J. Fluid Mech. Vol. 502, pp. 309 - 333.

Eiswirth, R. T., Bart, H. J., Ganguli, A. and Kenig, E. Y., 2012a, Experimental and Numerical Investigation of Binary Coalescence; Liquid Bridge Building and Internal Flow Fields, Phys. Fluids Vol. 24.

Eiswirth, R. T., 2014, Binary Droplet Coalescence of Free Rising Droplets, Ph.D. Thesis, University of Kaiserslautern.

Elemans, P.H.M. and Bos, H. L., 1993, Transient Phenomena in Dispersive Mixing, Chem. Eng. Science Vol. 48, pp. 267 – 276.

Eow, J.S., Ghadiri, M., and Sharif, A., 2002, Electrostatic and Hydrodynamic Separation of Aqueous Drops in a Flowing Viscous Oil, Chem. Eng. and Processing Vol. 41, pp. 649 – 657.

Eow, J.S., Ghadiri, M., 2003, Motion, Deformation and Break-up of Aqueous Drops in Oils Under High Electric Field Strengths, Chem. Eng. and Processing Vol. 42, pp. 259 – 272.

Friedlander, S.K., 1977, Smoke, Dust and Haze, Wiley, New York.

Fu, X.Y. and Ishii, M., 2002, Two-Group Interfacial Area Transport in Vertical Air–Water Flow, I. Mechanistic Model, Nucl. Eng. Des. Vol. 219, pp. 143 – 168.

Gaitzsch, F., Gäbler, A., and Kraume, M., 2011, Analysis of Droplet Expulsion in Stagnant Single Water-in-oil-in-water Double Emulsion Globules, Chem. Eng. Science Vol. 66, pp. 4663 – 4669.

Gebauer, F., Hlawitschka, M. W. and Bart, H. J., 2015, CFD Aided Investigation of Single Droplet Coalescence, Chinese Journal of Chem. Eng. Vol. 24, pp. 249 - 252.

Grace, H. P., 1982, Dispersion Phenomena in High Viscosity Immiscible Fluid Systems and Application of Static Mixers as Dispersion Devices in Such Systems, Journal of Chem. Eng. Communications Vol. 14, pp. 225 – 277.

Han, L., Luo, H. and Liu, Y., 2011, A Theoretical Model for Droplet Breakup in Turbulent Dispersions, Chem. Eng. Science Vol. 66, pp. 766 - 776.

Han, L., Gong, S., Li, Y., Gao, N., Fu, J., Luo, H. and Liu, Z., 2014, Influence of Energy Spectrum Distribution on Drop Breakage in Turbulent Flows, Chem. Eng. Science Vol. 117, pp. 55 - 70.

Hikibi, T., Takamasa, T. and Ishii, M., 2001, Interfacial Area Transport of Bubbly Flow in a Small Diameter Pipe, Journal of Nuclear Science and Tech. Vol. 38, pp. 614 - 620.

Hirt, C. W. and Nichols, B. D., 1981, Volume of Fluid (VOF) method for the Dynamics of Free Boundaries, Journal of Comp. Phys. Vol. 39, pp. 201 – 225.

Howarth, W. J., 1964, Coalescence of Drops in a Turbulent Flow Field, Chem. Eng. Science Vol. 19, pp. 33 - 38.

Jansen, K. M. B., Agretof, W. G. M. and Mellema, J., 2000, Droplet Breakup in Concentrated Emulsions, Journal of Rheology Vol. 45.

Jeffreys, G.V. and Davies, G.A., 1971, Coalescence of Liquid Droplets and Liquid Dispersion: Recent Advances in Liquid–Liquid Extraction, Pergamon Press, Oxford, UK, pp. 495.

Kalkach-Navarro, S., Lahey, R. T. and Drew, D. A., 1994, Analysis of Bubbly/slug Flow Regime Transition, Nuclear Eng. And Science Vol. 151, pp. 15 - 39.

Kamp, J. and Kraume, M., 2014, Influence of Drop Size and Superimposed Mass Transfer on Coalescence in Liquid/liquid Dispersions – Test Cell Design for Single Drop Investigations, Chem. Eng. Research and Design Vol. 92, pp. 635 - 643.

Kentish, S. E., Stevens, G. W. and Pratt H. R. C., 1998, Estimation of Coalescence and Breakage Rate Constants within a Kuhni Column, Industrial and Eng. Chem. Research Vol. 37, pp. 1099 – 1106.

Klaseboer, E., Chevaillier, J. P., Gourdon, C. and Masbernat, O., 2000, Film Drainge between Colliding Drops at Constant Approach Velocity: Experiments and Modelling, Journal of Colloid and Interface Science Vol. 229, pp. 274 – 285.

Kocamustafaogullari, G. and Ishii, M., 1995, Foundation of the Interfacial Area Transport Equation and Its Closure Relations, Int. Journal of Heat and Mass Transfer Vol. 38, pp. 481 - 493.

Komosawa, I., Otake, T. and Kamojima, M., 1980, Wake Behavior and its Effect on Interaction between Spherical-cap Bubbles, Journal of Chem. Eng. Of Japan Vol. 13, pp. 103 – 109.

Konno, M., Aoki, M. and Saito, S., 1988, Coalescence of Dispersed Drops in an Agitated Tank, Journal of Chem. Eng. Vol. 21, pp. 3335 – 3338.

Kopriwa, N., Buchbender, F., Ayesteran, J., Kalem, M., Pfennig, A., 2012, A Critical Review of the Application of Drop-Population Balances for the Design of Solvent Extraction Columns: I. Concept of Solving Drop-Population Balances and Modelling Breakage and Coalescence, Solvent Extraction Ion Exchange Vol. 30, pp. 683 – 723.

Laakkonen, M., Alopaeus, V. and Aittamaa, J., 2006, Validation of Bubble Breakage, Coalescence and Mass Transfer Models for Gas-Liquid Dispersion in Agitated Vessel, Chem. Eng. Science Vol. 61, pp. 218 – 228.

Lan, W., Jing, S., Guo, X. and Li, S., 2017, Study on "Interface – Shrinkage – Driven" Breakup of Droplets in Co-Flowing Microfluidic Devices, Chem. Eng. Science Vol. 158, pp. 58 - 63.

Lee, C.H., Erikson, L. E. and Glasgow, L. A., 1987a, Bubble Breakup and Coalescence in Turbulent Gas–Liquid Dispersions, Chem. Eng. Commun. Vol. 59, pp. 65 – 84.

Lee, C.H., Erikson, L. E. and Glasgow, L. A., 1987b, Dynamics of Bubble Size Distribution in Turbulent Gas–Liquid Dispersions, Chem. Eng. Commun. Vol. 61, pp. 181 – 195.

Lehr, F. and Mewes, D., 1999, A Transport Equation for the Interfacial Area Density Applied to Bubble Columns, Chem. Eng. Science Vol. 56, pp. 1159 - 1166.

Lehr, F. and Mewes, D., 2002, Bubble Size Distributions and Flow Fields in Bubble Columns, Journal of Al. Chem. Vol. 48, pp. 2426 - 2443.

Levenspiel, O., 2001, *Chemical Reaction Engineering*, Third Ed., John Wiley and Sons, New York.

Liao, Y. and Lucas, D., 2009, A Literature Review of Theoretical Models for Drop and Bubble Breakup in Turbulent Dispersions, Chem. Eng. Science 64, pp. 3389 - 3406.

Liu, H., Jing, S., Fang, Q. and Li, S., 2016, Droplet Breakup in a Square-sectioned Pulsed Disc and Doughnut Column, Ind. Eng. Chem. Res. Vol. 55, pp. 2242 – 2251.

Luo, H. and Svendsen, H. F., 1996, Theoretical Model for Drop and Bubble Breakup in Turbulent Dispersions, Fluid Mech. and Transport Phenomena Vol. 42, pp. 1225 - 1233.

Mackay, G.D.M., Mason, S.G., 1963, The Gravity Approach and Coalescence of Fluid Drops at Liquid Interfaces, Canadian J. of Chem. Eng. Vol. 41, pp. 203 – 212.

Maindarkar, S. N., Raikar, N. B., Bongers, B. and Henson, M. A., 2011, Incorporating Emulsion Drop Coalescence into Population Balance Equation Models of High Pressure Homogenization, Colloids and Surfaces A: Physicochemical and Engineering Aspects Vol. 396, pp. 63 - 73.

Marchisio, D. L., Vigil, R. D. and Fox, R. O., 2003, Quadrature Method of Moments for Aggregation-Breakage Processes, Journal of Colloid and Interface Science Vol. 258, pp. 322 – 334.

Marchisio, D. L. and Fox, R. O., 2005, Solution of Population Balance Equations Using the Direct Quadrature Method of Moments, Journal of Aerosol Science Vol. 36, pp. 43 – 73.

MATLAB Release 2016a. The MathWorks, Inc., Natick, Massachusetts, United States.

Mignard, D., Amin., L and Ni, X.-W., 2004, Modelling of Droplet Breakage Probabilities in an Oscillatory Baffled Reactor, Chem. Eng. Science Vol. 59, pp. 2189 - 2200.

Mitra, T. and Ghosh, P., 2007, Binary Coalescence of Water Drops in Organic Media in Presence of Ionic Surfactants and Salts, Journal of Dispersion Science and Tech. Vol 28, pp. 785 - 792.

Mitra, T. and Ghosh, P., 2007, Binary Coalescence of Water Drops in Organic Media in Presence of Ionic Surfactants and Salts, Journal of Dispersion Science and Tech. Vol 28, pp. 785 - 792.

Mitre, J. F., Lage, P. L. C., Souza, M. A., Silva, E., Barca, L. F., Moraes, A. O. S., Coutinho, R. C. C. and Fonseca, E. F., 2014, Droplet Breakage and Coalescence Models for the Flow of Water-in-Oil Emulsions through a Valve-like Element, Chem. Eng. Research and Design Vol. 92, pp. 2493 - 2508.

Mousavichoubeh, M., Shariaty-Niassar, M. and Ghadiri, M., 2011, The Effect of Interfacial Tension on Secondary Drop Formation in Electro-coalescence of Water Droplets in Oil, Chem. Eng. Science Vol. 66, pp. 5330 - 5337.

Narsimhan, G., Gupta, J.P., 1979, A Model for Transitional Breakage Probability of Droplets in Agitated Lean Liquid–Liquid Dispersions, Chem. Eng. Science Vol. 34, pp. 257 – 265.

Ni, X., Mignard, D., Saye, B., Johnstone, J. C. and Pereira, N., 2001, On the Evaluation of Droplet Breakage and Coalescence Rates in an Oscillatory Bafflet Reactor, Chem. Eng. Science Vol. 57, pp. 2101 - 2114.

Osher, S. and Sethian, J.A., 1988, Front Propagating with Curvature-dependent Speed: Algorithm Based on Hamilton–Jacobi Formulations, Journal of Comp. Phys. Vol. 79, pp. 12 – 49.

Pozrikidis, C., 1990, The Deformation of a Liquid Drop Moving Normal to a Plane Wall, Journal of Fluid Mech. Vol. 215, pp. 331 - 363.

Prince, M. J. and Blanch, H. W., 1990, Bubble Coalescence and Breakup in Air-sparged Bubble Columns, Journal of Al. Chem. Vol. 36, pp. 1485 - 1499.

Rallison, J. M., 1984, The Deformation of Small Viscous Drops and Bubbles in Shear Flows, Annu. Rev. Fluid Mech. Vol. 16, pp. 45 - 66.

Ramkrishna, D., *Population Balances: Theory and Applications to Particulate Systems in Engineering,* Purdue University, School of Chem. Eng., West Lafayette, India.

Reddy, S. R. and Fogler, H. S., 1980, Emulsion Stability of Acoustically Formed Emulsions, Journal of Phys. Chem. Vol. 84, pp. 1570 – 1575.

Reichert, M. D. and Walker, L. M., 2015, Coalescence Behaviour of Oil Droplets Coated in Irreversibly-adsorbed Surfactant Layers, Journal of Colloidal and Interface Science Vol. 449, pp. 480 - 487.

Rider, W.J. and Kothe, D.B., 1998, Reconstructing Volume Tracking, Journal of Comp. Phys. Vol. 141, pp. 112 – 152.

Rommel, W., Meon, W., Blass, E., 1992, Hydrodynamic Modeling of Droplet Coalescence at Liquid–Liquid Interfaces, Sep. Science and Tech. Vol. 27, pp. 129 – 159.

Rozentsvaig, A.K., 1985, Mechanism of the Comminution of Drops during the Mixing of Dilute Emulsions with Turbine-driven Agitators, Journal of Appl. Chem. Vol. 6, pp. 1191 – 1198.

Rozentsvaig, A.K., Strashinskii, C.S., 2016, Identification of Models of Transfer Processes in Complex Disperse Systems, Appl. Math. Science Vol. 24, pp. 1151 – 1161.

Sagert, N. H., Quinn, M. J., 1976, The Coalescence of H_2S and CO_2 Bubbles in Water, The Canadian J. of Chem. Eng. Vol. 54, pp. 392 – 398.

Scheele, G.F., and Leng, D.E., 1971, An Experimental Study of Factors which Promote Coalescence of Two Colliding Drops Suspended in Water, Int. Chem. Eng. Science Vol. 26, pp. 1867 – 1879.

Silva, L. F. L. R., Damian, R. B. and Lage, P. L. C., 2008, Implementation and Analysis of Numerical Solution of the Population Balance Equation in CFD Packages, Computers and Chemical Eng. Vol. 32, pp. 2933 – 2945.

Silva, L. F. L. R and Lage, P. L. C., 2013, Development and Implementation of a Polydispersed Multiphase Flow Model in OpenFOAM, Computers and Chem. Eng. Vol. 35, pp. 2653 – 2666.

Skelland, A. H. P. and Kanel, J. S., 1992, Simulation of Mass Transfer in a Batch Agitated Liquid-liquid Dispersion, Ind. Chem. Eng. Res. Vol. 31, pp. 908 – 920.

Solsvik, J. and Jakobsen, H. A., 2014, Solution of the Dynamic Population Balance Equation Describing Breakage-Coalescence Systems in Agitated Vessels: The Least Squares Method, The Canadian Journal of Chem. Eng. Vol. 92, pp. 266 -287.

Sovova, H., 1981, Breakage and Coalescence of Drops in a Batch Stirred Vessel – Comparison of Models and Experiments, Chem. Eng. Science Vol. 36, pp. 1567 - 1573.

Stevens, G. W., Pratt, H. R. C. and Tai, D. R., 1990, Droplet Coalescence in Aqueous Electrolyte Solutions, Journal of Colloid Interface Science Vol. 136, pp. 470 – 479.

Stewart, C. W., 1995, Bubble Interaction in Low-viscosity Liquids, Int. Journal of Multiphase Flow Vol. 21, pp. 1037 - 1046.

Sun, X., Kim, S., Ishii, M. and Beus, S. G., 2004, Modeling of Bubble Coalescence and Disintegration in Confined Upward Two-Phase Flow, Nucl. Eng. Des. Vol. 230, pp. 3 – 26.

Takada, N., Misawa, M., Tomiyama, A. and Fujiwara, S., 2000, Numerical Simulation of Two and Three Dimensional Two Phase Fluid Motion by Lattice Boltzmann Method, Computer Phys. Communications Vol. 129, pp. 233 – 246.

Tamminen, J., Lahdenperä, E., Koiranen, T., Kuronen, T., Eerola, T., Lensu, L. and Kälviäinen, H., 2017, Determination of Single Droplet Sizes, Velocities and Concentrations with Image Analysis for Reactive Extraction of Copper, Chem. Eng. Science Vol. 167, pp. 54 – 65.

Tamminen, J., Sainio, T. and Paatero, E., 2013, Intensification of Metal Extraction with High Shear Mixing, Chem. Eng. and Proc. Vol. 73, pp. 119 – 128.

Thoroddsen, S. T., Takehara, K. and Etoh, T. G., 2005, The Coalescence Speed of a Pendant and a Sessile Drop, Journal of Fluid Mech. Vol. 527, pp. 85 – 114.

Tobin, T. and Ramkrishna, D., 1992, Coalescence of Charged Droplets in Agitated Liquid-Liquid Dispersions, AlChe Journal Vol. 38, pp. 1199 – 1205.

Tsouris, C., Shin, W. T. and Yiacoumi, S., 1998, Pumping, Spraying and Mixing of Fluids by Electric Fields, The Canadian Journal of Chem. Eng. Vol. 76, pp. 589 - 599.

Unverdi, S.O. and Tryggvason, G., 1992, A Front Tracking Method for Viscous, Incompressible, Multi-fluid Flows, Journal of Comp. Phys. Vol. 100, pp. 25 – 37.

Verschueren, M., van de Vosse, F.N. and Meijer, H.E.H., 2001, Diffuse-interface Modelling of Thermocapillary Instabilities in a Hele–Shaw Cell, Journal of Fluid Mech. Vol. 434, pp. 153 – 166.

Villwock, J., Gebauer, F., Kamp, J., Bart, H. J. and Kraume, M., 2014, Systematic Analysis of Single Droplet Coalescence, Chemical Eng. and Tech. Vol. 37, pp. 1103 - 1111.

Wang, J., Lu, P., Wang, Z., Yang, Z. and Mao Z. S., 2008, Numerical Simulation of Unsteady Mass Transfer by the Level-Set Method, Chem. Eng. Science Vol. 63, pp. 3141 – 3151.

Wang, T. F., Wang, J. and Jin, Y., 2003, A Novel Theoretical Breakup Kernel Function for Bubbles/Droplets in a Turbulent Flow, Chem. Eng. Science Vol. 58, pp. 4629 - 4637.

Wang, T. F., Wang, J. and Jin, Y., 2005b, Population Balance Model for Gas-Liquid Flows: Influence of Bubble Coalescence and Breakup Models, Ind. And Eng. Chem. Research Vol. 44, pp. 7540 - 7549.

Wang, W., Li, K., Wang, P., Hao, S. and Gong, J., 2014, Effect of Interfacial Dilational Rheology on the Breakage of Dispersed Droplets in a Dilute Oil-Water Emulsion, Colloids and Surfaces A: Physico Chem. Eng. AspectsVol. 441, pp. 43-50.

Wegener, M. and Paschedag, A. R., 2011, The Effect of Soluble Anionic Surfactants on Rise Velocity and Mass Transfer at Single Droplets in Systems with Marangoni Instabilities, Int. Journal of Heat and Mass Transfer Vol. 55, pp. 1561 - 1573.

Wegener, M., Paul, N. and Kraume, M., 2014, Fluid Dynamics and Mass Transfer at Single Droplets in Liquid/liquid Systems, Int. Journal of Heat and Mass Transfer Vol. 71, pp. 475 - 495.

Wieringa, J. A., VanDieren, F., Janssen, J. J. M. and Agterof, W. G. M., 1996, Droplet Break-up Mechanisms During Emulsification in Colloid Mills at High

Dispersed Phase Volume Fraction, Chem. Eng. Research and Design Vol. 74, pp. 554 - 562.

Wright, H. and Ramkrishna, D., 1994, Factors Affecting Coalescence Frequency of Droplets in a Stirred Liquid-Liquid Dispersion, AlChe Journal Vol. 40, pp. 767 – 776.

Wu, Q., Kim, S. and Ishii, N., 1998, One-group Interfacial Area Transport in Vertical Bubbly Flow, Int. Journal of Heat and Mass Transfer Vol. 41, pp. 1103 - 1112.

Xu, J.H., Li, S.W., Tan, J., Wang, Y.J. and Luo, G.S., 2006, Preparation of Highly Monodisperse Droplet in a T-junction Microfluidic Device, AIChE Journal Vol. 52, pp. 3005 – 3010.

Yang, C. and Mao, Z. S., 2005, Numerical Simulation of Interphase Mass Transfer with the Level Set Approach, Chem. Eng. Science Vol. 60, pp. 2643 - 2660.

Zhang, Y., Liu, Y., Ji, R., Cai, B., Wang, F. and Liu, R., 2012, Discussion of the Drop Rest Phenomenon at Millimeter Scale and Coalescence of Droplets at Micrometer Scale, Journal of Dispersion Science and Tech. Vol. 33, pp. 1700 - 1707.